University of Cincinnati

Date: 5/3/2017

I, Zhizhen Wu, hereby submit this original work as part of the requirements for the degree of Doctor of Philosophy in Electrical Engineering.

It is entitled:

Flexible Microsensors based on polysilicon thin film for Monitoring Traumatic Brain Injury (TBI)

Student's name: **Zhizhen Wu**

This work and its defense approved by:

Committee chair: Chong Ahn, Ph.D.

Committee member: Punit Boolchand, Ph.D.

Committee member: Leyla Esfandiari, Ph.D.

Committee member: Jed Hartings, Ph.D.

Committee member: Chunyan Li, Ph.D.

Committee member: Ian Papautsky, Ph.D.

29042

FLEXIBLE MICROSENSORS BASED ON POLYSILICON FOR MONITORING TRAUMATIC BRAIN INJURY (TBI)

A thesis submitted to the
Division of Research and Advanced Studies
of the University of Cincinnati
in partial fulfillment of the requirements for the degree of

DOCTOR OF PHILOSOPHY

in the Department of Electrical and Computer Engineering and Computer Science
of the College of Engineering

2017

By

Zhizhen Wu

B.E., Nankai University, China, 2005
M.S., Nankai University, 2008

Committee Chair: Chong H. Ahn, Ph.D.

ABSTRACT

Pressure and temperature are parameters essential for brain monitoring. Currently, the intracranial pressure (ICP) and intracranial temperature (ICT) are measured by the separate sensors/catheters in clinic. Although integrated ICP and ICT sensors with low cost and minimal damage to brain is highly favored, the integration of the sensors involves complicate assembly and packaging process, and also increases the diameter of micro-catheters. Researches have been done to develop integrated pressure and temperature sensors on the same platform, especially on flexible substrate, to minimize the damage to brain caused by the device implantation. However, the developed sensors are either merely prove-of-concept or difficult to be manufactured due to the complicate and costly process.

This work proposes and explores novel approaches to develop the integrated flexible ICP and ICT sensors with low cost and simple process. High quality polysilicon thin film was directly grown on flexible substrate as the sensing material for both ICP and ICT sensors with simple, fast, and low cost aluminum induced crystallization (AIC) process. The polycrystalline structure of the film was characterized and verified with XRD, SEM, TEM and EDS measurements. The results showed a continuous P-type polysilicon film with the crystals' average size of 49 nm. Based on the polysilicon thin film, a flexible thermistor array was designed, developed and characterized for brain temperature monitoring. The developed polysilicon thermistors achieved good *in vitro* performance with a sensitivity of -0.0031/°C, response time of 1.5 s, resolution of 0.1 °C, thermal hysteresis less than 0.1°C, and long term

stability with drift less than 0.3 °C for 3 days of continuous operation in water. *In vivo* tests of the polysilicon thermistor showed a low noise level of 0.025±0.03 °C and the expected transient temperature increase associated with cortical spreading depolarization.

In addition, polysilicon based flexible pressure sensor was developed and characterized for ICP measurement. The gauge factor of polysilicon thin film was characterized with a value of 10.316. The dimensions of the flexible piezoresistive pressure sensor were designed and optimized with COMSOL multiphysics simulation to achieve high sensitivity and linearity. The developed flexible pressure sensor showed a sensitivity of 6×10^{-4} / mmHg, resolution of 1 mmHg, and hysteresis of less than 1 mmHg for the pressure range of 10 to 20 mmHg, which totally met the requirements of ICP monitoring. Finally, a 1 × 4 integrated flexible pressure and temperature sensor array was developed for monitoring the temperature and possible pressure vectors in the traumatic brain injury (TBI). The real-time measurements of pressure and temperature were performed in an immolated brain model for monitoring any pressure vectors or gradients. The preliminary experiment results showed that the developed sensor array had high enough sensitivity to detect the pressure differences or gradients in brain if any.

In conclusion, this work has proposed, developed and fully characterized innovative polysilicon-based flexible temperature and pressure sensors for ICP and ICT monitoring. The development of polysilicon thin film on flexible polyimide with simple, low cost and high yield has been shown. The polysilicon-based temperature and pressure sensors have meet requirements the ICP and ICT monitoring with high sensitivity, high resolution, fast response, and low hysteresis, and can be very beneficial to brain monitoring.

ACKNOWLEDGMENTS

First and foremost, I would like to express my sincere gratitude to my advisor, Dr. Chong Ahn. His skillful guidance in both my technical and my personal development was priceless. I've learned so much from his passion and enthusiasm for new ideas, great insight into research work. I deeply appreciate his tremendous support in my research and patience of continuous training me to be an effective researcher. He is my lifelong mentor and role model in both research and my personal life.

In addition, I would like to thank my supervisory committee members, Dr. Jed Hartings, Dr. Ian Papautsky, Dr. Chunyan Li, Dr. Punit Boolchand, and Dr. Leyla Esfandiari for their valuable time, suggestions and comments. I would like to give a special thanks to Dr. Hartings for his insight and guidance in brain monitoring research work, and help in my journal paper reviewing. I also would like to thank Dr. Li for the *in vivo* test results for my devices. I would like to thank Dr. Papautsky for the valuable feedback about the arrangement of the content in my thesis work, Dr. Leyla Esfandiari for the suggestions about my future career, and Dr. Punit Boolchand for the comments for the polysilicon material.

Many thanks are to Ronald Flenniken and Jefferey Simkins at cleanroom center. Ron provided tremendous help for me to go through all the optimization processes of my polysilicon

material with lots of discussions about the microfabrication. Jeff gave me all kinds of supports in setting up the equipments, micromachining the components for the measurement setup.

I also thank students in Dr. Papautsky's, Dr. Heinkenfeld's, and Dr. Steckl's groups for their help. Special thanks to my colleagues at the BioMEMS Lab for their friendship and support, especially Siddhant Awasthi for developing the interface circuit and helping the measurement setup.

Finally, I would like to thank my family, my parents Yue Wu and Xiaoling Hu and my sister Zhimei Wu for their unconditional love, for being supportive and encouraging, for providing motivation and always being there for me.

TABLE OF CONTENTS

LIST OF FIGURES iii

LIST OF TABLES viii

CHAPTER 1 INTRODUCTION 1

Traumatic brain injury (TBI) monitoring 1
Previous work 4
Research motivation 10
Scope of work 11
Chapter Summaries 12

CHAPTER 2 POLYSILICON FILM DEVELOPED ON FLEXIBLE POLYIMIDE 14

Introduction 14
Aluminum Induced Crystallization (AIC) 16
Polysilicon thin film developed with AIC on polyimide 19
Polysilicon thin film characterization 24
Summary 35

CHAPTER 3 FLEXIBLE TEMPERATURE SENSOR BASED ON POLYSILICON 36

Introduction 36
Sensor design and fabrication 39
In Vitro measurement 49
In Vivo measurement 59
Summary 63

CHAPTER 4 FLEXIBLE PRESSURE SENSOR BASED ON POLYSILICON 64

Introduction 64
Gauge Factor of polysilicon thin film 66
Flexible pressure sensor design and microfabrication 71
Experimental results 80
Summary 86

CHAPTER 5 POLYSILICON PRESSURE SENSOR ARRAY 87

Introduction 87
Pressure sensor array design and microfabrication 89
Interface circuit 91
Experimental results...94
Summary 102

CHAPTER 6 CONCLUSIONS 103

Summary of research 103

REFERENCES 106

LIST OF FIGURES

Figure		Page
1-1	Flexible, large-area network of pressure and thermal sensors with organic transistor active matrixes on polyimide substrate: graphite-containing rubber was used as the sensing material for pressure sensor, and organic diodes as sheet-type thermal sensors. Pressure sensor showed a resolution of 10 kPa, and temperature sensor with a resolution of 10 °C, which were too low to for ICP and ICT measurement.	6
1-2	Flexible capacitive pressure sensors with microstructured SBSs elastomers as dielectric layer showed high sensitivity in medium and low pressure regimes, with demonstration of *In vivo* ICP measurement.	7
1-3	Fully printed, multifunctional highly sensitive e-whisker arrays developed as a proof of concept to integrate highly sensitive strain and temperature sensors on flexible substrate.	8
1-4	Multifunctional sensors developed with single crystal silicon-nanomembrane transferred on flexible polyimide for simultaneous sensing of pressure and temperature.	9
2-1	Illustration of the diffusion and layer exchange of aluminum induced crystallization process: (a) amorphous silicon and aluminum layer with the same thickness, (b) silicon and aluminum atoms inter-diffused into each other's layer during annealing, (c) Silicon and aluminum layers totally exchange the position and a continuous polysilicon layer is formed under the aluminum after annealing is done.	18
2-2	Flexible PI2611 film (a) developed on silicon wafer; (b) peeled off from the wafer.	20
2-3	Thickness of sputtered amorphous silicon and aluminum layer measured by profilometer	22
2-4	(a) Amorphous silicon and aluminum layer sputtered on PI2611 before annealing; (b) The stack layer after annealing. Color change can be clearly seen due to the layer exchange...	23
2-5	Polysilicon film on flexible PI2611 substrate (a) before getting peeled off from silicon wafer, (b) peeled off from silicon wafer.	24

2-6 XRD results for samples annealed for 1(a), 2(b) and 3(c) hours: the peaks appear at 2θ = 28.5°<111> and 47.3°<220> for all three samples of polysilicon thin film developed on PI2611 substrate.. 26

2-7 TEM result shows the fully polycrystalline characterization of polysilicon film..........27

2-8 SEM picture showing the continuous and dense microcrystals of developed polysilicon film 28

2-9 EDS results showing the embedding of Al atoms in the formed polysilicon film: the weight ratio between Al and Si is 7.6%:92.4%; and atom number ratio is 7.9%: 92.1%..........29

2-10 Designed polysilicon pattern for sheet resistance measurement based on TLM. 30

2-11 Developed pattern for measuring sheet resistance of polysilicon thin film and the contact resistance (a) on PI2611film peeled off from silicon wafer; (b) under microscope. 32

2-12 Linear I-V curve shows the contact between polysilicon and aluminum is Ohmic-contact. 33

2-13 Resistance change with length/width ratio of resistor 34

3-1 Concept and device design: polysilicon thermistors array with four sensing elements (R_1 & R_2: 20 μm ×160 μm, R_3 & R_4: 200 μm ×160 μm), ECoG microelectrodes are placed along for in vivo test of association between ECoG depolarization signal and local temperature change under stimulus... 40

3-2 SEM picture of silicon nitride layer sputtered on PI2611 substrate, showing a clear interface between PI2611 and silicon nitride. 42

3-3 EDS analysis of silicon nitride layer and PI2611 substrate... 43

3-4 Summary of the microfabrication process. 44

3-5 Polysilicon-based temperature sensor array: (a) developed flexible devices, (b) sensor pattern under microscope..........45

3-6 Temperature profile of the device with (a) 100μA after 10 minutes shows an elevated temperature of the device of 323.00K with environmental temperature of 293.15K (room temperature); (b) 5μA after 10 minutes shows the temperature of device of 293.15K without obvious self-heating; (c) device temperature change with different input currents..........48

3-7 Sensitivity test: the sensor demonstrates sensitivity of -0.0031/°C for polysilicon thermistor R_1 & R_2, and -0.0025/°C for R_3 & R_4..........50

3-8 Long term stability test in air: (a) Polysilicon resistance measurement in a constant temperature oven with temperature around 37.2°C for 3 days; (b) Resistance drift V.S. temperature drift... 52

3-9 Long term stability test in water: (a) shows the resistance of one polysilicon thermistor measured for 3 days; (b) shows the resistance-drift in three days

measured for five samples. The resistance drifts of the polysilicon thermistors were less than 0.08 %, which corresponds to less than 0.3 °C. 54

3-10 Response time test: The time constant and response time are found to be around 0.8 s and 1.5 s for R_1 & R_2, and 0.8 s and 2.2 s for R_3 & R_4. 56

3-11 Thermal cycle test: the thermal hysteresis is less than 0.1°C for the temperature sensor for R_1 & R_2; and 1°C for R_3 & R_4 after three thermal cycles from 30 °C to 45 °C. 57

3-12 Resolution test: The sensor's resistance changes with each temperature step clearly shows that the sensor can realize a resolution of 0.1 °C. 58

3-13 Measured in vivo noise level for polysilicon thermistors: $R_1$with the dimension of 20 μm ×160 μm: 0.025±0.03 °C; R_3 with the dimension of 200 μm ×160 μm: 0.07±0.06 °C 60

3-14 Transient response of polysilicon thermistors to in vivo stimulus: brain cortical temperature showed a transient increase (0.35±0.06 for R_1 & R_2; 0.23±0.07 for R_3 & R_4; n=4) and then slowly recovered to its baseline value during spreading depolarization...61

4-1 Polysilicon resistors developed on flexible polyimide substrate for gauge factor test... 67

4-2 Gauge factor test: (a) Instron® loading cell (b) polysilicon resistor used for the measurement, and (c) polysilicon the resistor fixed on the loading cell............................69

4-3 Gauge factor measurement results: mean gauge factor of three samples is 10.316 70

4-4 Hysteresis curve for 2 strain cycles: the hysteresis is less than 0.3%... 70

4-5 Polysilicon-based flexible pressure sensor: the polysilicon elements out of membrane act as temperature sensor and the elements on the membrane act as pressure sensor. 72

4-6 Displacement of membrane under (top) 1 mmHg; (bottom) 35 mmHg... 75

4-7 Stress distribution along the thickness of membrane under (top) 1 mmHg; (bottom) 35 mmHg. 76

4-8 Simulation of longitudinal strain and stress distribution of the cut plane 0.5 μm from the top surface of membrane under the pressure of 1mmHg (a, b) and 35 mmHg (c. d)... 77

4-9 Dimensions of pressure sensor...78

4-10 Summary of microfabrication process. 79

4-11 Polysilicon piezoresistor pattern on membrane under microscope: aluminum connection was used to connect two polysilicon radical resistors and prevent transverse effect... 80

4-12 Test setup: (a) water column was used to apply pressure to the sensor, and a three valve was used to control the height of the water, thus the applied temperature. Replaceable adapters were fabricated with milling machine and were used to hold the pressure sensor. (b) Two types of adapters for planar pressure sensor and curved pressure sensor respectively. (c) The planar form of pressure sensor attached to the adapter for testing. (d) Pressure sensor wrapped around a 2 mm diameter tube and placed in the adapter for measurement. 82

4-13 The developed pressure sensor showed a linear change with pressure and a sensitivity of 6×10^{-4} / mmHg. 83

4-14 The pressure sensor showed a stable resistance at each pressure and a clear increase with every pressure step of 1 mmHg for the pressure range of 1 mmHg to 30 mmHg 84

4-15 The pressure sensor showed a hysteresis of less than 1 mmHg for a cycle ranging from 10 to 20 mmHg........85

5-1 Illustration of brain monitoring: (a) Current approach: single ICP, the real-time directional pressure gradient is not detectable; (b) New approach: lab-on-a-tube with pressure sensor arrays for monitoring pressure gradient and evaluating the pressure vectors within the skull. 88

5-2 Spirally-assembled lab-on-a-tube integrated with pressure sensor array and temperature sensors........89

5-3 Layout of pressure and temperature sensor array. 90

5-4 Fabricated sensor array devices... 91

5-5 Block diagram of the circuitry 92

5-6 Current source IC Schematic... 92

5-7 PCB of designed circuit. 93

5-8 Temperature sensors of two adjacent sensing units responded to temperature change. Voltage decreased for both temperature sensors with the same slope as temperature increased, and the voltage got stabled after hotplate reached to the set temperature of 40 °C.... 95

5-9 Pressure sensors of two adjacent units responded to both applied pressure and temperature. Pressures of 1 mmHg, 2 mmHg, and 5 mmHg were applied on the two elements and about 0.8 mV, 1.5 mV and 4 mV output voltages change were generated respectively. No interference is shown between the two sensors, indicating a low cross-talk.... 96

5-10 Test setup: a brain emulation model was developed for real-time pressure and temperature monitoring. 10 μA input constant current was applied interface circuit and output voltage was recorded with Labview program with the 100 Hz frequency and displayed with laptop... 98

5-11 Real-time dynamic pressure and temperature measurement with a balloon expansion: the output voltage of all three pressure sensors changed with the pressure with the same slope, which increased when pushing the syringe to expand the balloon volume and increase the pressure inside the closed spherical ball, and decreased when pulling the syringe; the output voltage of temperature sensors also changed when pressure changes: which means temperature increased when agar pushed against the sensor. 100

5-12 Comparison of normalized output voltage pressure of pressure sensors in three sensing units: Output voltages overlap well for three sensors, which mean there is no pressure gradient in the experiment 101

LIST OF TABLES

Table 1. Thermal conductivities at room temperature for the materials used in the thermal simulation……………………………………………………………………………………47

Table 2. Parameters of PI2611 and Silicon nitride used in the membrane strain and displacement simulation……………………………………………………………………………………73

CHAPTER 1

INTRODUCTION

Traumatic brain injury (TBI) monitoring

Traumatic brain injury (TBI) is an epidemic. In the US each year, 1.7 million people experience TBI; 52,000 die and 275,000 require hospitalization[1]. Severe TBI (sTBI) is commonly defined as coma despite initial resuscitation, and occurs in approximately 10 % of hospital admissions[2–4]. Of patients who survive sTBI, only 31-53% experience favorable functional outcome by 6 months [5–8] and more than three-quarters are left with some form of functional disability[9]. However, the severity of the initial injury alone is a poor prognostic marker[10].

Survivors of a severe primary injury require care in an intensive care unit (ICU), where secondary brain injuries play an important role in determining outcome1[1]. Neurological deterioration occurs in 27 % of patients, which increases the TBI-associated mortality from 9.6 % to 56.4 %[12]. Pharmacological neuroprotective agents have so far failed to demonstrate a statistically significant effect when given after TBI and there is currently no clinically proven means to improve neurological recovery after TBI[13]. Current management strategies are therefore directed towards providing an optimal physiological environment in order to minimize secondary insults that can cause additional neurological injury and further compromise the

regenerative processes[14, 15]. Monitoring the brain after acute injury is central to the practice of neurocritical care for patients with a wide range of disorders including TBI, ischemic and hemorrhagic stroke. It is critical that safe and accurate means of monitoring the key physiological parameters are available to facilitate prompt intervention when necessary.

Intracranial pressure (ICP), the physiological parameter measured the most for TBI patients, is the pressure inside the skull that fills in around the brain and spinal. Its value, conventionally referenced to the atmospheric pressure and expressed in millimeters of mercury, is maintained in a range between 7 and 15 mmHg for adults, 3-6 mmHg in children, and 1.5-6 mmHg in term infants[16]. An increase in ICP usually happens in sTBI because of resistance to cerebrospinal fluid (CSF) flow between intracerebral compartments secondary to brain swelling or expansion of intracranial mass lesions, or because CSF outflow is obstructed[17]. A number of studies have shown that high ICP is strongly associated with poor outcome. Data suggests that elevated ICP impacts outcome: each 10 mmHg of ICP recorded < 48 hours from TBI increases the odds of death threefold[18] and elevations to 20 mmHg for just 30 minutes increase the odds for poor functional outcome by fourfold[19].

All current clinical available methods for ICP monitoring are invasive. Catheters of various mechanisms such as intraventricular catheter[20], air pouch balloon catheter (Speigelberg) [21], Fibreoptic catheter (Camino) [22] and Silicon pressure sensor-tip catheter (Codman) [23] have been used. Among them, the intraventricular catheter with CSF drainage function is considered as the “gold standard” of ICP monitoring but bears infection problem. Silicon pressure sensor-tip catheter has shown comparable performance to that of intraventricular catheter and can be another good option[24].

In additional to ICP, intracranial temperature (ICT) is another critical parameter used to monitor patients subject to intensive neurosurgical monitoring. ICT is different from the body's core temperature and largely dependent on the metabolic activity of brain tissue[25]. It has been shown that, in cases of trauma, the brain is extremely sensitive and vulnerable to small temperature variations[26]. Soukup et al. reported poor outcome at 3 months in patients with TBI who showed extremes of brain temperature[27]. Brain temperatures within the range of 36.5 °C to 38 °C during the first 24 hours were associated with a lower probability of death (10–20%). Brain temperature outside this range was associated with a higher probability of death and with poor 3-month neurological outcomes[28]. Evidence for the adverse effects of a small increase in brain temperature on secondary neuronal damage[29] and mortality[30, 31] is now extensive. Both non-invasive and invasive methods are clinically available for brain temperature measurement. MRI[32] and CT[33] technologies have been popular for non-invasive measurement; while invasive brain temperature measurements are usually based on thermistor and integrated with ICP (Camino, Neurovent)[34, 35] or partial oxygen pressure (Licox, Codman)[36, 37] measurements. Although having the advantage of being non-invasive, MRI and CT measurements are less accurate than the invasive ones and can only measure brain temperature discontinuously.

Currently, the ICP and ICT are measured by separate sensors on different platform. The integration of the sensors to develop multi-functional micro-catheters involves wiring, assembly, and packaging processes which have been regarded as some of the most challenging tasks due to their high complexity and manufacturing cost. In addition, the diameter of micro-catheters increases with sensor's integration[38]. Thus, the development of integrated ICP and ICT sensors with minimal crosstalk on a single platform using simple process with low cost is quite attractive. Flexible substrate can be a good choice as the platform to minimize the damage caused by the

device implantation as well as fit to the non-flat structure of tissue. Furthermore, it is ideal that the ICP and ICT sensors can be easily integrated with other biosensors and electrocorticalgraphy microelectrodes to obtain a profound insight of the pathophysiological status and evolvement of brain injury.

Previous work

Numerous works have been done to develop flexible pressure and temperature sensors for biomedical applications. Flexible temperature sensors are usually developed with resistance temperature detector or thermistors. It is relatively simple to develop flexible temperature as sensing material such as metal can be easily developed on flexible substrate to meet the requirements of ICT measurement without concerning about processing temperature limit[39, 40]. However, it is difficult to develop flexible pressure sensor, especially in low pressure range (<10 kPa), due to the lack of available high sensitive pressure sensing material on flexible substrate.

Rigid silicon piezoresistive pressure sensor was tried to bond to flexible substrate with flip-chip bonding method[41]. However, the process with assembling and wire bonding was very complicated, time-consuming, and costly. Some early work also tried to use metal alloy as sensing material for flexible pressure sensor. . Lichtenwalner et al developed a temperature and strain sensor array using thin film Pt as resistance temperature detector (RTD) and NiCr as the piezoresistive pressure-sensing material[42]. However, the low gauge factor of NiCr (~1.7) prevented it from developing high sensitive and resolution pressure sensor. Another pioneer work was done by Someya et al by developing a conformable, flexible, large-area network of

pressure and thermal sensors with organic transistor active matrixes on polyimide substrate[43, 44].As shown in Fig. 1-1, Graphite-containing rubber was used as the piezoresistive sensing material for pressure sensor, and organic diodes were used as sheet-type thermal sensors. The organic transistors were integrated with sensor layer to read the data from sensors. However, for pressure sensing, the resistance of the rubbery sheet was changed with the resolution of 10 kPa, and for temperature sensing, the results showed a resolution of 10 °C. The resolution for both pressure and pressure sensor is too low to realize functional biomedical measurement.

To achieve high sensitivity of pressure sensor, sensing mechanisms such as capacitance and piezoelectricity have been extensively explored[45-49]. Bao's group has done lots of pioneering work in this filed. By microstructuring polydimethylsiloxane (PDMS) [45, 46], styrene-butadiene-styrene (SBS) [47] elastomers as dielectric layer, flexible capacitive pressure sensors with high sensitivity in medium and low pressure regimes, fast response and relaxation time were developed. A resonant circuit was also developed by integrating the high sensitive capacitive pressure sensor with antenna to realize wireless measurement. An *in vivo* ICP measurement test was demonstrated as shown in Fig. 1-2. Akiyama et al developed flexible piezoelectric pressure sensors using oriented aluminum nitride thin films prepared on polyethylene terephthalate (PET) [48]. Human pulse wave form was measured by holding the sensor between the thumb and middle finger. Li et al developed flexible dual-mode (capacitive and resonant mode) pressure sensor for ICP measurement using piezoelectric PVDF-TrFE polymer diaphragm [49]. The capacitive and piezoelectric pressure sensors can fulfill the sensitivity requirement for ICP monitoring. However, piezoelectric sensors require complex support electronics for sensing real static

pressure. Furthermore, the sensors with AC signals may induce severe cross-talk and noise to other integrated sensors during multimodal measurement.

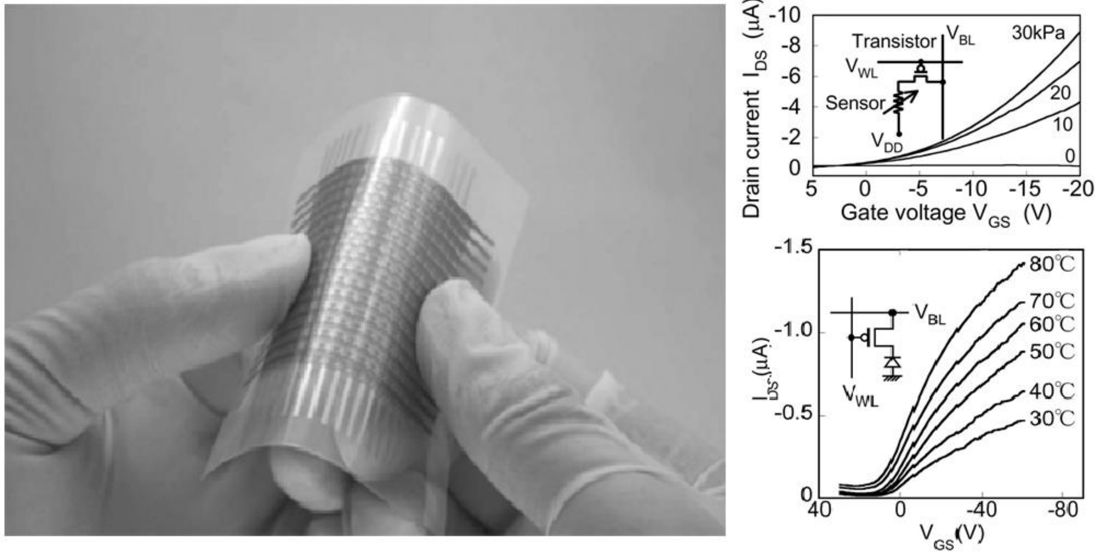

Figure 1-1. Flexible, large-area network of pressure and thermal sensors with organic transistor active matrixes on polyimide substrate: graphite-containing rubber was used as the sensing material for pressure sensor, and organic diodes as sheet-type thermal sensors. Pressure sensor showed a resolution of 10 kPa, and temperature sensor with a resolution of 10 °C, which were too low to for ICP and ICT measurement[43, 44].

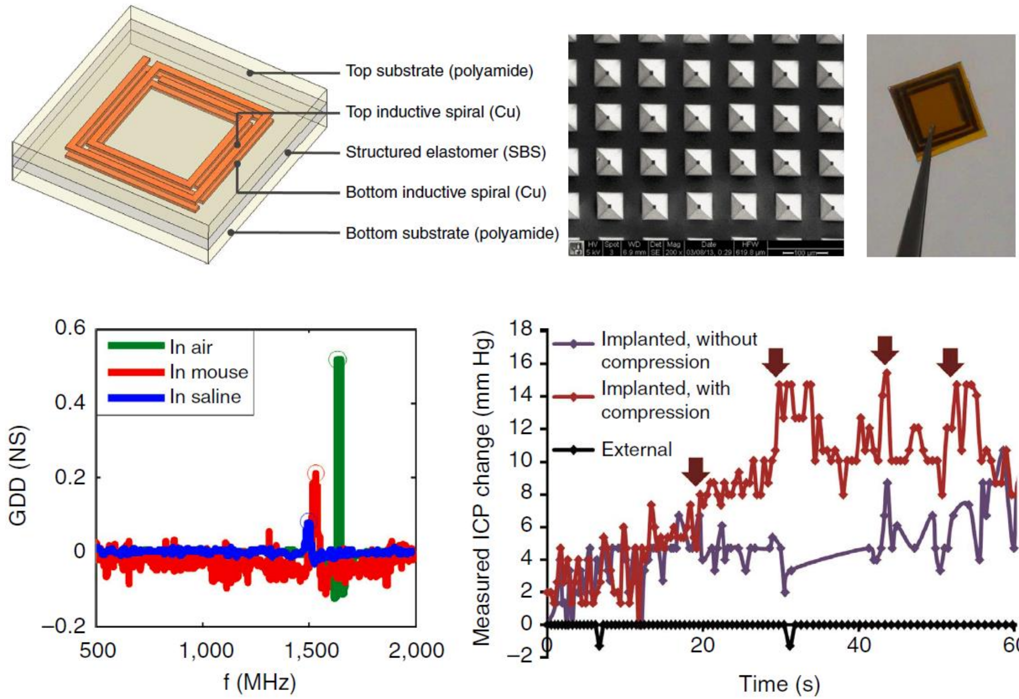

Figure 1-2. Flexible capacitive pressure sensors with microstructured SBSs elastomers as dielectric layer showed high sensitivity in medium and low pressure regimes, with demonstration of *In vivo* ICP measurement [47].

To achieve high sensitivity, simple signal process, and easy integration with other sensors with minimal cross-talk, in recent years, many researchers have been working on the development of high sensitive piezoresistive material on flexible substrate. Composite material of nanoparticles[50, 51], nanowires[52, 53], and nanotube[54, 55] is one of the main trends. Harada et al developed fully printed, multifunctional highly sensitive e-whisker arrays as a proof of concept to integrate highly sensitive strain and temperature sensors[50]. As shown in Fig. 1-3, a carbon nano tube (CNT)-Ag nano particle (NP) film was printed for pressure sensing by measuring the resistance change, and the printed poly(3,4-ethylenedioxythiophene)-poly(styrenesulfonate) (PEDOT:PSS)-CNT composite film was used for temperature sensing. Gong et al[52] demonstrated

that an AuNWs-impregnated tissue paper sandwiched between a blank PDMS sheet and a patterned PDMS sheet with interdigitated electrode arrays, leading to a superior wearable pressure sensor with a sensitivity of 1.14 kPa^{-1}. However, most of the developed devices are still under prove of concept, and have difficulty for in vitro/in vivo tests. The characterizations in liquid have not been reported yet.

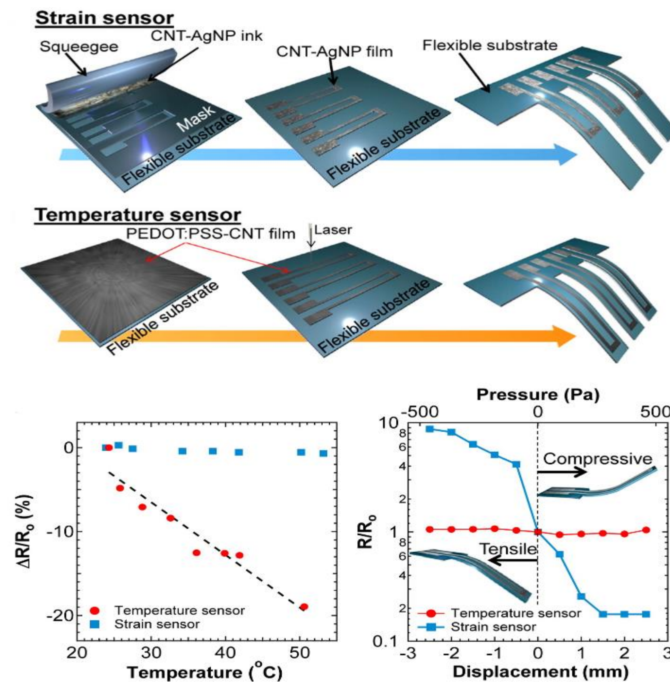

Figure 1-3. Fully printed, multifunctional highly sensitive e-whisker arrays were developed as a proof of concept to integrate highly sensitive strain and temperature sensors on flexible substrate[50].

Instead of exploring new piezoresistive materials on flexible substrate, Roger's group are dedicated to develop high sensitive pressure sensor with traditional single crystal silicon material by transferring silicon nanomembrane or nanoribbons on flexible substrate, and has done lots of

pioneer work[56-58] (Fig. 1-4). Multifunctional sensors have been developed based on single crystal silicon-nanomembrane for simultaneous sensing of both intracranial pressure (ICP) and intracranial temperature (ICT) [57]. *In vivo* tests were conducted for wireless pressure and temperature monitoring in the intracranial space of rats. And the results showed comparable results between the developed sensors and the commercial ones. By far, it is one of the most promising and suitable devices for *in vivo* multimodal brain monitoring and integration of multiple sensors. The only disadvantage lies in the complicate and expensive process of developing and transferring the silicon nanomembrane/nanoribbon.

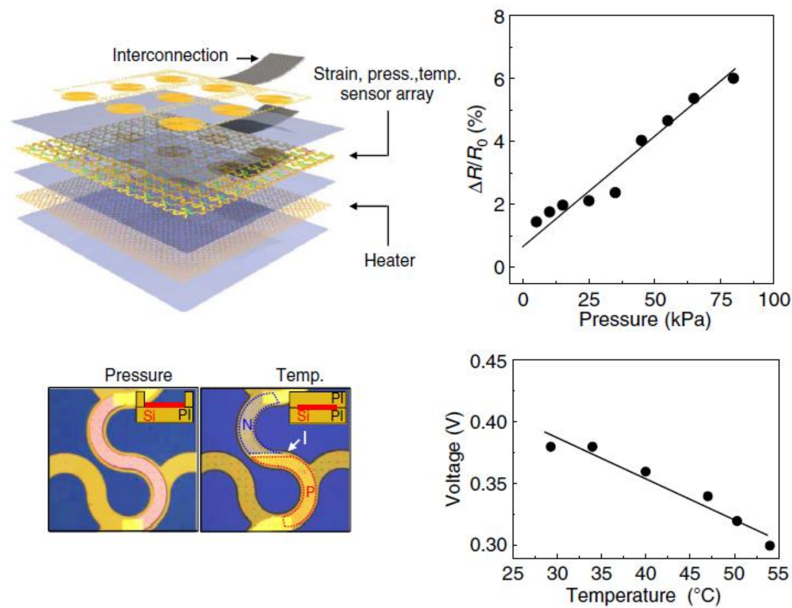

Figure 1-4. Multifunctional sensors have been developed with single crystal silicon-nanomembrane transferred on flexible polyimide for simultaneous sensing of pressure and temperature[56].

Research Motivation

The clinical significance of brain monitoring, specifically multimodal monitoring has triggered a considerable interest and demand for developing integrated ICP and ICT sensors with minimal invasion and crosstalk. Current clinical available catheters which simultaneously measure ICP and ICT are developed by -integrating individual ICP and ICT sensor together, and thus have the problems of complicated assembling, wiring process, and large diameter caused by the integration.

It is ideal to develop ICP and ICT sensors on the same platform. Flexible substrate, as a platform has the advantage of inducing minimal tissue damage. Flexible pressure and temperature sensors have been explored extensively in recent years. However, most newly developed high sensitive flexible pressure sensors are based on capacitive or piezoelectric principles which tend to cause cross-talk when integrating with other sensors and induce high frequency noises. To minimize crosstalk between sensors, high sensitive piezoresistive materials have been extensively explored. Nano composite materials are popular nowadays but they are still under prove-of-concept, and the characterization in liquid environment has not been reported yet. Flexible single crystal silicon nanomembrane based piezoresistive pressure sensor is by far the most promising approach, but has limitation of practical application because of the complicate and costly microfabrication process.

This work has utilized a method to develop polysilicon thin film directly on flexible polyimide, and applied the developed polysilicon thin film for the development of flexible ICP and ICT sensors.

The development of polysilicon thin film on flexible polyimide substrate is based on aluminum induced crystallization (AIC) process. This simple process enables the crystallization of silicon at low temperature suitable for polyimide substrate with high uniformity, low cost and fast process time, which leads to a high throughout and yield of high sensitive ICP and ICT sensors.

Polysilicon thin film was used as the sensing material for both flexible ICP and ICT sensors. The mechanism of pressure sensing is based on the piezoresisitivity of the polysilicon film and temperature sensing is based on the temperature coefficient of resistance (TCR) of the film. Both ICP and ICT sensors measure the resistance change. The DC signal driven nature ensures simple interface circuit for signal processing and readout, , and minimal interference to other sensors.

Scope of work

In this work, the development of polysilicon thin film on a flexible polyimide substrate and the applications of the developed polysilicon thin film for flexible ICP and ICT sensors have been explored and researched.

AIC has been proven to be able to decrease the crystallization temperature of amorphous silicon and form polysilicon thin film. However, direct formation of the polysilicon thin film on flexible substrate and further exploration of gauge factor, TCR properties of the polysilicon film for developing pressure and temperature sensor haven't been reported yet. In this work, high quality polysilicon thin film was developed on free standing polyimide substrate with the low cost, simple, and fast AIC process. The gauge factor and TCR of the polysilicon film were characterized for further design and development of flexible pressure and temperature sensor.

The design, microfabrication, and characterization of the flexible pressure and temperature sensors and sensor array based on polysilicon thin film are presented. The test results show that the developed sensors have high sensitivity and can meet the requirements of ICP and ICT measurement in brain. In addition, the DC driven sensors and sensor array have the advantage of simple signal processing, minimal interference and are suitable for the multiple sensors integrated for the multimodal brain monitoring.

Chapter summaries

Following this introduction, Chapter 2 will describe the process and parameters of developing high quality polysilicon thin film on flexible PI2611 substrate with aluminum induced crystallization (AIC). The polycrystalline structure and atom content of the film will be verified with XRD, TEM, SED, EDS measurements. Further sheet resistance measurement of the polysilicon thin film by transfer length method (TLM) will be discussed to verify P-type nature

of the developed polysilicon film, which eliminates high temperature doping process for l sensors development with the polysilicon film.

Chapter 3 will present a flexible polysilicon-based thermistor array developed with polysilicon film on polyimide for high spatial, temporal resolution brain temperature monitoring, as well as investigating the correlation between brain temperature and electrocorticalgraphy change for injured brain. The design, fabrication process of the thermistor array will be described. The development of silicon nitride film as extra ion/moisture barrier layer will be illustrated. *In vitro* tests to characterize the sensitivity, long term stability, response time, resolution, hysteresis and the results will be shown. *In vivo* noise level and correlation between temperature and ECoG signals results will be presented.

Chapter 4 will introduce a flexible polysilicon-based pressure sensor for the ICP measurement. Characterization of piezoresistivity for the developed polysilicon film and the results will be discussed. Based on the measured gauge factor, the flexible pressure design with the assistance of COMSOL simulation will be presented. The fabrication process of the pressure sensor and test setup will be described. *In vitro* tests to characterize the sensitivity, resolution, and hysteresis of pressure sensor will be presented.

In Chapter 5, a prototype of flexible polysilicon-based temperature and pressure sensor array will be introduced to measure pressure gradient. The fabrication and *in vitro* tests of the sensor array will be presented.

Finally, Chapter 6 will conclude and summarize this work and will provide prospective on the remaining challenges and future directions.

CHAPTER 2

POLYSILICON DEVELOPED ON FLEXIBLE POLYIMIDE

Introduction

Being sensitive to both temperature and pressure, polysilicon can be a very good choice as sensing material for ICP and ICT sensors development. Depending on the developing process and doping level of polysilicon, the GF and temperature coefficient can be adjusted in a wide range[58]. The production of polycrystalline silicon is normally done by crystallization of amorphous silicon (a-Si) and solid phase crystallization (SPC) was the first technique employed to crystallize a-Si. But the crystallization temperature of SPC is too high (~ 600 °C) for flexible substrate and the time required for full crystallization is ultra-long.

To lower the crystallization temperature of polysilicon and develop it on flexible substrate, approaches such as PECVD[59, 60], laser annealing[61, 62] have been explored. However, neutral polysilicon thin film is formed with PECVD process and additional high temperature doping process is still needed to develop electrical device from the film. Laser annealing has the problems of non-uniform crystallization and high cost. Another prevalent low crystallization process for polysilicon is metal-induced crystallization[63-66]. Various metals such as Cu[63], Au[64],

Al[65], and Ni[66] have been used. The general driving force behind metal-induced crystallization is the reduction of the free energy of the silicon material during the transformation of the amorphous to the crystalline phase. When a-Si is in contact with certain metals, electronic screening of the covalent bonding in the Si material occurs according to Hiraki's screening model[67]. This effect weakens the Si bonds, and therefore, facilitates the inter-diffusion of the metal and silicon atoms. Among these metals, aluminum has unique advantages of not forming silicide and the possibility of acting as P-type dopant to avoid further doping process.

Nast et al. [65] proposed the technique of Aluminum induced crystallization (AIC), in which the crystallization process occurred at a temperature under the eutectic temperature of 577 °C. Temperatures for AIC to occur were reported as low as 165 °C [68]. Steffen Uhlig et al. developed polysilicon film on ceramic plates using the AIC process (annealing at 330 to 660°C for up to 6h)[69]. Gauge factors (GFs) of 4.5 to 17 and temperature coefficients of resistance (TCR) between -0.4 and -0.1%/K were obtained for the developed film. Patil et al. [70-72] reported on piezoresistive properties of polysilicon obtained by the AIC process (annealing at 475 up to 550 °C for 90 min) for tactile sensor applications. A polyimide layer was used as a sacrifice layer to build the membrane structure for the tactile sensor, and GFs were estimated to be in the range of 6.6 to 11.7 for an estimated strain of approximately 1.5×10^{-3} applied on the piezoresistors. However, to our best knowledge, the research work of developing polysilicon thin film on flexible substrate using AIC is still lacked, and the feasibility of developing flexible polysilicon-based pressure and temperature sensor using this process has not been explored and reported yet.

In this work, I present the development of polysilicon thin film directly on a flexible polyimide substrate using the AIC process. The polysilicon film developed on the flexible low-

stress polyimide PI2611 (HD Microsystems) was fully characterized using XRD, SEM, and TEM methods.

Aluminum Induced Crystallization (AIC)

In the aluminum induced crystallization (AIC) process, amorphous silicon (a-Si) and aluminum layers are deposited on the substrate and annealed at a temperature under the eutectic temperature of 577 °C. During annealing, Si and aluminum atoms inter-diffuse into each other's layer and lead to a complete layer exchange with sufficient annealing time. While Si atoms dissolve into aluminum layer, crystallization happens and forms poly-crystallization silicon film. Crystallization temperature of polysilicon as low as 150 °C have been reported for AIC.

Numerous studies have been conducted to gain an insight into the actual crystallization process of AIC[73-75]. Konno and Sinclair showed that AIC below the eutectic temperature was a solid phase process[73]. It has been suggested that prior to crystallization an extensive intermixing of Al and Si occurs. The resulting supersaturation of Si in Al is relieved through the nucleation and growth of Poly-Si. At the beginning Si nuclei grow in all directions within the Al layer until they are confined between the original Substrate/Al and Al/a-Si interfaces. In the following phase the Si grains go on growing laterally only when adjacent grains meet and form a continuous polycrystalline silicon film.

Since Si nuclei are confined between the original Substrate/Al and Al/a-Si interfaces, the thickness ratio of aluminum and amorphous layer is critical to develop a continuous polysilicon film. If the Si layer is thinner than the Al layer scarcity of Si material occurs, isolated islands of

crystalline silicon will grow with the height of original Al layer thickness, and prevent the formation of a continuous poly-Si layer prior to depletion of the silicon. If the Si layer is thicker than aluminum layer, a continuous poly-Si layer will be formed with the thickness of the original Al film. The surplus of Si material resulted in the formation of a Si network, visible after Al etching. Thus, it can be concluded that to form continuous poly-Si films under steady temperature conditions, the a-Si layer must be at least as thick as the Al layer, but that thicker a-Si layers will not give any advantage in the final thickness of the polycrystalline Si layer. The ideal thickness ratio of Al and Si layer is 1:1.

During the layer inter-diffusion, a small amount of aluminum is left and embedded in the poly-crystallized silicon film and a fraction of these aluminum atoms are located at substitutional sites, and therefore, electrically active leading to the P-type character polysilicon film. Thus, polysilicon thin film developed by AIC are P-type and high temperature doping process for developing devices can possibly be avoided, which can be very attractive for flexible substrates.

Fig. 2-1 illustrates the diffusion and layer exchange of the AIC process. The overall process leads to an exchange of layer positions, leaving the poly-Si film on the substrate with the Al layer on top.

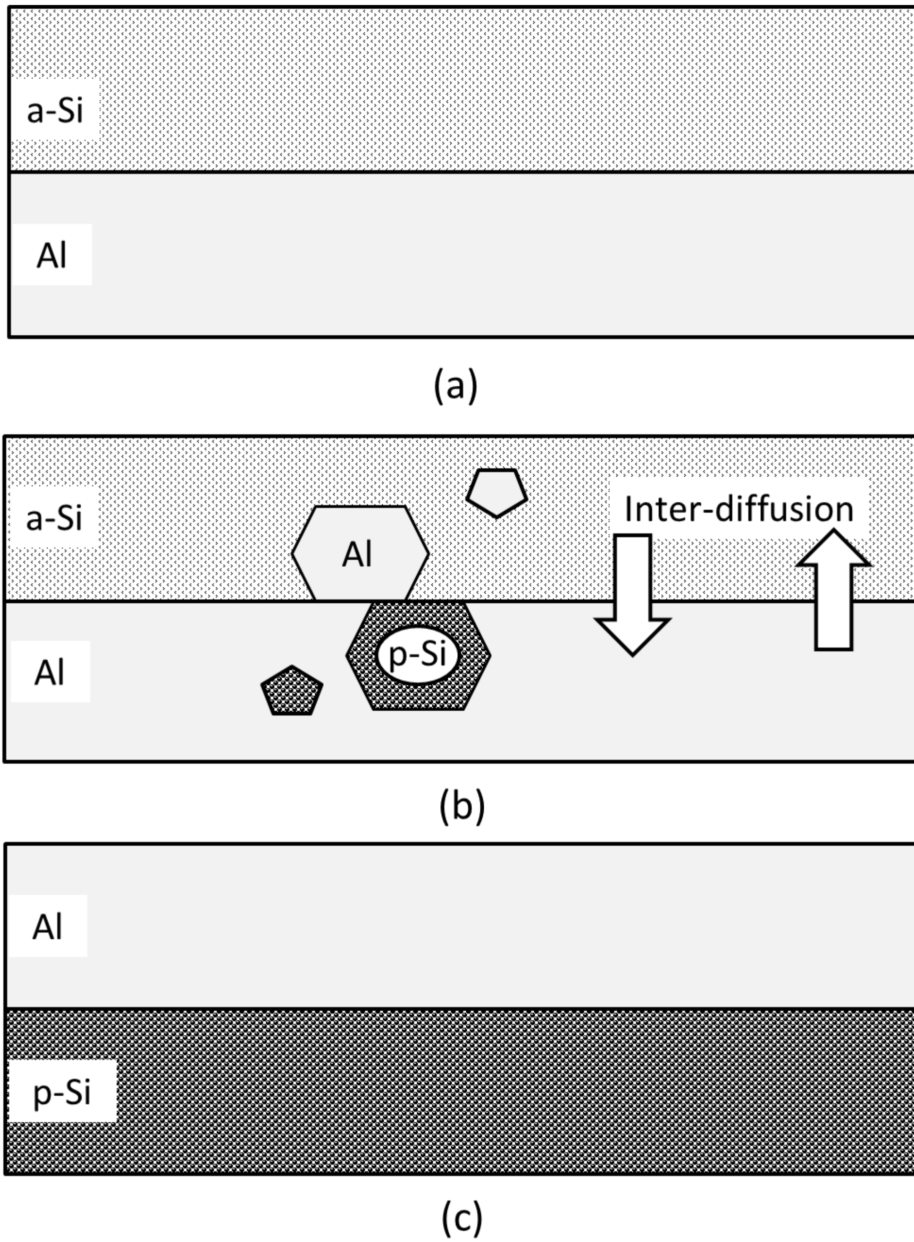

Figure 2-1. Illustration of the diffusion and layer exchange of aluminum induced crystallization process: (a) amorphous silicon and aluminum layer with the same thickness, (b) silicon and aluminum atoms inter-diffused into each other's layer during annealing, (c) Silicon and aluminum layers totally exchange the position and a continuous polysilicon layer is formed under the aluminum after annealing is done.

Polysilicon thin film developed with AIC on polyimide

Flexible polyimide substrate

Among all the flexible materials, polyimide is superior because of its biocompatibility, inertness to chemical etchant to sustain the microfabrication process, high glass transition temperature, which makes it possible to be used for high temperature process otherwise impossible for PMMA, PET.

As temperature of 300 ~ 400 °C needs to be applied for aluminum induced crystallization process, coefficient of thermal expansion (CTE) is another important parameter needs to be considered. In order to minimize thermal stress induced by the mismatch of CTE during annealing, the CTEs of substrate and amorphous / polycrystallized silicon should be as close as possible. While most polyimide have high CTE of ~30 ppm/°C, low stress PI2611 (HD microsystem) has an ultra-low CTE of 3 ppm/°C, which is close to the CTE of amorphous / polycrystallized silicon (2.6 ppm/°C). So, PI2611 was chosen as the material to develop the flexible substrate for polysilicon.

To develop flexible PI2611 film substrate, PI2611 precursor in liquid form (polyamic acid precursors dissolved in an n-methyl-pyrrolidone (NMP) based solvent carrier) was firstly spun on silicon wafer with proper spin-coat speed for desired film thickness. After spin-coating, the wafer was soft-baked at 90 °C and 150 °C for 90 seconds, respectively. Finally, the PI2611 coated wafer was placed in a programmable oven (Blue-M) and cured at 400 °C for 30 minutes in nitrogen gas, with a ramp rate of 4 °C/min to minimize the thermal stress. The curing process

converted the polyamic acid precursor into a fully aromatic, insoluble polyimide film and derived off the NMP solvent carrier. After curing, the adhesion between developed PI2611 film and silicon wafer was examined. Fig. 2-2 (a) shows PI2611 cured on a bare silicon wafer, and (b) shows PI2611 peeled off from the wafer. The adhesion strength was perfect in a way that was strong enough to hold PI2611 film flat during the whole fabrication process and week enough to be easily peeled off after the process.

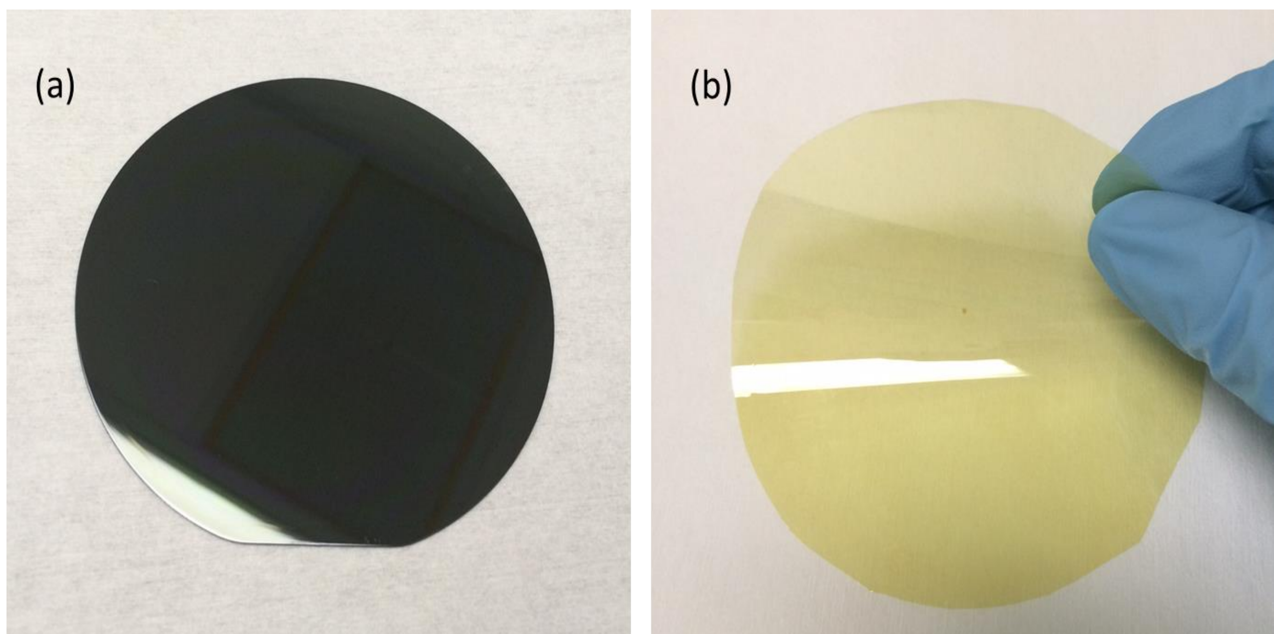

Figure 2-2. (a) Flexible PI2611 film developed on silicon wafer; (b) PI2611 film peeled off from the wafer.

Polysilicon developed on flexible substrate with AIC

After developing PI2611 film substrate on silicon wafer, a 200 nm aluminum thin layer was magnetron sputtered on PI2611, followed by RF sputtering of amorphous silicon thin layer with the same thickness using Denton Discovery 24 Sputtering System.

Since the thickness ratio of amorphous silicon and aluminum layer is critical for developing a continuous polysilicon film, it is necessary to ensure the thickness of sputtered amorphous silicon layer equal to, or a bit thicker than that of aluminum layer. Thickness monitor was used to accurately control the time needed for each layer's sputtering. The sputtered thickness was further measured and verified by profilometer (KLA Tencor P-15) with testing wafers. Photolithography, dry etching of amorphous silicon and profile measurement were done to determine the thickness of amorphous silicon, followed by photolithography, wet etching of aluminum and profile measurement to determine the thickness of aluminum layer. Fig. 2-3 shows the developed patterned for the measurement and the measured thickness of amorphous silicon and aluminum layer with the profilometer.

The sputtering power was adjusted to achieve low surface roughness and proper grain size of the aluminum, as the grain size of the aluminum layer affects the time required for the annealing process as well as the grain size of the formed amorphous polysilicon [74].

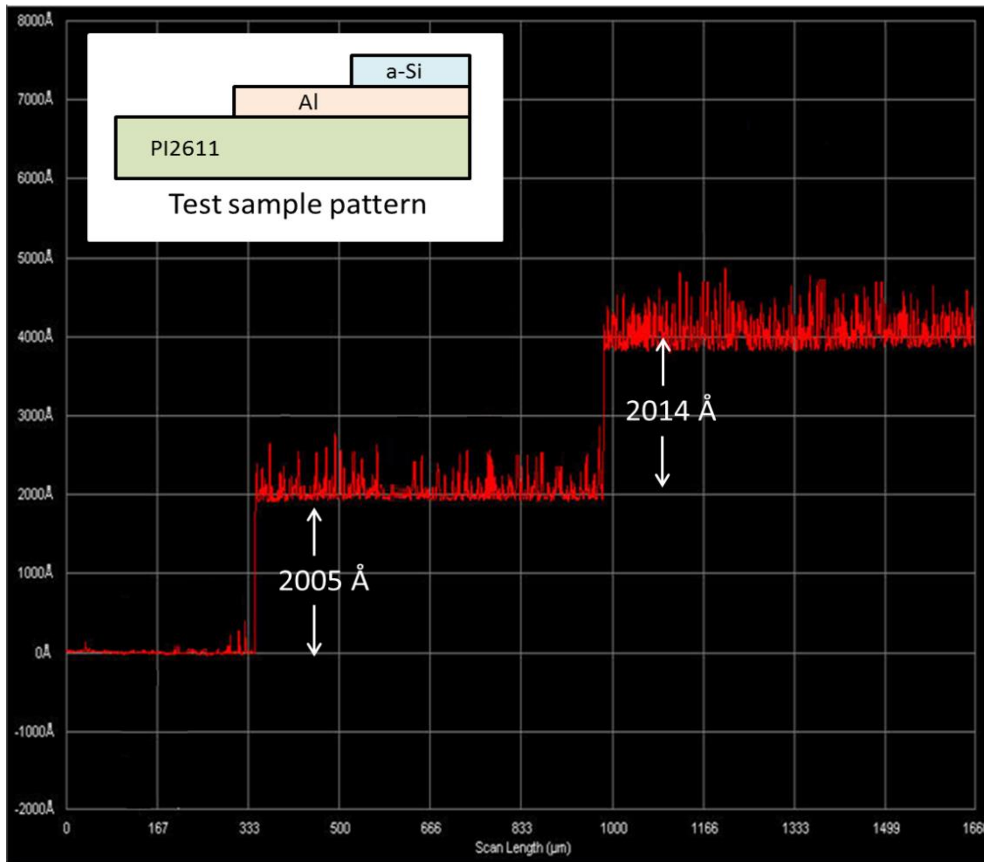

Figure 2-3. Thickness of sputtered amorphous silicon and aluminum layer measured by the profilometer.

After sputtering, the sample was annealed at 400 °C in nitrogen gas for AIC process to happen, with a ramp rate of 4 °C/min to minimize the thermal stress. Fig. 2-4 shows the sample before annealing (a) and after annealing (b). Due to the layer exchange of aluminum and silicon layer induced by AIC process, clear color difference can be seen between the samples. Before annealing, the sample showed the color of amorphous silicon layer; and after annealing, aluminum layer came to top and the sample shows the color of aluminum layer. The formerly-on-top amorphous silicon layer went to bottom and formed polysilicon thin film.

To expose the newly formed polysilicon thin film, the aluminum layer on top was etched away with aluminum etchant at 55 °C. Figure 2-4 shows the polysilicon thin film on PI2611 film coated on silicon wafer (a), peeled off from silicon wafer (b).

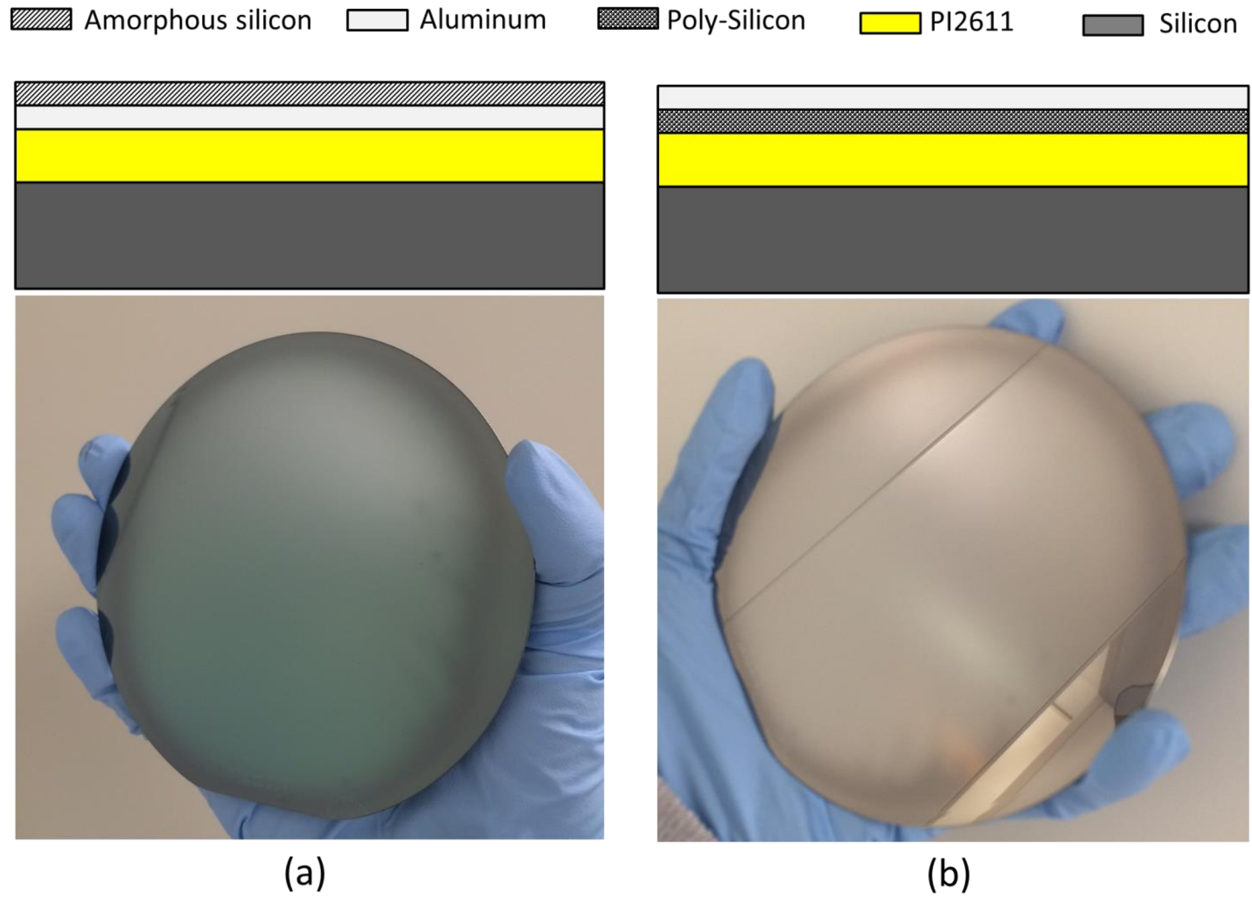

Figure 2-4. (a) Amorphous silicon and aluminum layer sputtered on PI2611 before annealing; (b) The stack layer after annealing. Layer exchange can be clearly seen from the color change.

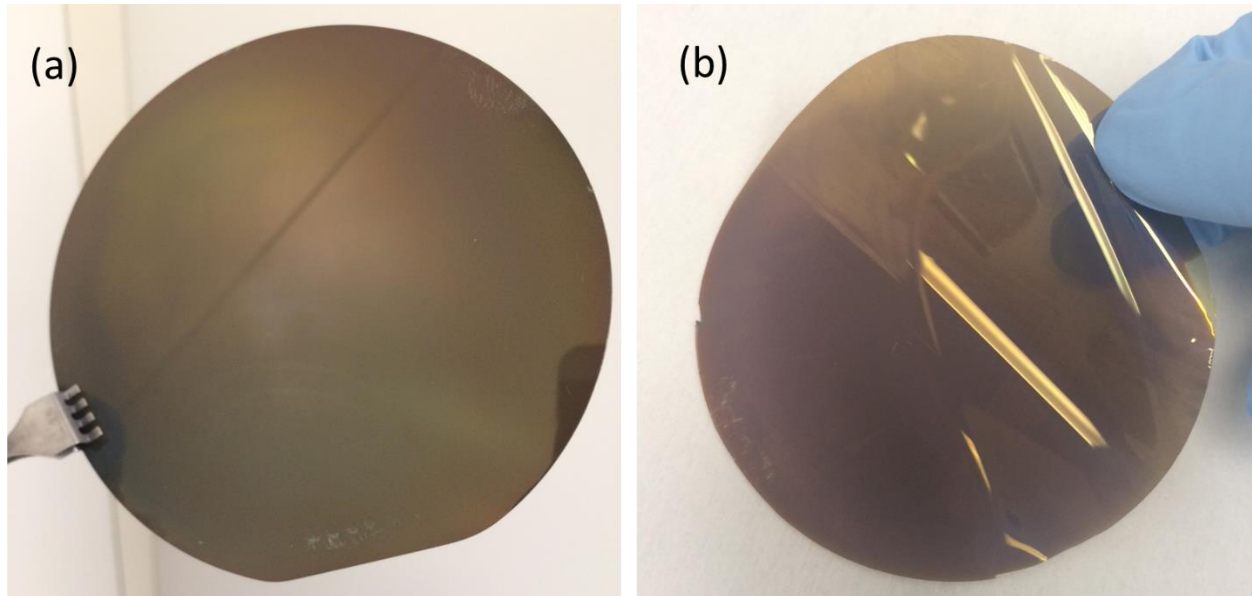

Figure 2-5. Polysilicon film on flexible PI2611 substrate (a) before getting peeled off from silicon wafer, (b) after peeled off from silicon wafer

Polysilicon thin film characterization

X-Ray diffraction (XRD) results

XRD measurements were performed using X'Pert Pro MPD system (PANalytical) to verify the crystallization of polysilicon. The samples annealed for 1, 2 and 3 hours were tested and the results are shown in Fig. 2-6. As shown in the figure, peaks appear at 2θ = 28.5°<111> and 47.3°<220> for all three samples of polysilicon thin film developed on PI2611 substrate, which proves the crystallization of silicon film. Furthermore, there is no obvious difference between the heights and widths of peaks, which represent the crystallization level. Thus, the crystallization process might be completed within 1 hour.

The crystallite size can be estimated from the high resolution X-ray diffraction data using the Scherrer relation[75] as:

$$B = 0.9\lambda/t\cos\theta, \quad (1)$$

where B is the full width at half maximum (FWHM), λ is the X-ray wavelength, and t is the diameter of the crystal. Peak <111> was considered for estimating the grain size of the polysilicon film. With FWHM of 0.144 °, the average size of the crystals of polysilicon film was about 49 nm.

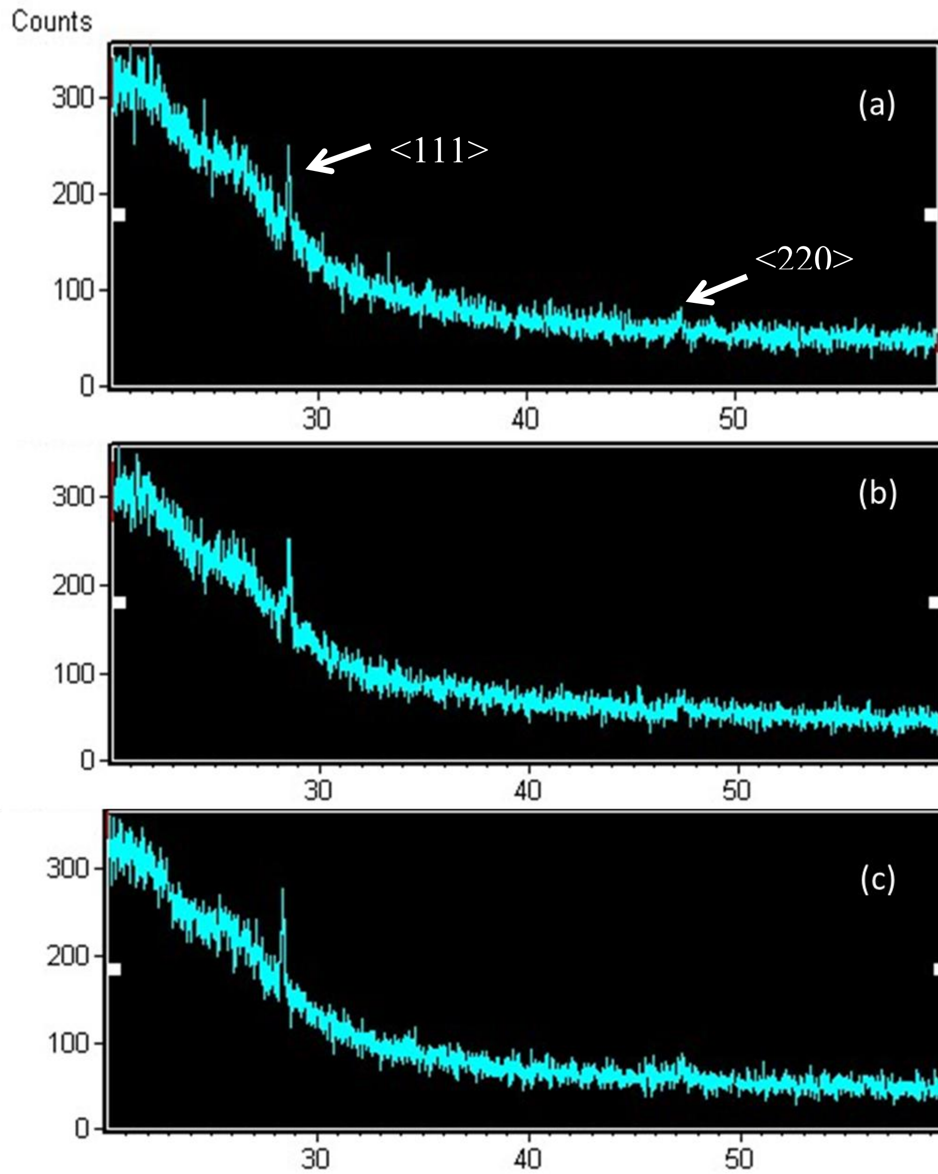

Figure 2-6. XRD results for samples annealed for 1(a), 2(b) and 3(c) hours: the peaks appear at 2θ = 28.5°<111> and 47.3°<220> for all three samples of polysilicon thin film developed on PI2611 substrate.

TEM results

To further inspect the extent of crystallization and conform that crystallization was completed within 1 hour, TEM measurement was performed with a FEI CM20 TEM system. To prepare the sample for measurement, polysilicon film developed on PI2611 substrate was first immersed in concentrated HF acid to lift the polysilicon film off of the substrate. The lifted polysilicon film was then immersed in DI water to wash away HF acid. Finally, the film was carefully transferred onto a copper grid and dried naturally in air. Fig.2-7 shows the TEM results.

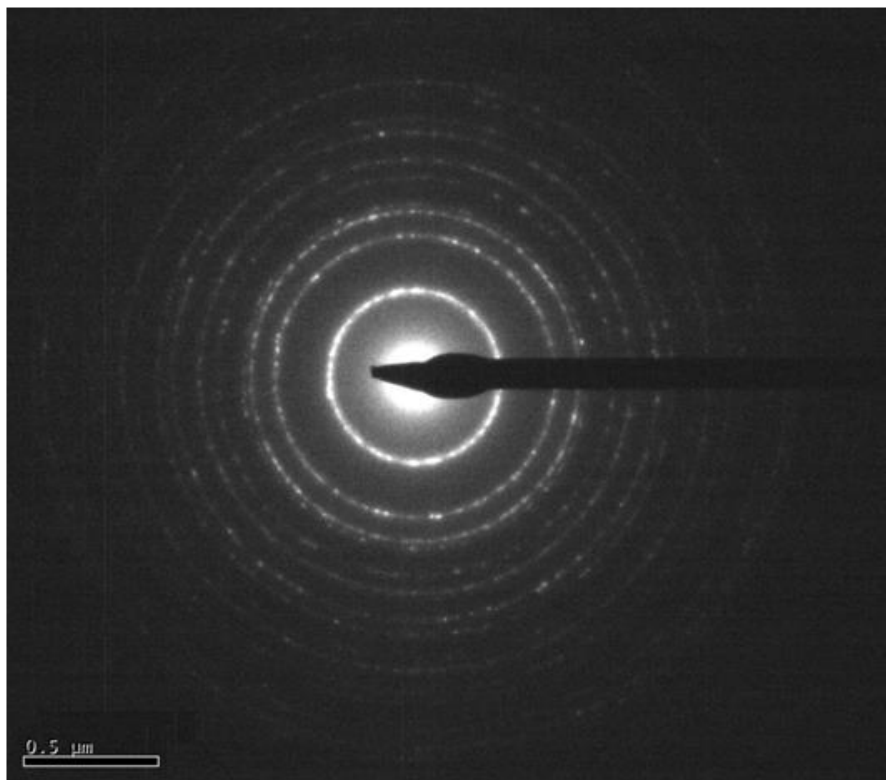

Figure 2-7. TEM result shows the fully polycrystalline characterization of polysilicon film.

The picture is void of any cloudy areas that would reflect amorphous character. Instead, clear circles formed by independent dots, which represent polycrystalline nature, are observed.

SEM results

Fig.2-8 is the SEM picture of surface morphology of the developed polysilicon film (using FEI XL30 ESEM). As shown in the picture, a continuous polysilicon film has been successfully attained.

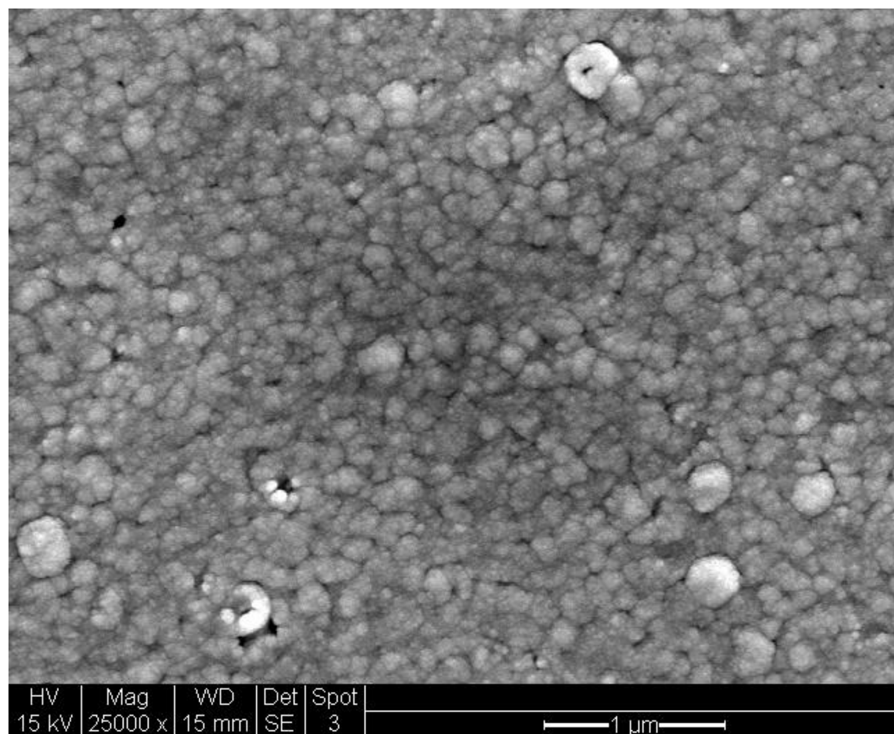

Figure 2-8. SEM picture showing the continuous and dense microcrystals of developed polysilicon film.

EDS results

To examine whether aluminum atoms were embedded in the formed polysilicon film, the polysilicon film was examined with energy dispersive spectroscopy (EDS) and the result is shown in Fig. 2-9. As shown in the figure, the film has aluminum and silicon content with the At. % (atom) ratio of 2.75 %: 97.25 %. This analysis confirms that a small amount of aluminum was embedded in the final crystallized film and could possibly act as a p-type dopant in the polysilicon film.

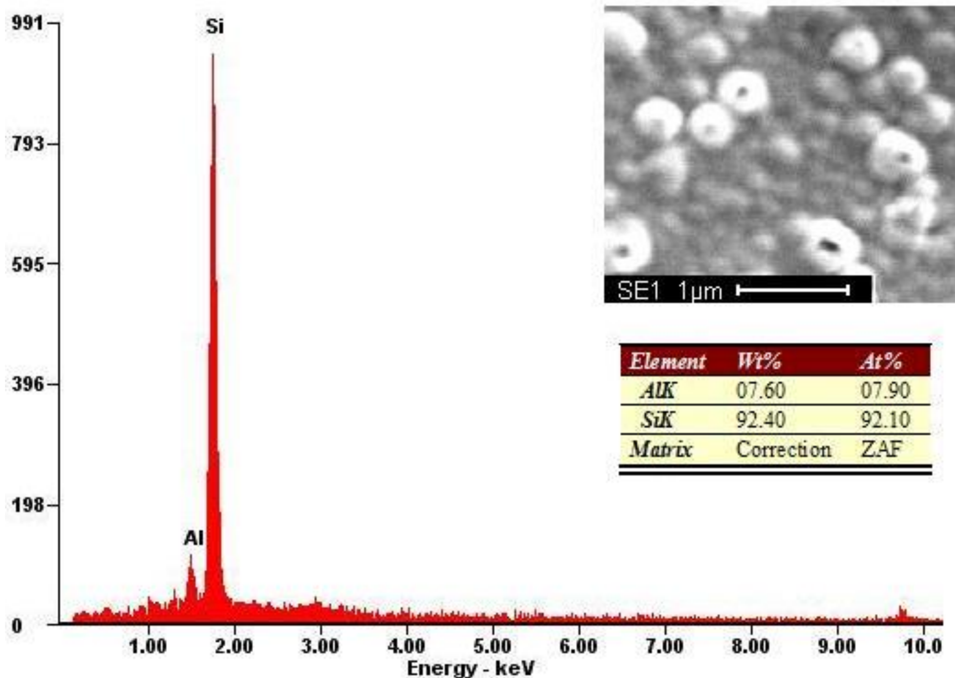

Element	Wt%	At%
AlK	07.60	07.90
SiK	92.40	92.10
Matrix	Correction	ZAF

Figure 2-9. EDS results showing the embedding of Al atoms in the formed polysilicon film: the weight ratio between Al and Si is 7.6%:92.4%; and atom number ratio is 7.9%: 92.1%.

Sheet resistance measurement

Sheet resistance of the developed polysilicon thin film was measured based on the transfer length method (TLM) [76]. AS shown in Fig. 2-10, the resistance of each polysilicon resistor can be expressed by Equation (2).

$$R_{total} = R_{\square} \cdot L/W + 2R_{C,} \quad (2)$$

where R□ is the sheet resistance of polysilicon film, L is the length of the resistor, W is the width of the resistor, and R_C is the contact resistance between polysilicon and aluminum. In the limit of a zero-length resistor, the residual resistance would be just twice the contact resistance.

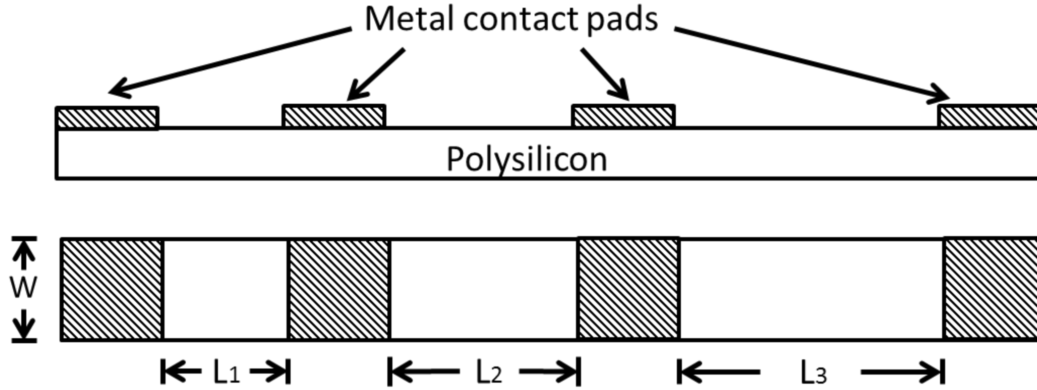

Figure 2-10. Designed polysilicon pattern for sheet resistance measurement based on TLM.

The polysilicon resistor pattern was developed by standard photolithography and wet etching the polysilicon thin film with polysilicon etchant (Hydrofluoric acid (HF) : Nitric acid (HNO_3) : DI water = 5 : 30 : 100). A 250 nm aluminum layer was then evaporated, followed by photolithography and wet etching with aluminum etchant to develop aluminum contact pads and electrical leads for polysilicon resistors. Another PI2611 passivation layer was coated on top and annealed. The annealing process was also aiming to generate ohmic-contact between aluminum leads and polysilicon resistors. The developed pattern for testing is shown in Fig. 2-11.

As shown in Fig. 2-11 (b), the length/width ratios of resistors are 0.7 (between contact pad 1&2), 1.7 (2&3), and 2.7 (3&4), respectively. The contact type was first investigated by sweeping voltage from -20 mV to 20 mV and measuring the output current. The linear I-V curve in Fig. 2-12 shows that the contact between polysilicon and aluminum is Ohmic.

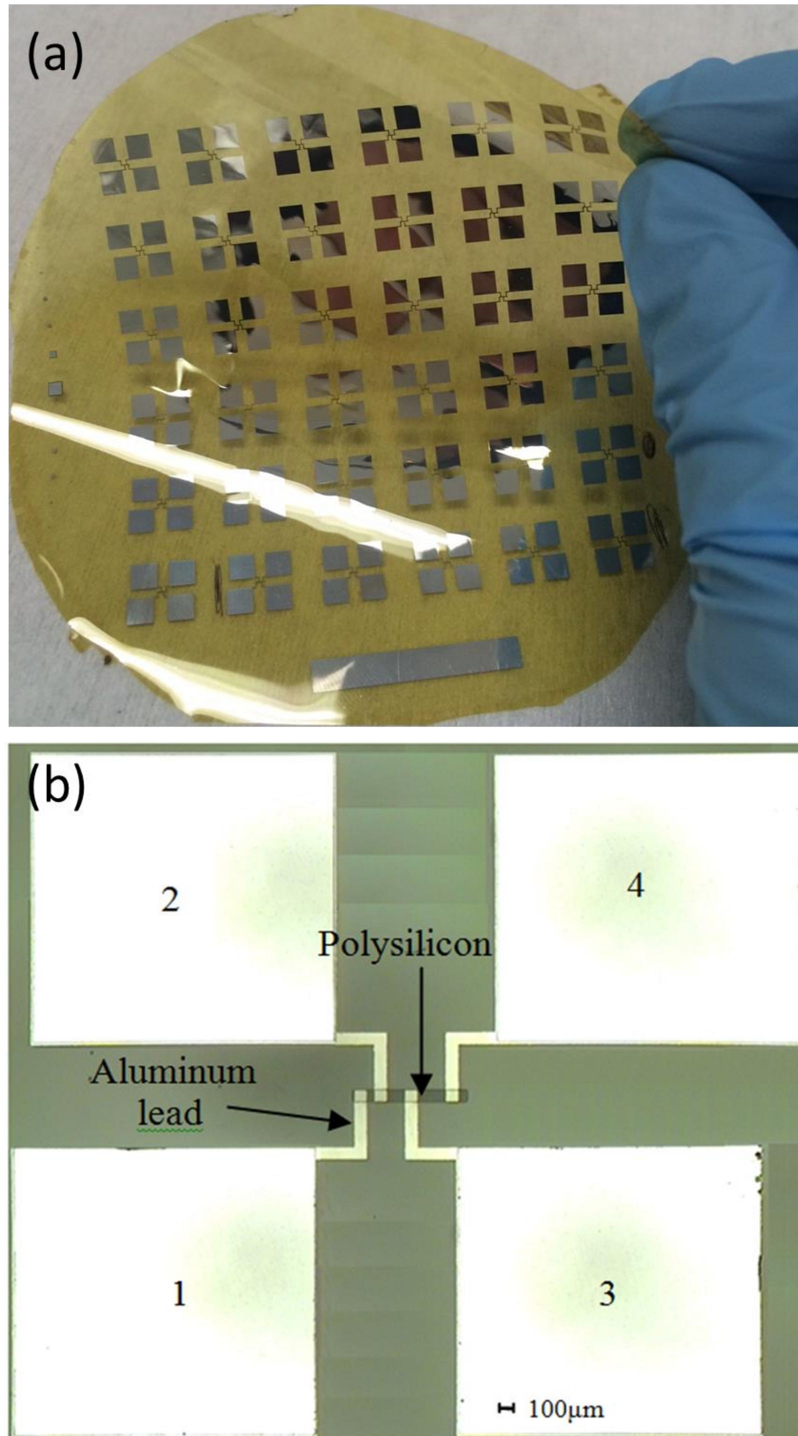

Figure 2-11. Developed pattern for measuring sheet resistance of polysilicon thin film and the contact resistance (a) on PI2611film peeled off from silicon wafer and (b) under microscope.

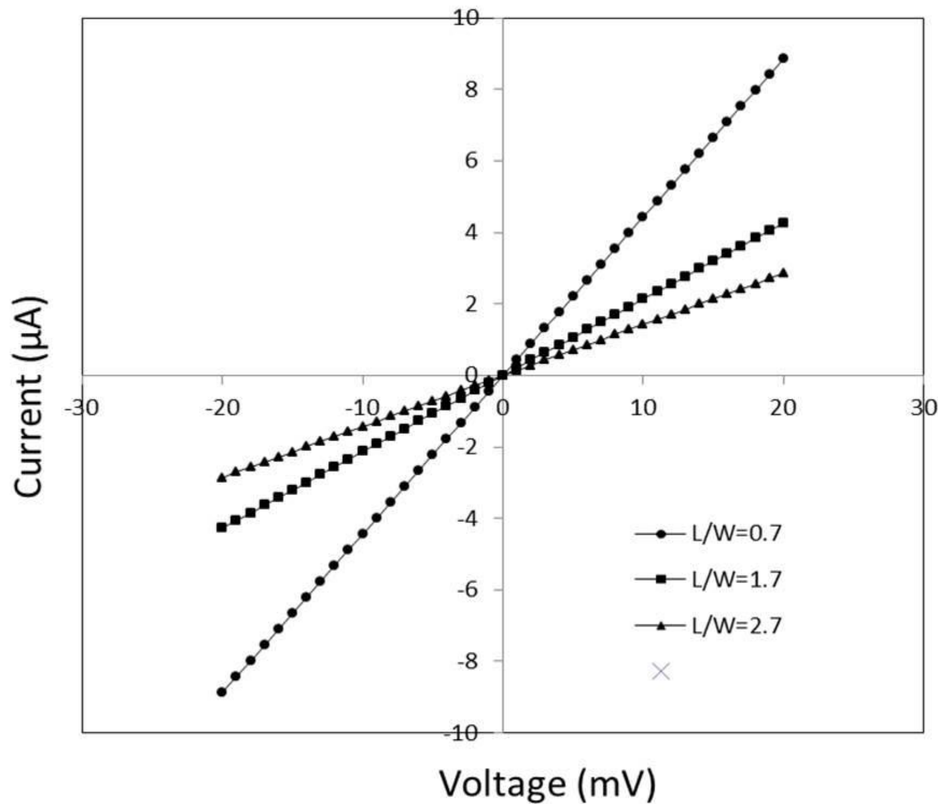

Figure 2-12. Linear I-V curve shows the contact between polysilicon and aluminum is Ohmic-contact.

The resistance R_{total} measured from the I-V curve is plotted versus length and width ratio (L/W) and shown in Fig. 2-13. As shown in the figure, resistance increases linearly with the length/width ratio. The fitted line with Equation 2 shows R_{total}= 2.46 L/W + 0.50, which means the sheet resistance of the developed polysilicon film is 2.46 KΩ, and the contact resistance between polysilicon and aluminum is 250 Ω. Compared to other works[77, 78], the contact

resistance obtained here is relatively large due to the low annealing temperature we used to form the ohmic-contact. However, it is still small compared to the resistance of the developed polysilicon resistor.

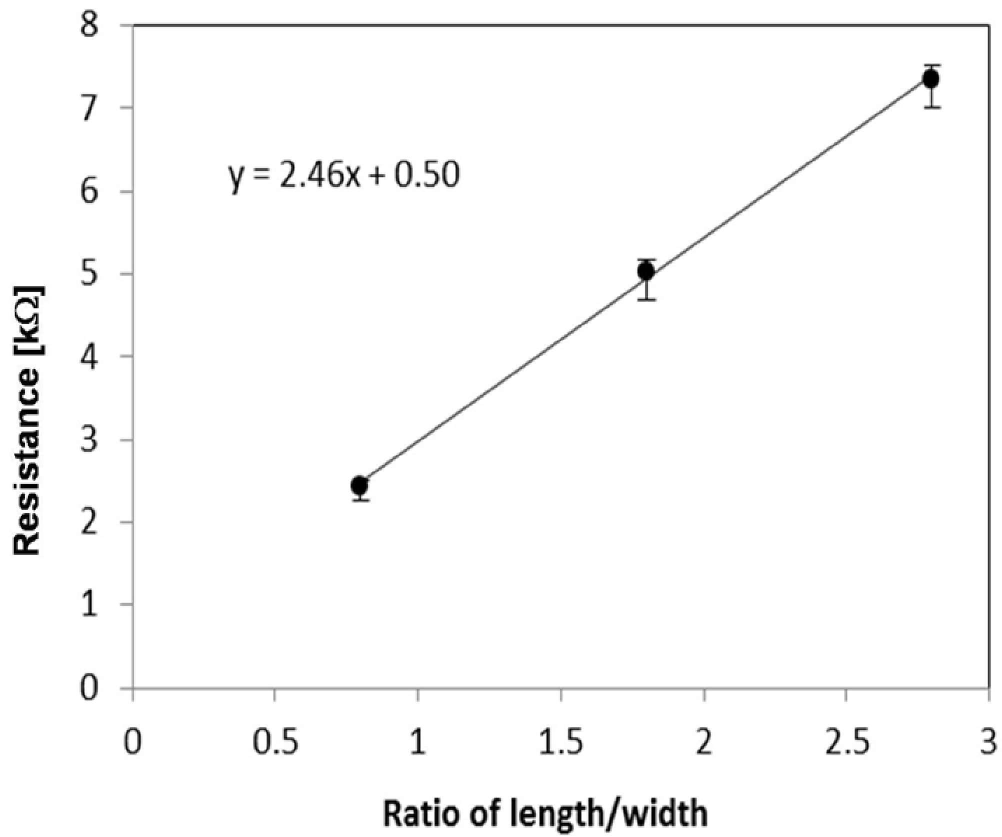

Figure 2-13. Resistance change with length/width ratio of resistor.

Summary

A high quality polysilicon thin film with the thickness of 200 nm has been successfully developed on flexible PI2611 substrate with aluminum induced crystallization (AIC). The polycrystalline structure of the film was verified with XRD measurements. The results showed the main crystallization direction of <111> and <220>, and the crystals' average size of 49 nm. TEM measurement showed a full crystallization of polysilicon film annealed at 400 °C for 1 hour. SEM results showed a high quality continuous polysilicon film without any void. EDS showed the polysilicon thin film had embedded aluminum atoms with atom percentage of 2.75%. Further sheet resistance measurement of the polysilicon thin film with transfer length method (TLM) showed a sheet resistance of 2.45 kΩ. It proved that the embedded aluminum atoms acted as P-type dopant for the polysilicon film and the doping concentration was about $\sim 10^{19}$. Therefore, high temperature doping process which damages the flexible substrate can also be avoided when developing electrical devices with the polysilicon film.

The work shows that high quality polysilicon thin film can be directly developed on flexible substrate with ultra-simple, low cost, and fast process. With the wafer-size based high yield and uniformity, the developed polysilicon thin film shows a great potential for developing manufactural polysilicon-based flexible devices.

CHAPTER 3

POLYSILICON BASED FLEXIBLE TEMPERATURE SENSOR

Introduction

Brain temperature reflects the balance of neural metabolic heat production, cerebral blood flow and the temperature of incoming arterial blood [79-81]. Studies have shown the temperature inside brain is not homogeneous. In humans, the temperatures around the center of the brain are 0.5 ~ 1 °C higher than those of the epidural space[82]. For the injured brain, the temperature variation throughout brain or between viable tissue and regions of ischemia become more evident. Schwab et al[83] showed that temperature in the ventricles exceeded epidural temperature by up to 2.0 °C for patients with severe middle cerebral artery (MCA) infarction. Marshall[84] also observed higher temperatures in ischemic brain regions compared to normal brain. Despite these studies, a systematic investigation of temperature variation across the injured human brain is still needed. An accurate and high spatial resolution method to monitor the brain, characterizing temperature at the level of local microvasculature and functional cell groups, would aid in understanding pathological processes developing in the injured brain. Furthermore, it is known that the injured brain is extremely sensitive and vulnerable to small temperature variations. Thus,

in order to improve temperature control and treatment of the injured brain using focal brain thermotherapy[85, 86], accurate measurement of the temperature profile is required.

Currently, ultrasound thermometry, microwave radiometry and magnetic resonance thermometry[87-90] are usually used for non-invasive brain temperature monitoring. However, these approaches always suffer from low temporal and spatial resolution. Advanced Proton chemical shift imaging (CSI) sequences in MR thermometry was shown to measure temperature distributions with one minute and a low spatial resolution of 3-4 mm[91]. Furthermore, artifacts can be induced by different composition of tissue, tissue motion, and external filed drift[92]. Thrippleton et al[93] reported a discrepancy of 0.7 °C between the temperature measured with MR and the absolute temperature measured by a fiber-optic method. Marshall et al.[84] performed a MRSI validation study at 1.5 T, finding a standard deviation of 1.2 °C through the repeating measurements on individual voxels which is inaccurate for reliable brain activity monitoring.

In order to obtain accurate and real-time temperature information, various implantable temperature sensors and probes have been developed using the principles of optical fiber[92], resistance temperature detector (RTD)[93], thermocouple[94, 95,] and thermistor[96, 97]. However, temperature arrays, which can directly measure the brain spatial temperature variation, are scarcely available and technologically challenging. Optical fibers are difficult to be integrated into a single platform, and multiple fibers/needles are needed for thermal mapping which will largely increase the damage caused by fiber insertion[98]. Metal based RTDs measure the resistance changes with temperature with high accuracy and repeatability and multiple RTDs can be easily integrated on one platform. However, due to its large pattern size, the RTD lacks the capacity to measure temperature with high spatial resolution. Thermocouple measures temperature-dependent voltage generated at the junction of two distinct metal wires due to

thermoelectric effect, but the thin film based thermocouples always suffer from measurement error due to their low junction voltage[99].

On the other hand, thermistors with semiconducting materials such as amorphous germanium[100], amorphous silicon[101], and vanadium oxide[102] have a large variation of resistance and a high sensitivity to temperature change, and thus are a good candidate for a brain temperature sensing array with high spatial and temporal resolution. Kuttner et al[100] developed amorphous germanium thermistor arrays on glass substrate with a sensitive area of 0.014 mm^2 each and an inter distances of 0.4 mm for the investigation of biological temperature fields. Billard et al[102] developed a vanadium oxide thermistor array on glass for localized temperature field measurements in brain. The developed thermistor arrays showed a high sensitivity of 0.2 ~ 0.4 %/°C of temperature. Nonetheless, both of the works developed thermistor arrays on rigid glass substrate with high mechanical stiffness. Cerebral monitoring, however, prefers flexible platform that can be inserted into the brain with minimal tissue damage.

In this work, we have developed a polysilicon thermistor array on flexible polyimide substrate with structural flexibility for brain temperature monitoring. Polysilicon thin film has been utilized as the sensing material for thermistors for a long time[103-106]. The temperature coefficient of resistance (TCR) of polysilicon can be selected over a wide range, both positive and negative, through developing temperature and selective doping[105]. To develop polysilicon on flexible polyimide substrate, polysilicon thin film in this work was formed using aluminum induced crystallization (AIC) process as described in our previous work[107]. Polysilicon thermistors have been developed with the dimensions of 20 μm × 160 μm and 200 μm ×160 μm. *In vitro* tests of the sensor for the sensitivity, response time, thermal hysteresis, resolution, and long term stability have been successfully performed. In addition, *in vivo* tests of the sensor have

also been performed to determine noise levels and assess performance in measuring temperature responses to pathophysiologic processes.

Sensor design and fabrication

Sensor design

Four polysilicon thermistors and two electrocorticography (ECoG) electrodes were designed on a flexible polyimide substrate as shown in Fig. 3-1 Two polysilicon thermistor elements with the dimension of 20 μm ×160 μm were designed with the inter-distance of 450 μm. To compare performance, another two polysilicon thermistors with dimension of 200 μm ×160 μm were also added. The four polysilicon thermistors formed a sensing array for temperature measurement. Two ECoG electrodes with a radius of 25 μm were placed along the thermistor elements to measure associations between neural activity and local temperature. The lateral distance between ECoG electrodes and polysilicon resistors was set as 1mm.

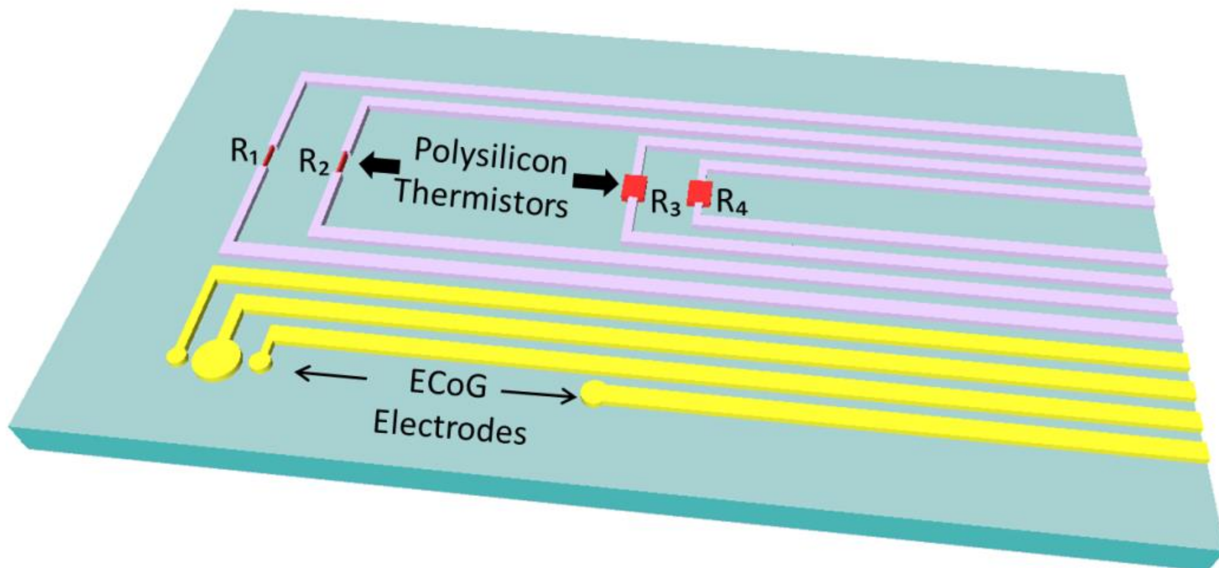

Figure 3-1. Concept and device design: polysilicon thermistors array with four sensing elements (R_1 & R_2: 20 μm ×160 μm, R_3 & R_4: 200 μm ×160 μm), ECoG microelectrodes are placed along for in vivo test of association between ECoG depolarization signal and local temperature change under stimulus.

Silicon nitride sputtering

High water and oxygen absorption or permeation of polyimide can limit the applications of polyimide based devices in water or air with high humidity[108], especially for BioMEMS applications in an aqueous environment (e.g. brain). The water absorption and oxygen permeation can cause drift or instability of the sensing signal throughout the measurement duration. Thus, an additional passivation layer is necessary to prevent or decrease the moisture and oxygen diffusion. Thin films such as aluminum oxide (Al_2O_3), silicon oxide (SiO_2) or

silicon nitride (SiN_X) have been deposited on the polyimide substrate to reduce the diffusion of water or humidity[109-112].

Here we used silicon nitride (SiN_X) film with the thickness of 100 nm as the passivation layer. The coefficient of thermal expansion (CTE) of silicon nitride thin film (3.3 ppm/ °C) is very close to that of polyimide substrate PI2611 (3 ppm/ °C), thus the stress induced by mismatch of thermal expansion under temperature change can be minimized. A thin film with the thickness of 100 nm was chosen to minimize its effect of mechanical strength and stiffness to PI2611 substrate. Silicon nitride film was RF sputtered on the polyimide film by Denton Discovery 24 Sputtering System with a silicon wafer as target and mixed gas of argon and nitrogen as the environmental and reactive gas. Optimized sputtering conditions with the distance between target and substrate of 2 inch, base pressure of 10^{-7} pa, sputtering power of 200 W, and nitrogen-to -argon ratio of 2:1 were used to obtain a dense silicon nitride film which can effectively block the moisture or oxygen.

Sputtered silicon nitride film was etched in buffered HF to test the density. The film can be considered as an effective passive layer only if the etching rate is less than 10 nm/min. The etching rate in buffered HF of sputtered silicon nitride film in this work was less than 6 nm/min.

Fig. 3-2 shows the SEM picture of silicon nitride layer sputtered on PI2611 substrate. The interface of sputtered silicon nitride layer and PI2611 is clearly shown in the figure. For the test sample, 200 nm thick silicon nitride thin film was sputtered. Then SEM result shows the same thickness as expected.

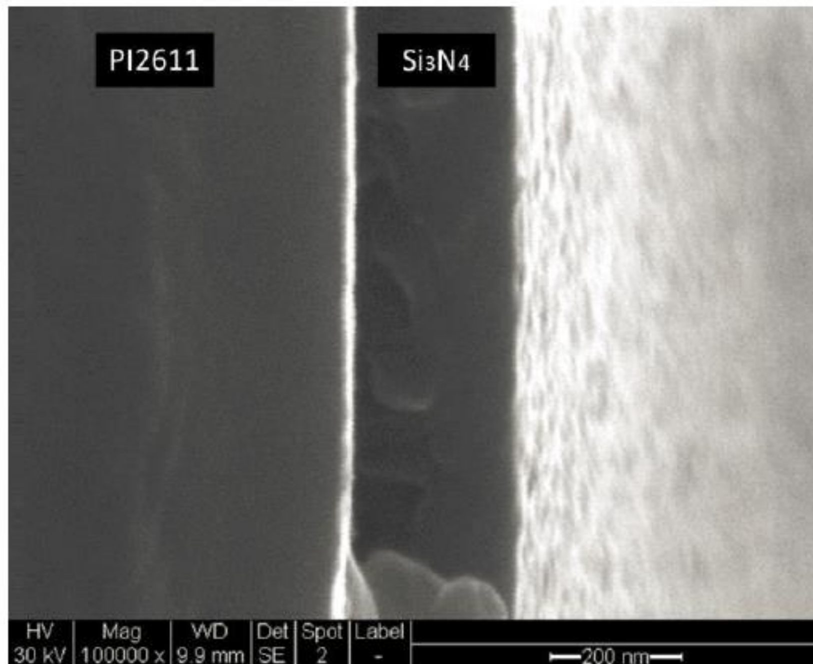

Figure 3-2. SEM picture of silicon nitride layer sputtered on PI2611 substrate, showing a clear interface between PI2611 and silicon nitride.

To further verify the element constitution of silicon nitride layer, EDS analysis was carried out and the results showed reasonable constitution of Si and N element in the film. Fig. 3-3 shows the EDS results for both PI2611 substrate and sputtered silicon nitride layer. The high peak of carbon at PI2611 on the substrate side clearly shows the constitution of carbon-rich PI2611. The high peaks of Si and N element at silicon nitride layer side show the constitution of Si and N element of the silicon nitride layer.

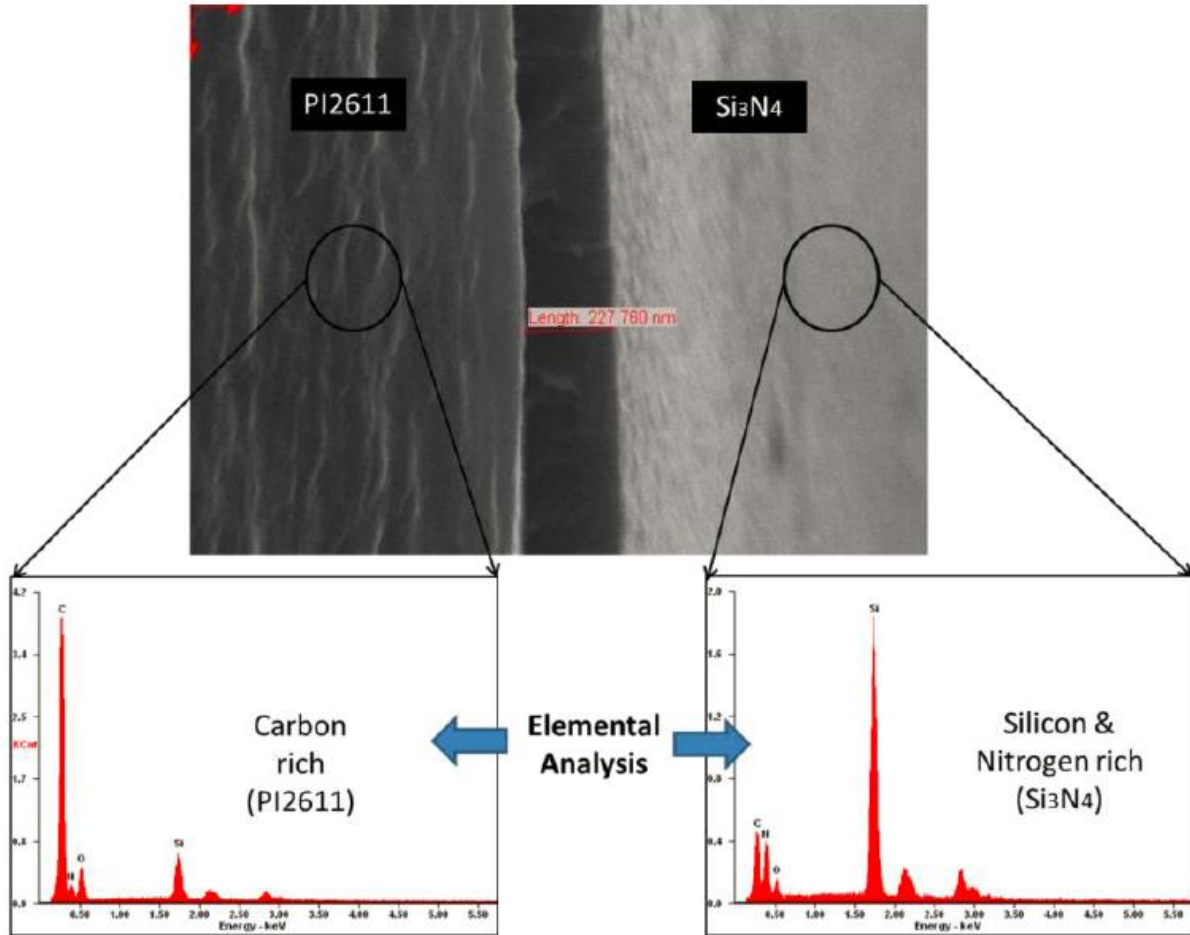

Figure 3-3. EDS analysis of silicon nitride layer and PI2611 substrate.

Microfabrication process

A summary of the microfabrication process is described in Fig. 3-4. After obtaining the 200 nm thick polysilicon film on a 7 µm thick PI2611 substrate with AIC, polysilicon thin film was patterned to form a resistor with the standard photolithography process, followed by the development of e electrical leads with 250 nm aluminum evaporation and etching. 12 nm/120 nm Ti/Au film was then deposited and patterned to form the ECoG pattern. Another 7 µm thick

PI2611 layer was coated on top of the fabricated metal and polysilicon patterns. Then, a 100 nm thickness of silicon nitride layer was sputtered on the top of the PI2611 layer as the final passivation layer.

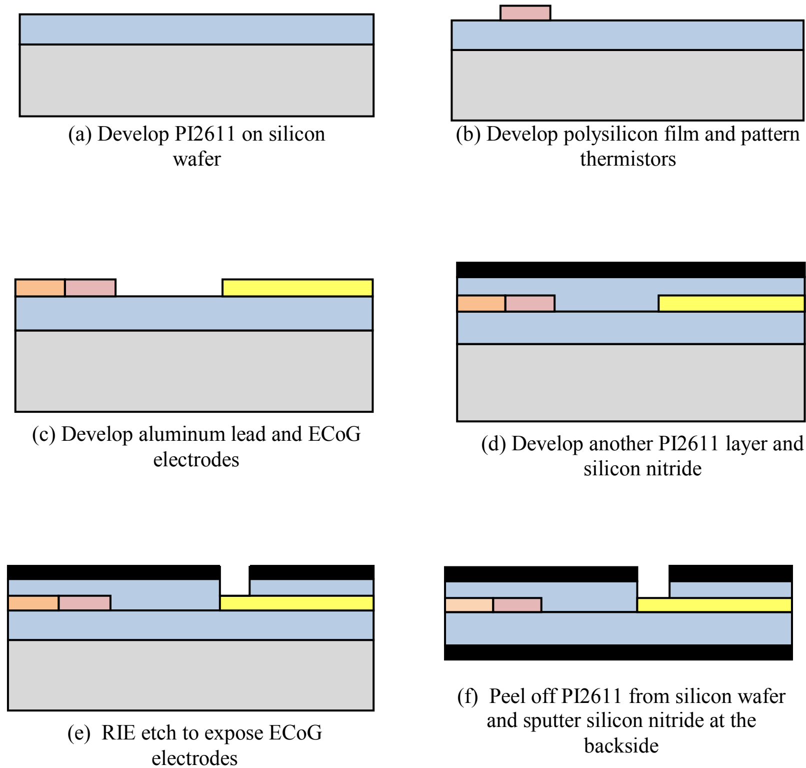

Figure 3-4. Summary of the microfabrication process.

To expose the ECoG pattern and contact pads, dry etching with CF_4 and O_2 plasma was performed to etch away both PI2611 and the passivation layer of silicon nitride. Finally the device was peeled off from the silicon wafer and a 100 nm thick silicon nitride layer was sputtered on the backside of the device. So both front side and backside of the device were protected with the passivation layer. In addition, with silicon nitride film at both sides of the device, the possible residual stress in silicon nitride film can be balanced.

The device was laser cut (Oxford lasers) into a desired size and bonded with connectors using silver paste. Epoxy was applied to further strengthen the contact between the connector and the contact pads. Pt nanoparticles (NP) were electrochemically deposited on ECoG electrodes with optimized roughness factor and iridium oxide was electrodeposited to form heterostructured ECoG electrodes. The impedance of ECoG electrodes was characterized by performing electrochemical impedance spectroscopy (EIS) based on the procedures described in our previous paper[109]. The average impedances of Pt/IrOx electrodes are 4.72 ± 1.06 kΩ (n=6) at 1 kHz. Fig. 3-5 shows the fabricated device and pattern under a microscope.

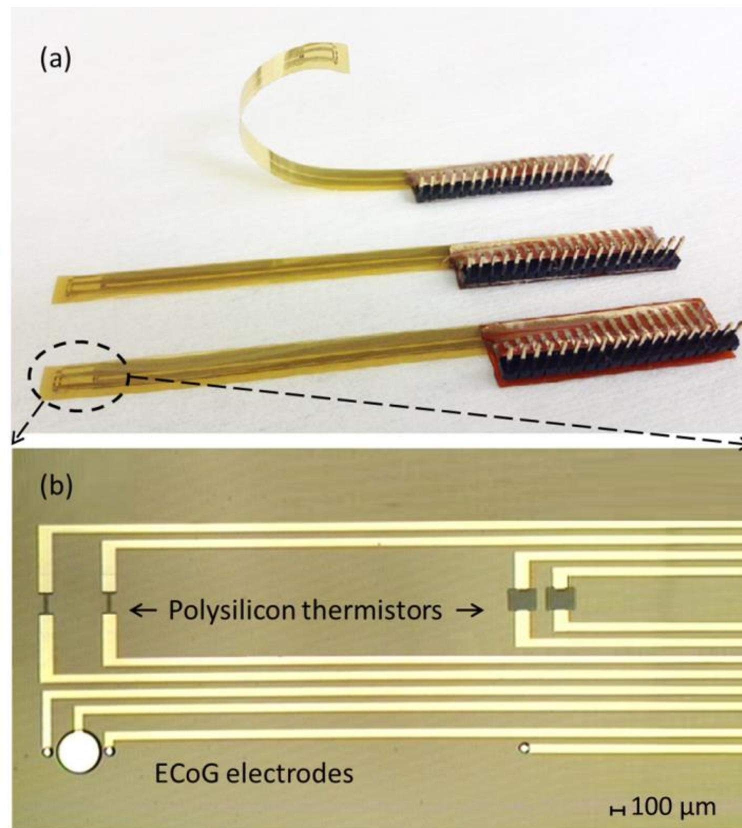

Figure 3-5. Polysilicon-based temperature sensors array: (a) developed flexible devices and (b) sensor pattern under microscope.

Thermal Simulation

Polyimide has numerous advantages as a flexible substrate for biomedical applications. However, it has poor heat dissipation with very low thermal conductivity (0. 52 W/ (K*m)) compared to traditional silicon substrate (155 W/ (K*m)). For biomedical devices, a passivation layer is also needed to prevent contamination from the outer environment, which further deters heat dissipation. For sensors developed with polysilicon film on polyimide substrate, if the driving current of the sensor is high enough to produce an obvious temperature increase, it can introduce large errors in the sensor and also instability in performance during long term application. Thus, it is necessary to characterize the device's temperature profile with the driving current and ensure that the current does not cause temperature increases due to self-heating.

To investigate the temperature profile and determine the proper input, COMSOL Multiphysics 4.4 was used to simulate the temperature profile with different current inputs. A device configuration of the polysilicon pattern sandwiched by two 7 μm-thick polyimide films at the top and bottom was used for simulation. The dimensions of the polysilicon pattern and aluminum lead used for simulation were the same as the design presented above. Table 1 shows the thermal conductivity at room temperature for the materials used in the simulation.

The "Heat transfer in solid" module was used for the boundary conditions between the aluminum electrical lead, polysilicon pattern, and PI2611 substrate. Heat flux convection was used for the boundary condition between PI2611 substrate and the air. DC input currents with

amplitude ranging from 5 to 100 μA were simulated. Temperatures of the polysilicon device with varying input currents are shown in Fig. 3-6.

Table 1. Thermal conductivity at room temperature for the materials used in the simulation.

	K (W/ (k*m))
PI2611	0.104
Polysilicon	155
Aluminum	238

As shown in Fig.3-6, the device was heated up to 323.00 K (ambient temperature: 293.15 K) with 100 μA after 10 minutes, while an input current of 5μA reached only 293.15 K without obvious self-heating. In the latter case, any temperature increase is clearly smaller than the required resolution of biomedical temperature sensing of 0.1 °C.

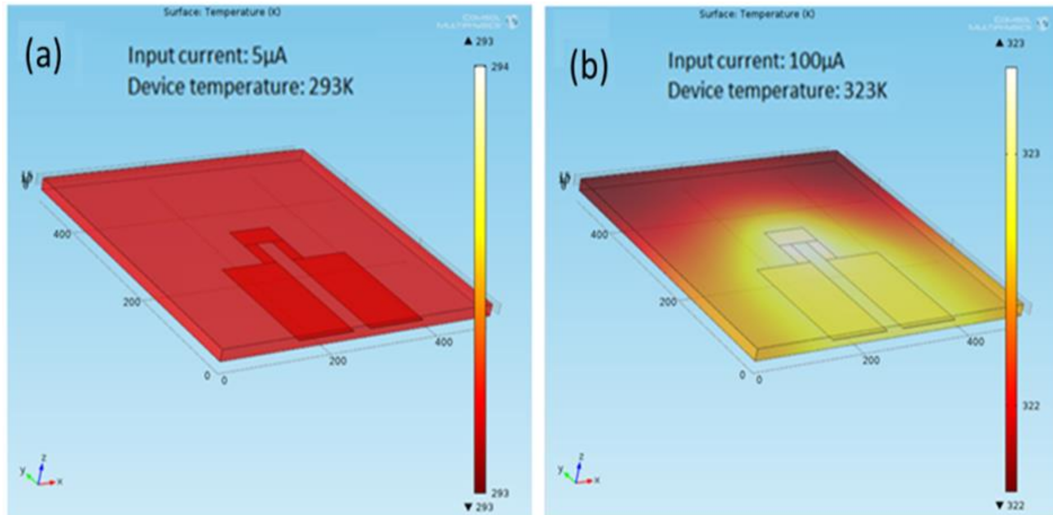

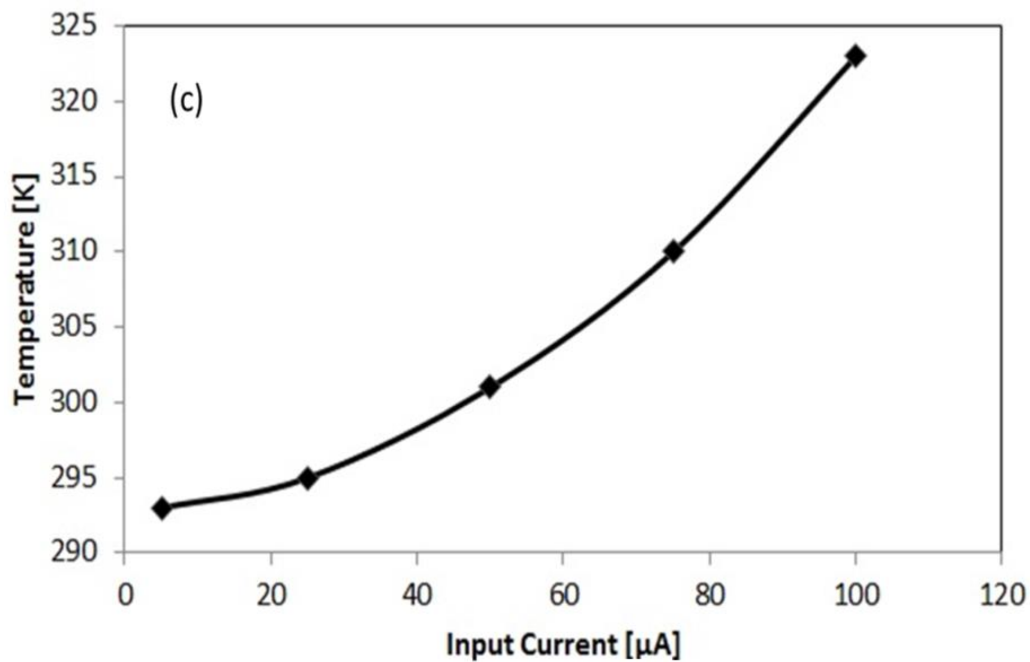

Figure 3-6. Temperature profile of the device with (a) 100 μA after 10 minutes shows an elevated temperature of the device of 323.00 K with environmental temperature of 293.15 K (room temperature); (b) 5 μA after 10 minutes shows the temperature of device of 293.15 K without obvious self-heating and (c) device temperature change with different input currents.

In vitro measurement

The developed flexible temperature sensor with polysilicon thermistor array was fully characterized in water for its sensitivity, response time, thermal hysteresis, resolution, and long term stability. The temperature sensor was submersed (submerging depth: 3 cm) in a water bath (1 liter) on a hot plate (Cole Parmer Series 04644). A high accuracy biomedical temperature probe (WPI® BAT-21) was attached to the temperature sensor and used to monitor the temperature in real-time. The probe tip and the polysilicon thermistor were positioned at the same height during the test to ensure they were exposed to the same environment. Polysilicon thermistor's resistance was measured by a digital multimeter (Agilent 34461A). Resistance and temperature data were acquired using Labview.

Sensitivity

The sensitivity of the polysilicon thermistor was obtained by measuring the sensing element's resistance variation while changing the environmental temperature. Temperature ranging from room temperature (~21 °C) to 60 °C was attained by increasing the hot plate's temperature with a ramping rate of 60 °C/hour. Four polysilicon elements for each dimension were tested. The resistance change with standard deviation (SD) is shown in Fig. 3-7. Polysilicon thermistors' resistance decreases with temperature in a linear fashion. For R_1 & R_2 with the dimension of 20 µm × 160 µm and resistance of 36.5 ± 0.3 kΩ, the sensitivity is -0.0031/°C (SD: 10^{-4}), while for R_3 & R_4 with the dimension of 200 µm × 160 µm and resistance

of 3.7± 0.2 kΩ , the sensitivity is -0.0025/°C (SD: 1.4 × 10^{-4}). Though the sensitivity of the developed polysilicon is about ten-orders lower than other thermistor materials such as amorphous germanium and silicon, it is comparable with gold-based RTD [15] that we previously developed for the brain temperature sensing and is sensitive enough for brain monitoring.

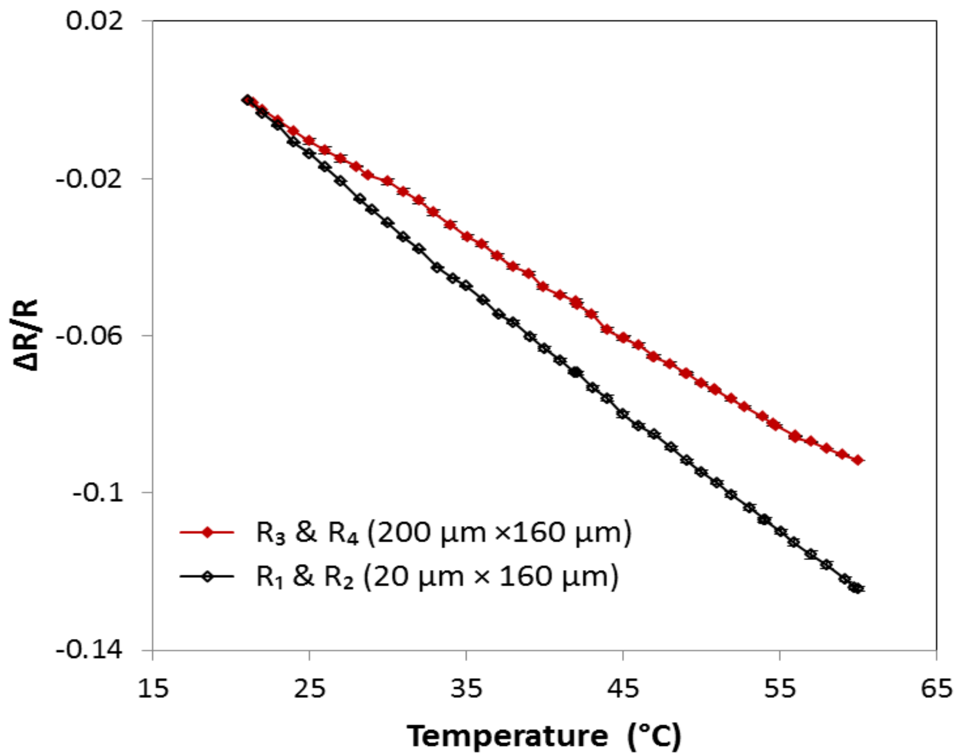

Figure 3-7. Sensitivity test: the sensor demonstrates sensitivity of -0.0031/°C for polysilicon thermistor R_1 & R_2, and -0.0025/°C for R_3 & R_4.

Long term stability Test

For biomedical monitoring applications, sensing materials needs to fulfill requirements of long term stability. To minimize stress induced by the polysilicon annealing process, which may

introduce instability, polyimide PI2611 with low stress and low CTE was chosen as the flexible substrate. Furthermore, a slow ramping rate was used for annealing to minimize the built-in stress between polyimide and polysilicon film. Long term instability of polysilicon resistor can also be induced by the grain boundaries in polysilicon film. Grain boundaries contain numerous dangling bonds, which can either trap a charge carrier or be saturated by an atom[110]. Trapped carriers give rise to a potential barrier, which increases the resistivity[111].The long term stability of the polysilicon material/device developed on polyimide substrate was examined in air firstly. The resistance of the developed polysilicon resistor was continuously measured with a digital multimeter (Agilent 34461A) and recorded with LabView, using a 5 μA DC input current to prevent self-heating. A commercial high accuracy WPI® IT-21 biomedical temperature probe was used to monitor the real-time temperature. The stability test was conducted in air by monitoring polysilicon resistor resistance and temperature simultaneously for a continuous duration of 3 days with data acquisition at 1 Hz. The test result is shown in Fig.3-8 (a). Fig.3-8 (b) shows the resistance drift. For 72 hours continuous operation, the resistance drifts for the polysilicon patterns were 12 ± 0.3 Ω, which equate to 0.3 ± 0.06 ºC drift as a temperature sensor. This result suggests that the developed polysilicon pattern can achieve an accuracy of 0.3 ºC over 3 days of continuous monitoring.

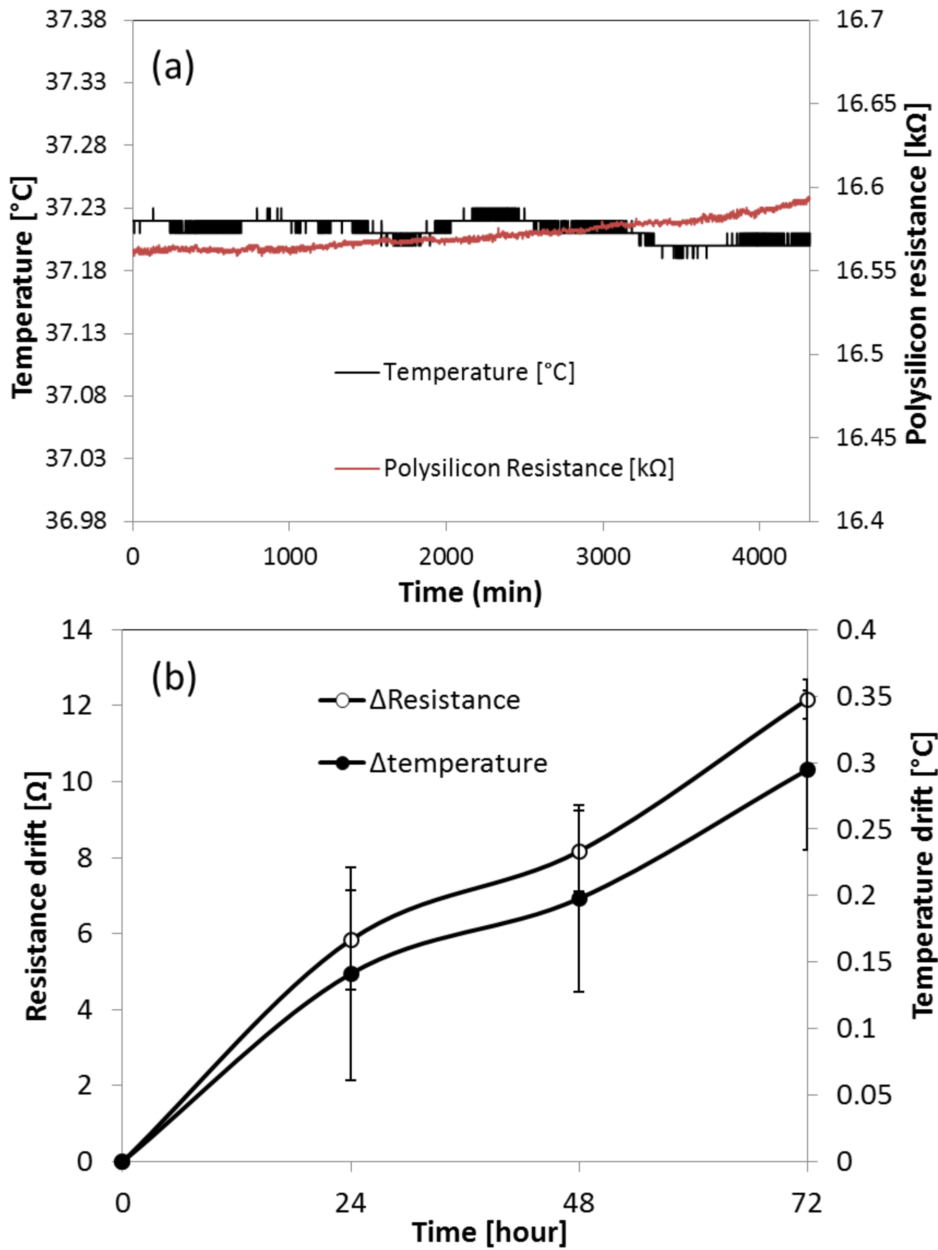

Figure 3-8. (a) Resistance drift V.S. temperature drift and (b) Long term stability test in air: Polysilicon resistance measurement in a constant temperature oven with temperature around 37.2 °C for 3 days.

After conforming the long term stability of polysilicon thin film in air, the stability was then tested in liquid. When exposing the polysilicon thin film in aqueous environment, hydrogen may diffuse in to the film and attach itself to the dangling bonds to form weak silicon-hydrogen bond, which easily get broken when the resistor is under thermal and electrical stress[112]. The forming and breaking of silicon-hydrogen bonds may cause additional resistance drift. In this work, dense silicon nitride layer has been sputtered on polyimide substrate as the moisture and ion barrier. The stability test in water was to examine the blocking effect of the sputtered silicon nitride film.

To test the long term stability of the polysilicon thermistors, the developed devices were submersed in a water bath at room temperature and resistances were measured continuously for 3 days. Fig. 3-9 (a) shows the measured resistance of one polysilicon thermistor and temperature with time and Fig. 3-9 (b) shows the resistance drift and corresponding temperature drift (with S.E.) over three days measured for five samples (three with 20 μm × 160 μm and two with 200 μm × 160 μm). As shown, the resistance drifts of the polysilicon thermistors were less than 0.08 %, corresponding to less than 0.3 °C. This result suggests that the developed temperature sensor can achieve a high accuracy of 0.3 °C over 3 days of continuous monitoring in an aqueous environment and is acceptable for the brain monitoring applications.

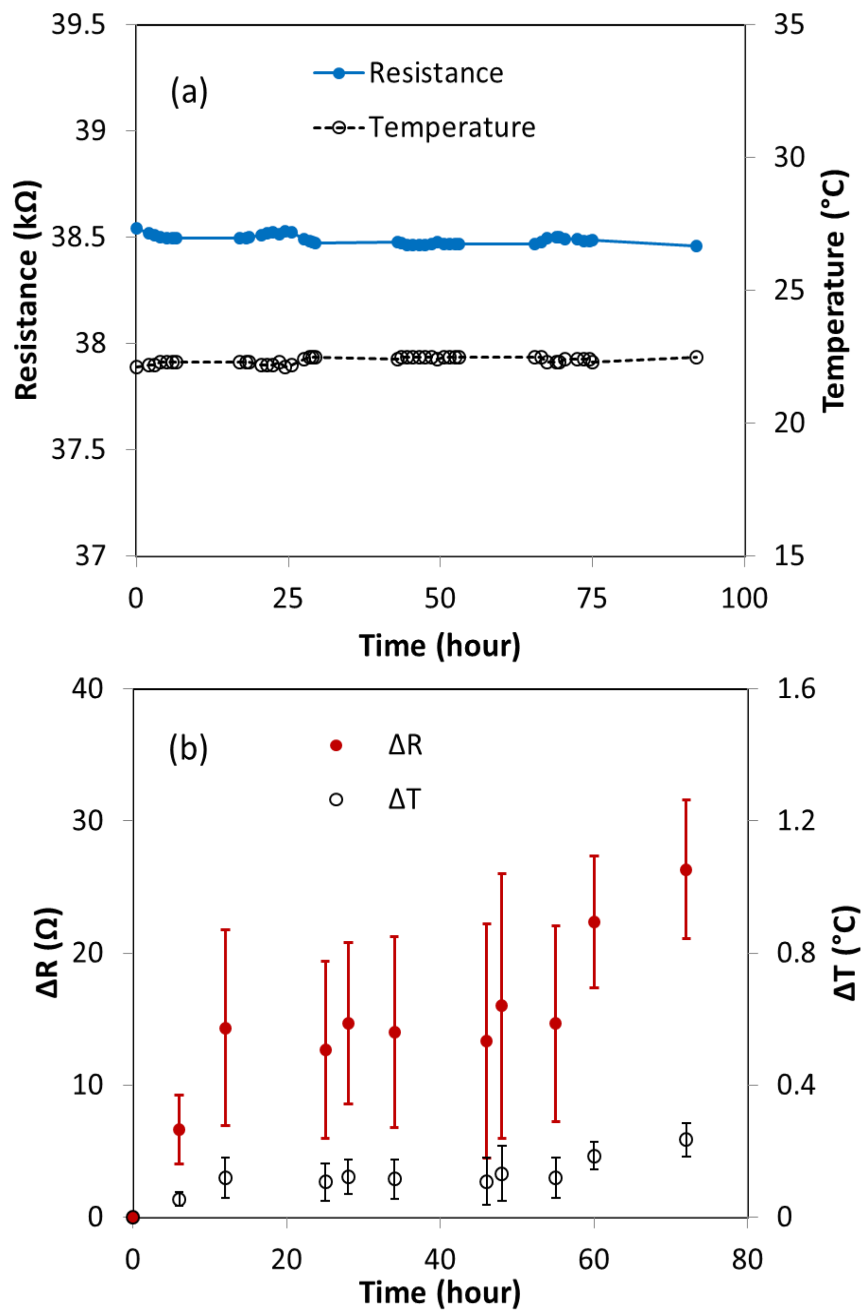

Figure 3-9. Long term stability test in water: (a) shows the resistance of one polysilicon thermistor measured for 3 days and (b) shows the resistance-drift in three days measured for five samples. The resistance drifts of the polysilicon thermistors were less than 0.08 %, which corresponds to less than 0.3 °C.

Response time

The temporal response of the polysilicon temperature sensor when exposed to instantaneous change in environment temperature is defined by two measures, the time constant and response time. Time constant is the time to reach 63.2 % of the complete step change in temperature. Response time is the time to reach 99.5 % of the final temperature in a step change.

The ability to track process changes depends on the sensor's thermal mass and proximity to the process. The time response for the sensor was determined by moving the sensor from the ambient air (~25 °C) into a water bath at 40 °C. The temperature range of 25 to 40 °C totally covered the physiologic temperature of brain.

Fig.3-10 shows the time course of the resistance change of the temperature sensor measured for three samples. The time constant and response time are found to be around 0.8 and 1.5 seconds for R_1 & R_2, and 0.8 s and 2.2 s for R_3 & R_4. Since brain temperature changes on a longer time scale, the response time of the developed polysilicon thermistor is fast enough for brain temperature sensing.

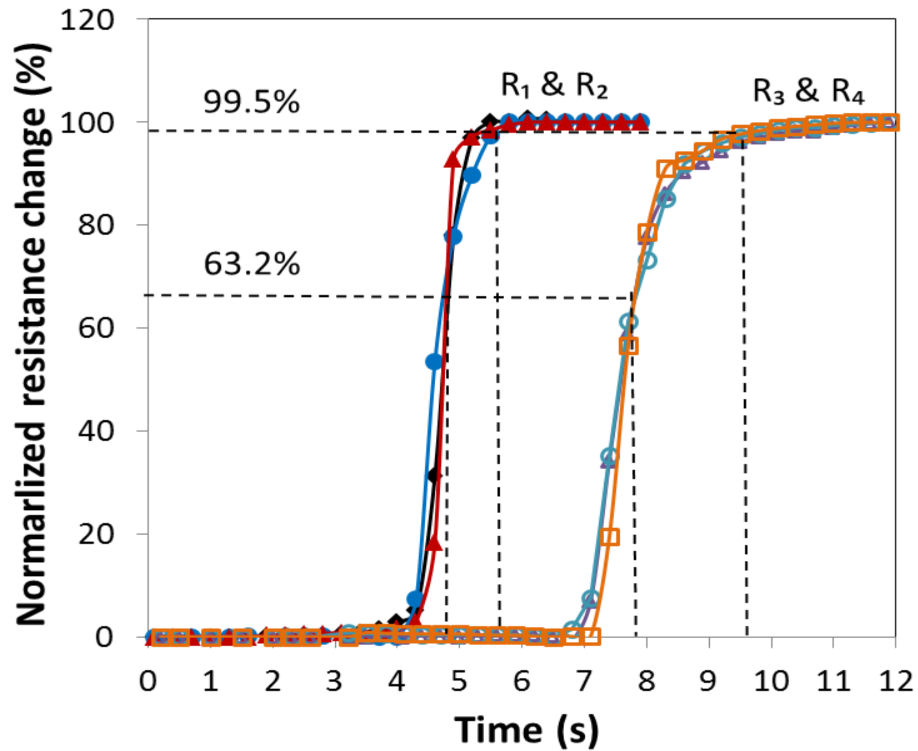

Fig.3-10. Response time test: The time constant and response time are found to be around 0.8 s and 1.5 s for R_1 & R_2, and 0.8 s and 2.2 s for R_3 & R_4.

Thermal hysteresis

Three cycles in the temperature range of 30 to 45 °C (which includes physiological temperature of brain) were applied to examine thermal hysteresis.

Fig. 3-11 (a) and (b) shows the relationship between temperature and resistance for R_1 & R_2, and R_3 & R_4 during the cycles, respectively. As shown in the figure, the thermal hysteresis is less than 0.1 °C for polysilicon elements R_1 & R_2 after three cycles, while for R_3 & R_4, the thermal hysteresis reaches 1°C.

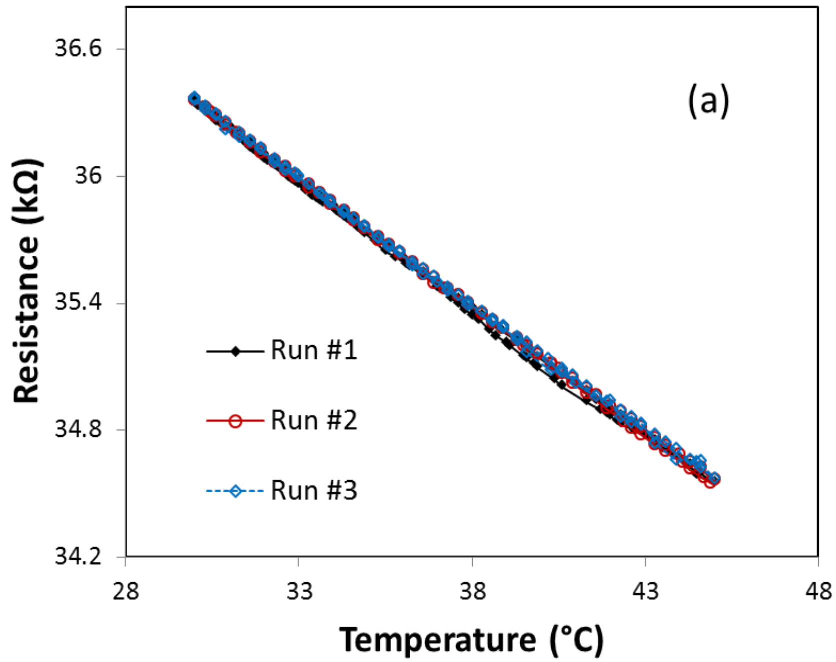

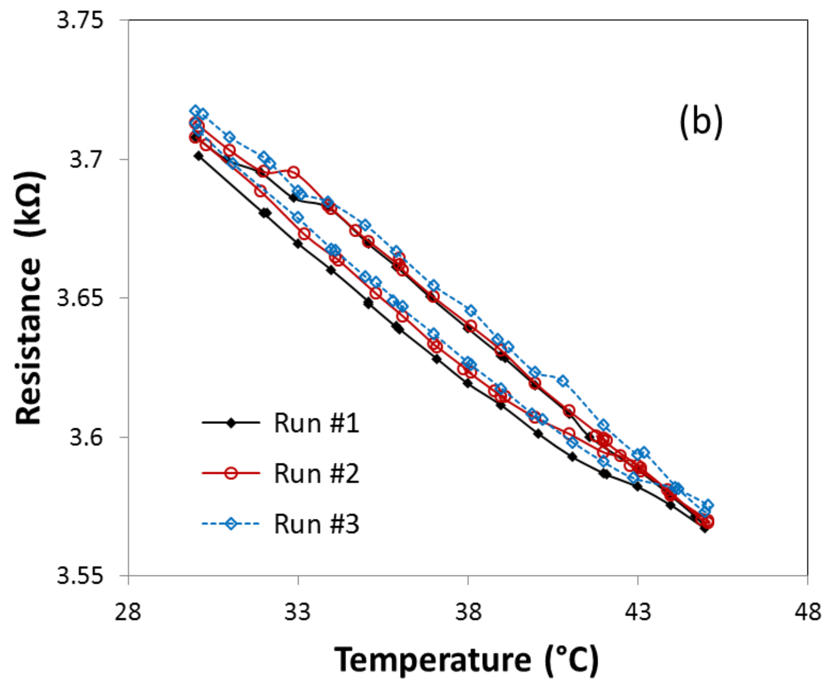

Figure 3-11. Thermal cycle test: the thermal hysteresis is less than 0.1°C for the temperature sensor for R_1 & R_2; and 1°C for R_3 & R_4 after three thermal cycles from 30 °C to 45 °C.

Resolution

Temperature steps of 0.1 °C were realized by a slow ramping rate of 5 °C/hour of the hot plate. The resistance of the temperature sensor was recorded when the reference temperature probe (BAT-21) showed an increase of 0.1 °C.

Recorded temperature and resistance are shown in Fig. 3-12. The sensor's resistance changes for both R_1 & R_2 and R_3 & R_4 with each temperature step clearly show that the sensor can realize a resolution of 0.1 °C, thus meeting requirements for brain temperature monitoring.

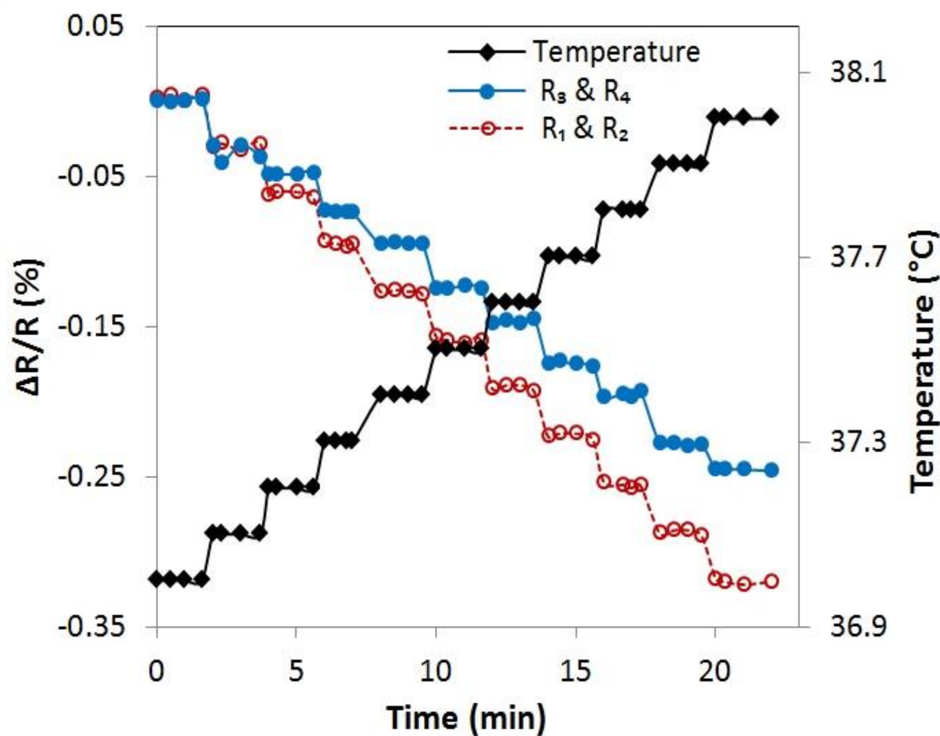

Figure 3-12. Resolution test: The sensor's resistance changes with each temperature step clearly shows that the sensor can realize a resolution of 0.1 °C.

In vivo measurement

All surgical procedures were performed in the animal surgical procedure room at the Feinstein Institute for Medical Research.

Two male Sprague-Dawley rats (250-400 gram) were used in the experiments. Animals were anesthetized with 5 % isoflurane and placed in a stereotaxic frame with a base heating pad. Animals were maintained on 2.5 % isoflurane delivered in room air through a nose cone throughout surgical procedures, and 1.5 % isoflurane throughout recordings. Two craniotomies were made in the right hemisphere. One was made over coordinate at AP 0-6 mm, ML 1-3 mm to place the polysilicon temperature sensing strip on the dura. The other was made at AP -2 mm, ML 1-2 mm to induce a spreading depolarization wave by a needle prick to the cortex. A 250 μm diameter Ag/AgCl wire reference electrode was implanted in the left hemisphere (AP 3 mm, ML 2 mm, DV -0.5 mm). Recordings began 24 hours after device implantation. To assess the polysilicon temperature performance, a spreading depolarization (SD) wave was elicited by needle prick at the frontal craniotomy and the wave was recorded as it propagated across the sensor array. All procedures complied with the NIH guidelines for the care and use of laboratory animals and were approved by the Feinstein Institute for Medical Research Committee on Use and Care of Animals.

In vivo noise level

The *in vivo* noise levels of the polysilicon temperature sensors were measured. In order to prevent self-heating of the polysilicon elements, 10 µA and 40 µA constant current were applied to R_1/R_2 polysilicon elements with the resistance of 36.5±0.3 kΩ and R_3/R_4 with the resistance of 4.0±0.1 kΩ, respectively. The experimental results are shown in Fig. 3-13. A total of 4 polysilicon elements for each dimension (n=4) were evaluated. In summary, the R_1/R_2 polysilicon exhibited less noise (0.025± 0.03 ºC) than the R_3/R_4 element (0.07± 0.06 ºC) by a factor of at least 2.8.

Compared to the noise level of gold-based RTD (0.035±0.04 °C) that we developed previously as a temperature sensor, the polysilicon thermistors with the dimension of 20 µm ×160 µm and larger resistance achieved a lower noise level and thus realized higher measurement accuracy.

Figure 3-13. Measured *in vivo* noise level for polysilicon thermistors: $R_1$with the dimension of 20 µm ×160 µm : 0.025±0.03 °C; R_3 with the dimension of 200 µm ×160 µm : 0.07±0.06 °C.

In vivo transient response

The needle prick model was employed as a mechanically induced "mini" traumatic brain injury causing one single spreading depolarization (SD) wave[113]. Two needle pricks were performed in two rats with a 1 hour interval. A representative recording is shown in Fig. 3-14.

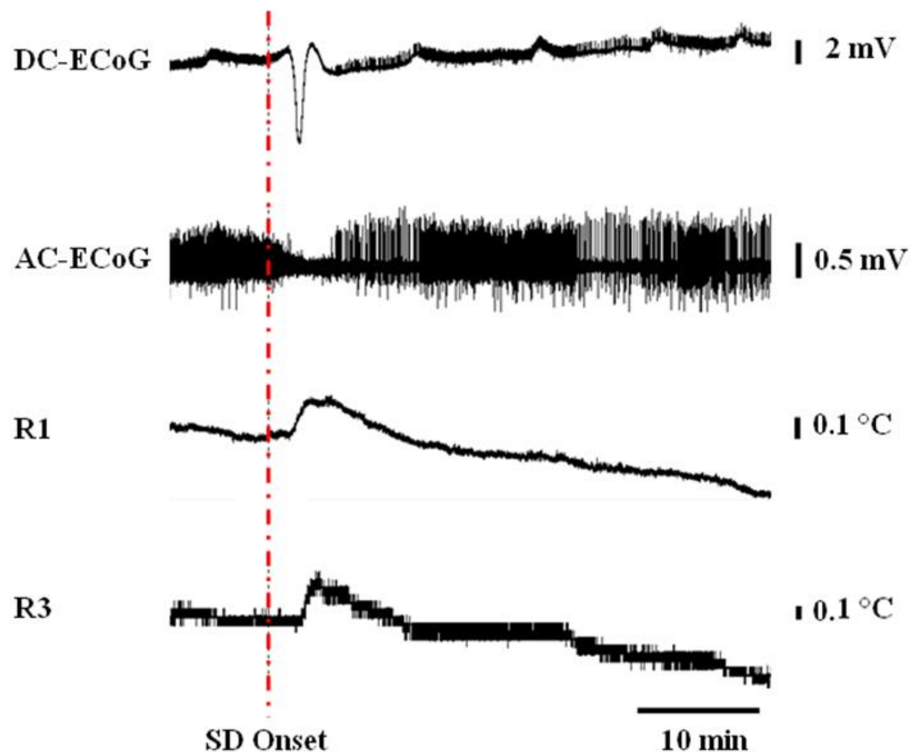

Figure 3-14. Transient response of polysilicon thermistors to *in vivo* stimulus: brain cortical temperature showed a transient increase (0.35±0.06 for R_1 & R_2; 0.23±0.07 for R_3 & R_4; n=4) and then slowly recovered to its baseline value during spreading depolarization.

Successful induction of the SD wave was confirmed by a DC negative shift (5.9±0.7 mV; n=4) and a transient suppression of spontaneous neural activity. During the SD, the brain cortical temperature showed a transient increase (0.35±0.06 for R_1 & R_2; 0.23±0.07 for R_3 & R_4; n=4) and then slowly recovered to its baseline value. The temperature sensing elements R_1 & R_2 with larger resistance showed higher sensitivity than the temperature sensing elements R_3 & R_4.

Summary

A flexible polysilicon-based thermistor array has been developed on thin polyimide substrate for brain temperature monitoring. The array has low mechanical stiffness and the ultra-small dimension of developed polysilicon thermistors can be applied for high spatial resolution measurement with sufficient accuracy and resolution. Comparison of polysilicon thermistors for two dimensions 20 μm × 160 μm and 200 μm × 160 μm showed the thermistors with larger resistance (20 μm × 160 μm) had better performance both *in vitro* and *in vivo*. The developed polysilicon thermistors with dimension of 20 μm × 160 μm has achieved good *in vitro* performance with a sensitivity of -0.0031/°C, response time of 1.5 s, a resolution of 0.1 °C, thermal hysteresis less than 0.1°C, and long term stability with drift less than 0.3 °C for 3 days of continuous operation in water. *In vivo* tests of the polysilicon thermistor showed a low noise level of 0.025±0.03 °C and the expected transient temperature increase associated with cortical spreading depolarization. The obtained results further suggest the superior performance of polysilicon thermistor compared to gold RTD.

CHAPTER 4

POLYSILICON BASED FLEXIBLE PRESSURE SENSOR

Introduction

Nearly three-quarters of neurological deterioration after sTBI is related to intracranial volume, and therefore intracranial pressure (ICP) [114]. High ICP is strongly associated with poor outcome, particularly if the period of intracranial hypertension is prolonged. Increased ICP can also cause actual shift of brain substance resulting in structural damage to the brain and to herniation through the tentorial hiatus or foramen magnum[115]. Although treatment is instituted at different levels depending on the pathology, ICP higher than 15 mm Hg is generally considered to be abnormal[116].

Monitoring ICP forms the cornerstone of modern neurocritical care and has been used as a marker of secondary brain injury for decades[114]. Currently, ICP is measured either through transducing the column of cerebrospinal fluid drained directly from the ventricle (through an external ventricular drain, or EVD)[20] or by means of a mini-strain gauge (Codman)[23] placed within the brain tissue. Typical mini-strain gauge catheters are approximately 1.5 mm in diameter with a single pressure sensor that allows for a global measure of pressure within the region of the probe. Each sensor must be placed through an individual burr hold drilled through the skull. Flexible pressure sensor, which can minimize the brain tissue damage as and be easily integrated with other sensors to realize multimodal brain monitoring, is on demand.

With regard to easy sensor integration, piezoresistive pressure sensors are always preferred because of the simple signal processing, minimal cross-talk, and relatively low energy consumption. Roger's group pioneers in this field by applying single crystal silicon-nanomembrane/nanoribbon transferred on flexible polyimide to develop multifunctional sensors for simultaneous sensing of intracranial pressure (ICP) and intracranial temperature (ICT) [57-58]. *In vivo* tests were conducted for pressure and temperature monitoring in the intracranial space of rats. The results showed comparable performance between the developed sensors and the commercial ones. By far, this approach can be considered as the most promising and suitable method for *in vivo* multimodal brain monitoring and integration of multiple sensors. However, the process of developing single crystal silicon nanomembrane/nanoribbon and transferring it to flexible substrate is quite complicate and expensive, which deters it from high yield and throughput of sensors.

In this work, we present an innovative polysilicon based flexible pressure sensor. Polysilicon, although with lower sensitivity to pressure comparing to single crystal silicon nanomembrane, has the advantage of being able to be directly developed on polyimide with simple, fast and low cost AIC process as showed in previous chapters. With proper design, the polysilicon based pressure sensor has achieved high sensitivity and resolution in low pressure range required for ICP measurement.

Gauge Factor of Polysilicon Thin Film

In order to check the feasibility of developing high sensitive pressure sensor in low pressure range as well as guide the pressure sensor design, the gauge factor of polysilicon thin film should be firstly characterized.

Fabrication of Characterization Device

To develop devices for gauge factor characterization, polysilicon film with the thickness of 200 nm was developed on 7 μm thick PI2611 substrate with AIC, followed by standard photolithography and polysilicon etching process to form polysilicon resistors patterns. A 200 nm thick aluminum layer was then evaporated and patterned to electrical leads for polysilicon resistors. Another 7 μm thick PI2611 film was developed as the passivation layer on the top. Finally, the PI2611 passivation layer was dry-etched using CF_4 and O_2 plasma to expose the aluminum contact pads for electrical input and measurement. The fabricated sample was then peeled off from the silicon substrate and cut into size for measurement. For electrical measurement, electrical wires were bonded to the aluminum contact pads with silver paste. Epoxy was applied to strengthen the contact between the wires and the contact pads.

Fig. 4-1 shows the fabricated devices on flexible polyimide film, which was peeled off from the silicon wafer, and the single device which was cut into size and bonded with electrical wires.

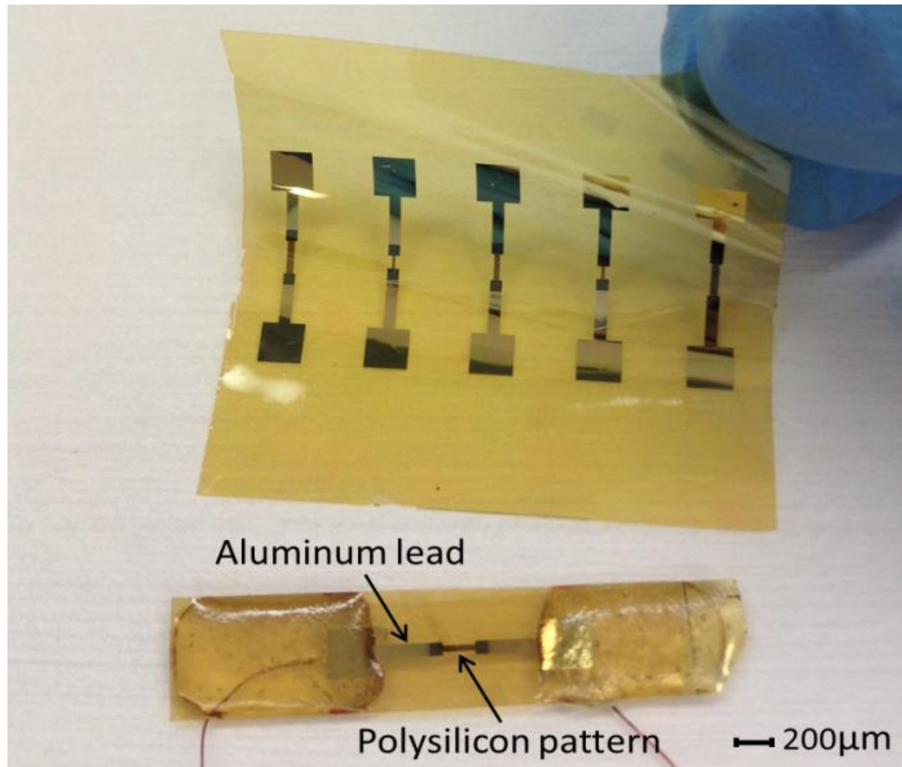

Figure 4-1. Polysilicon resistors developed on flexible polyimide substrate for gauge factor test.

Gauge factor test

Polysilicon resistors with length of 200 µm and width of 40 µm were developed and tested with Instron® 5948 loading cell to characterize the GF of polysilicon film developed on polyimide. Fig. 4-2 (a) shows the loading cell with Bluehill 3 instrument software to control the applied strain and the speed of strain change, (b) shows the polysilicon resistor used for the measurement, and (c) shows the resistor fixed on the loading cell. Strain from 0 to 0.01 was set to apply to the sample with a speed of 0.005/min under the control of Bluehill 3 instrument software. Resistance change with the applied strain was measured with digital multimeter and recorded by Labview program every second.

Fig. 4-3 shows the measured resistance change with strain for 3 samples. As shown in the figure, resistance of polysilicon piezoresistor increases linearly with the applied strain with a GF of 10.316. The GF of the polysilicon film developed on flexible polyimide substrate with AIC is comparable or even higher than that on traditional rigid substrate[117-120], demonstrating the feasibility of using the developed polysilicon thin film on flexible PI2611 substrate for high sensitive pressure sensing.

Hysteresis Test

To conduct hysteresis testing, tensile and relax mode was used in Instron® loading cell. Tensile strain increasing from 0 to 0.005 and then decreasing back to 0 with the speed of 0.005/min was applied to the testing sample. Two cycles of the strain were applied to the testing sample and the hysteresis curve is shown in Fig. 4-4. The hysteresis was less than 0.3 %.

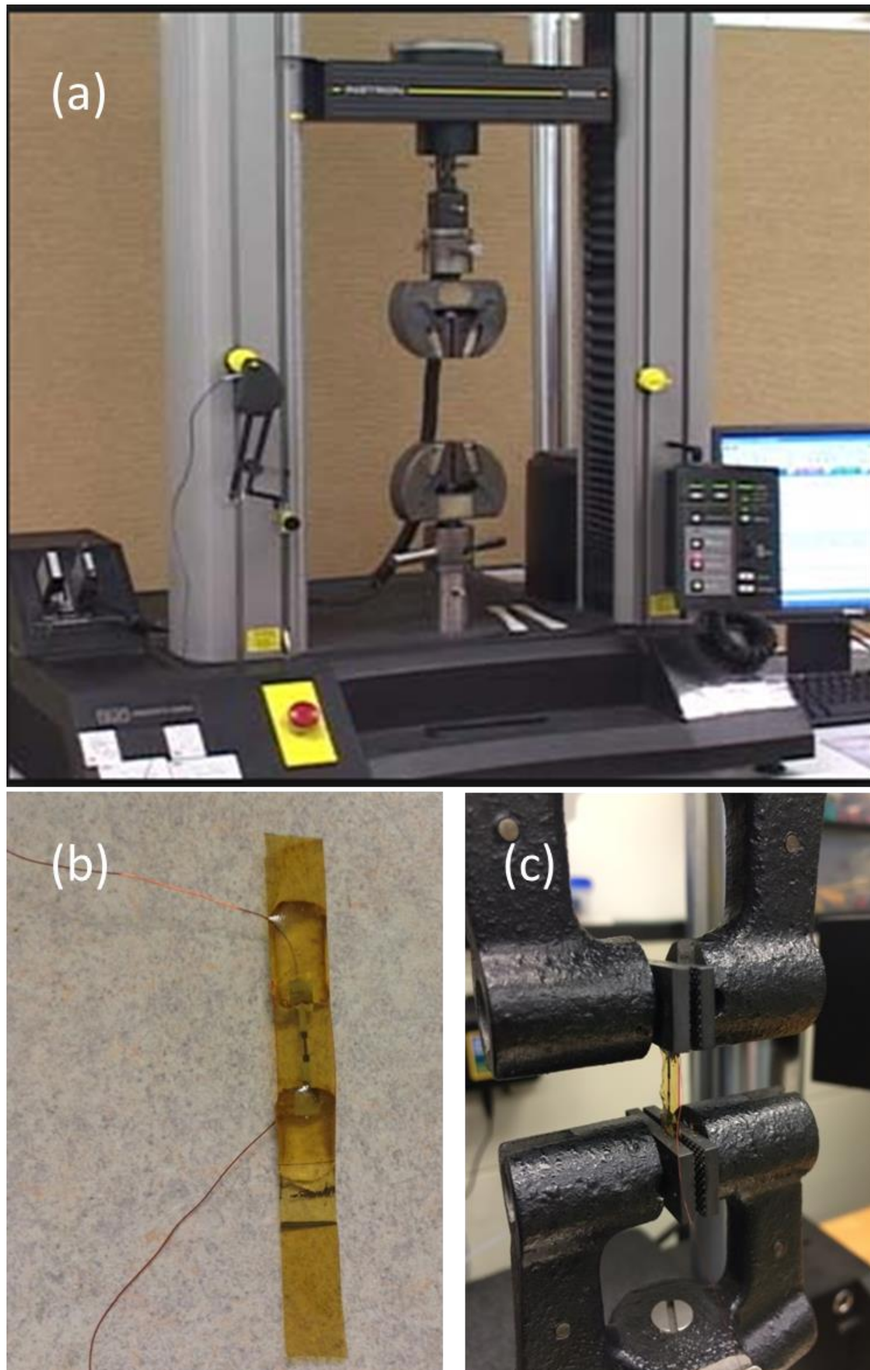

Figure 4-2. Gauge factor test: (a) Instron® loading cell (b) polysilicon resistor used for the measurement, and (c) polysilicon the resistor fixed on the loading cell.

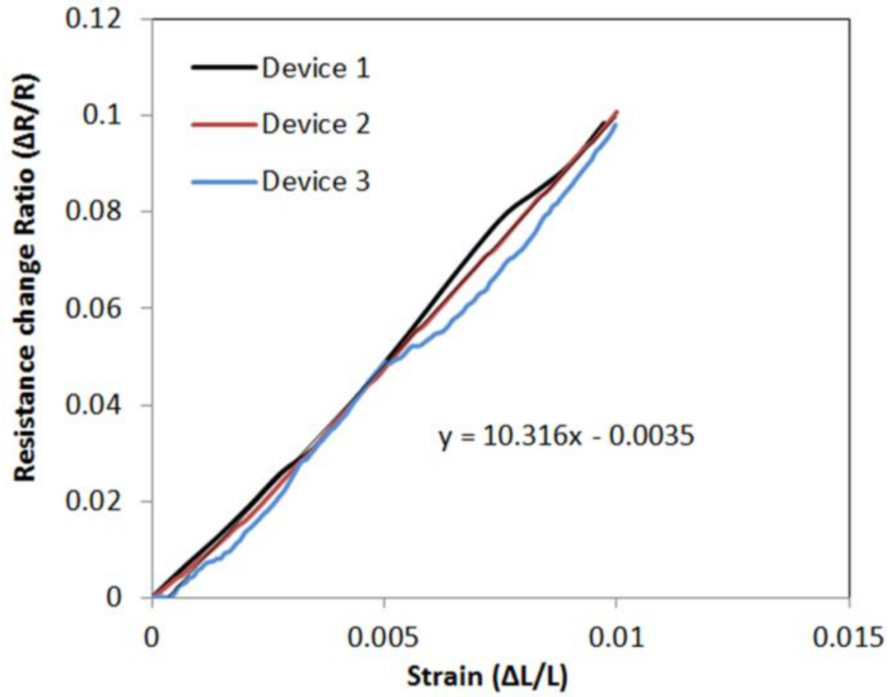

Figure 4-3. Gauge factor measurement results: mean gauge factor of three samples is 10.316.

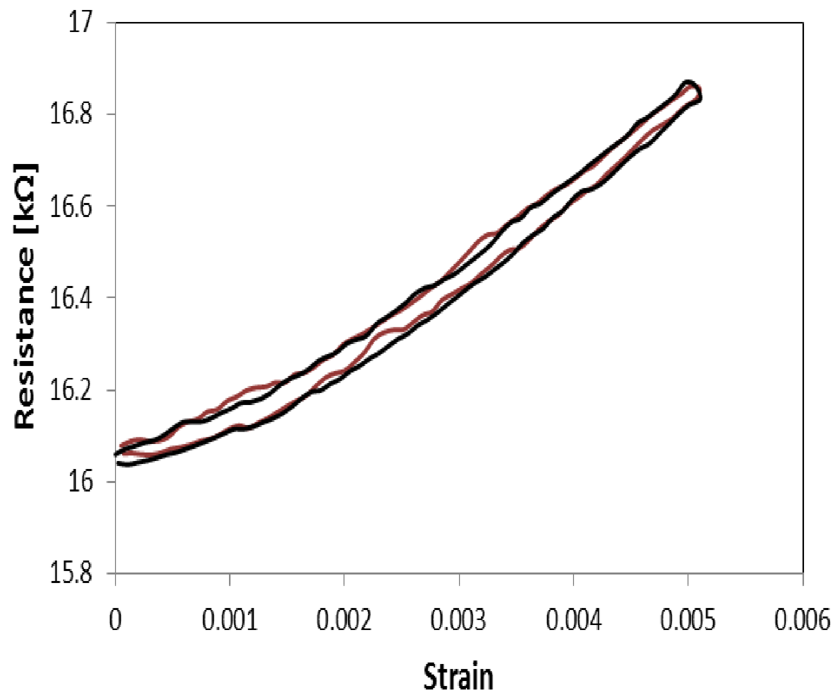

Figure 4-4. Hysteresis curve for 2 strain cycles: the hysteresis is less than 0.3 %.

Flexible pressure sensor design and microfabrication

Concept

Flexible piezoresistive pressure sensor based on polysilicon thin film is designed and shown in Fig. 4-5. Flexible polyimide is used as construction material to generate a cavity and form flexible polyimide membrane for pressure sensing. Polysilicon resistor placed on the membrane acts as piezoresistive element for pressure sensing. When the pressure is applied on the membrane, the flexible polyimide membrane will get deformed, thus generate strain/stress. The polysilicon piezoresistor placed on the membrane will experience the strain as the membrane and a resistance change will be induced according to its gauge factor. Applied pressure can be evaluated by measuring the polysilicon piezoresistor's resistance change. Polysilicon resistor is also placed out of the membrane. The resistance of this resistor is designed to calibrate against parasitic effects of temperature on the pressure determination. The resistor out of membrane can also be considered as an independent thermistor for temperature measurement. Thus, simultaneous pressure and temperature measurement can be achieved.

The changes of polysilicon resistance change (ΔR_1) on the membrane and apart from membrane (ΔR_2) are shown in equation (4-1) and (4-2) respectively.

$$\Delta R_1 = (GF \cdot \varepsilon + TCR \cdot \Delta T)R\,, \qquad (4\text{-}1)$$

$$\Delta R_2 = TCR \cdot \Delta T \cdot R\,, \qquad (4\text{-}2)$$

where GF is the gauge factor, and TCR is the temperature coefficient of resistance for polysilicon thin film.

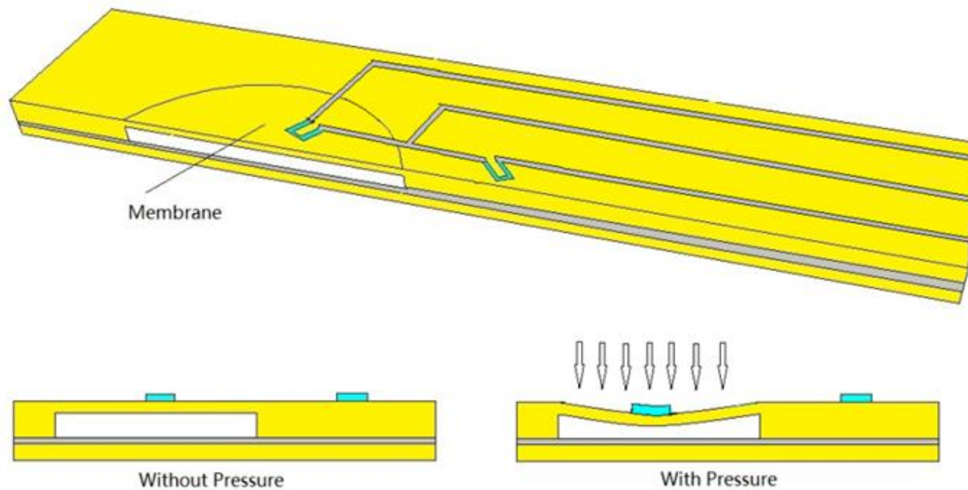

Figure 4-5. Polysilicon-based flexible pressure sensor: the polysilicon elements out of membrane act as temperature sensor and the elements on the membrane act as pressure sensor.

Simulation and design

The goal of piezoresistive pressure sensor design is achieving highest sensitivity while maintaining the linearity and stability. To get the proper membrane thickness and radius, the position of polysilicon piezoresistor on the membrane, as well as the gap height for membrane deformation, COMSOL Multiphysics 4.4 was used to simulate the displacement and Strain/Stress distribution of membrane under pressure. Solid module was used with fixed boundary and applied pressure on the surface.

Since silicon nitride film sputtered on PI2611 showed good passivation in aqueous biomedical environment in our previous work[121], a combined membrane with 100nm thick silicon nitride layer and PI2611 thin film was simulated. The parameters of silicon nitride and PI2611 used in the membrane strain and displacement simulation are listed in Table 2.

Table 2. Parameters of PI2611 and Silicon nitride used in the membrane strain and displacement simulation.

	Density $\rho(kg/m^3)$	Young's modulus $E(GPa)$	Poisson's ratio ν
PI2611	1400	8.5	0.35
Si_3N_4	3100	250	0.23

PI2611 membranes with different thickness and radius were simulated, and a membrane with the thickness of 5.5 µm and radius of 500 µm -showed good resutls. Fig. 4-6 shows the deformation of the membrane under 1 mmHg (a) and 35 mmHg (b) respectively. The largest deformation of membrane is at the center of the membrane. For the pressure of 35 mmHg, the largest deformation is 14 µm. Thus, a gap layer of 20 µm will be highenough for the membrane deformation.

To determine the position of the polysilicon piezoresistors along the thickness of the membrane, stress distribution along the thickness of membrane was simulated and shown in Fig. 4-7. As shown in the figure, the stress/strain is highest on the surface of the membrane, and the sensitivity will be the highest if the piezoresistors are placed on the surface. However, a passivation layer is always required for the pressure sensor to prevent the piezoresistors from any

contamination. Instead of placing the polysilicon piezoresistors on the surface of the membrane, the polysilicon pattern should be brought to the surface as close as possible, which means a thin passivation layer is preferred.

Fig. 4-8 shows the strain and stress distribution of a cut plane which has 0.5 μm distance to the surface. The largest longitude strain of 1 mmHg is about -2×10^{-5} at the edge, with the gauge factor of ~ 10, the resistance change will be around ~ 10^{-4} under 1 mmHg which is high enough for the measurement. Thus, the polysilicon piezoresistors were designed to be placed at the edge to achieve higher sensitivity and the passivation layer was designed as 0.5 μm. The length of polysilicon resistors was designed as 100 μm for the highest output[122].

A design of the pressure sensor's dimension is shown in Fig. 4-9. The membrane is constituted with 100 nm Silicon nitride layer and 5.5 μm PI2611 layer. Radical polysilicon resistors with the length of 100 μm and width of 15 μm are placed at the edge of the membrane, and covered with 0.5 μm passivation layer. Aluminum layer -is used for the transverse part of the resistors to eliminate any transverse strain which could cause resistance decreasing under pressure.

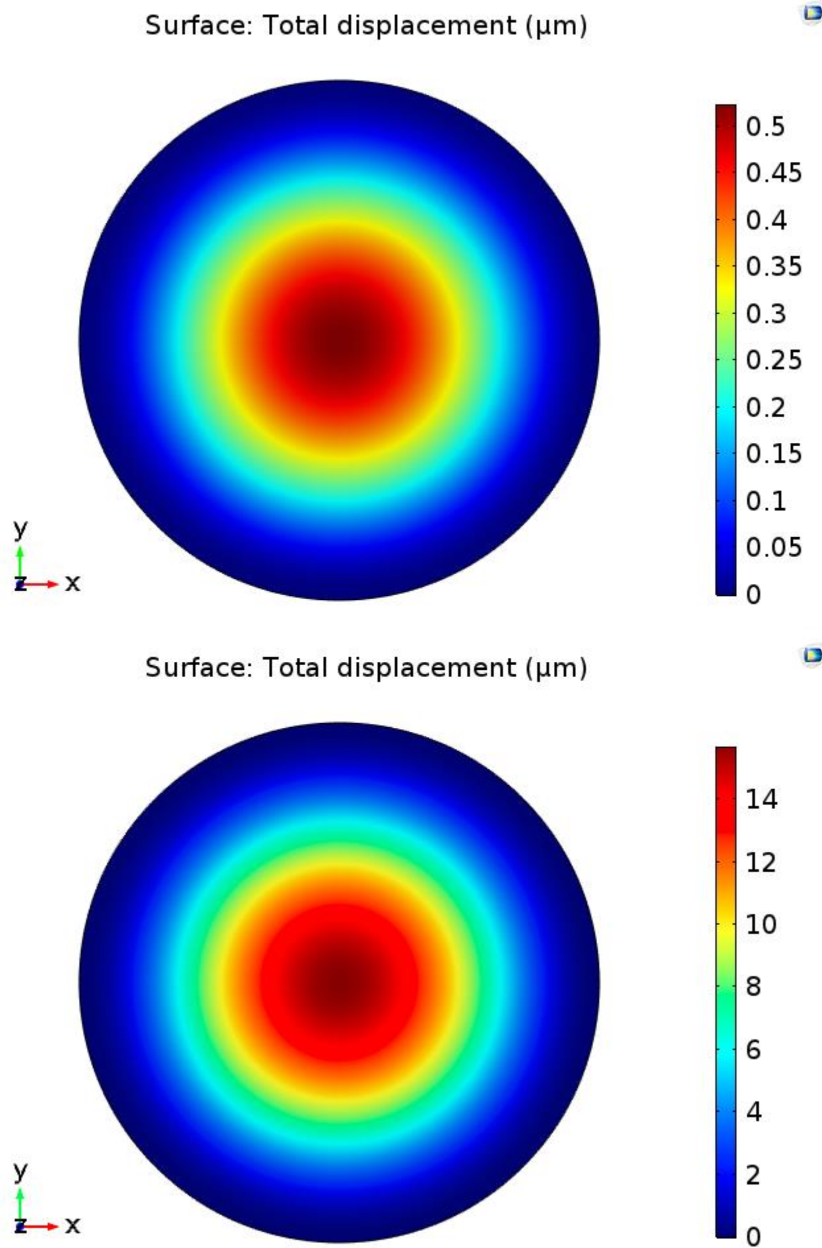

Figure 4-6. Displacement of membrane under (top) 1 mmHg and (bottom) 35 mmHg.

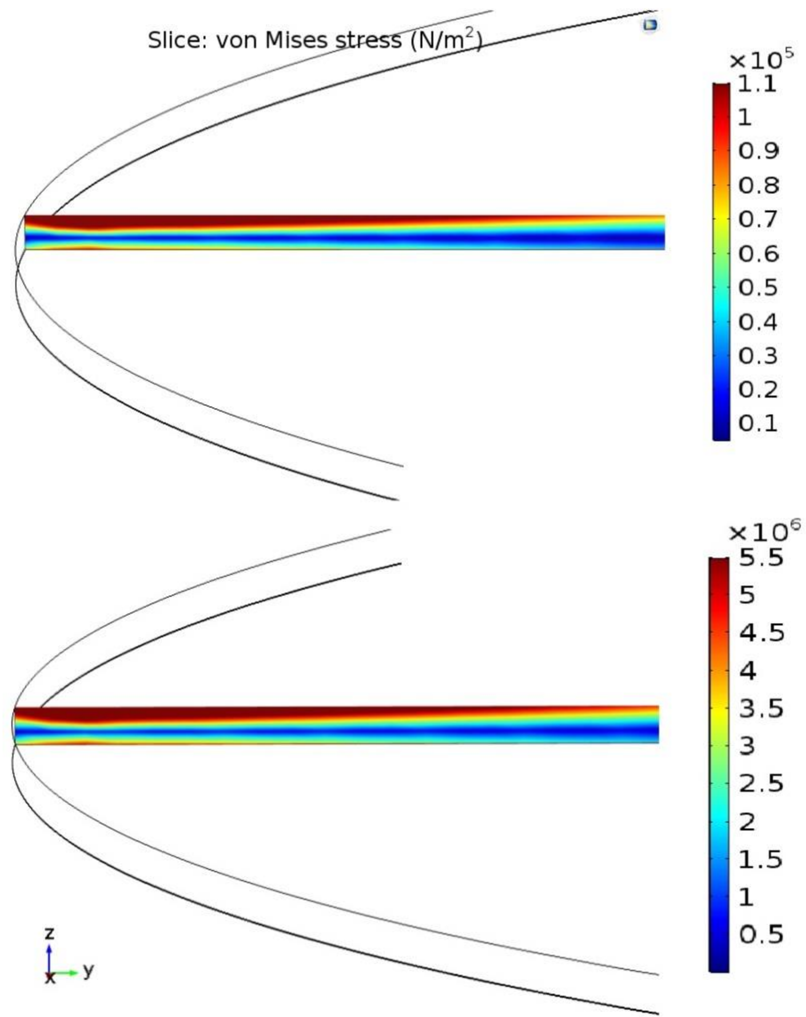

Figure 4-7. Stress distribution along the thickness of membrane under (top) 1 mmHg and (bottom) 35 mmHg.

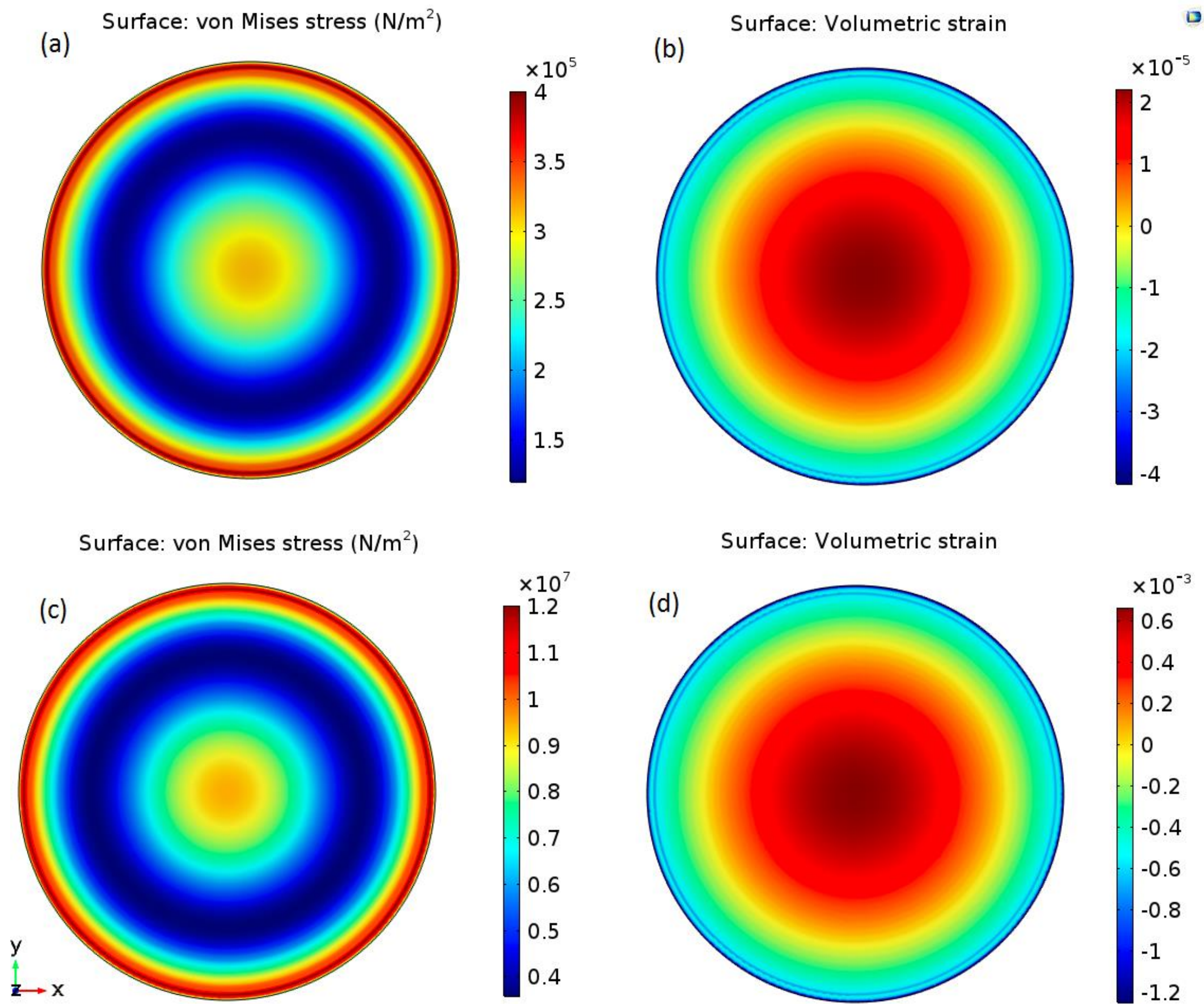

Figure 4-8. Simulation of longitudinal strain and stress distribution of the cut plane 0.5 μm from the top surface of membrane under the pressure of 1mmHg (a, b) and 35 mmHg (c. d).

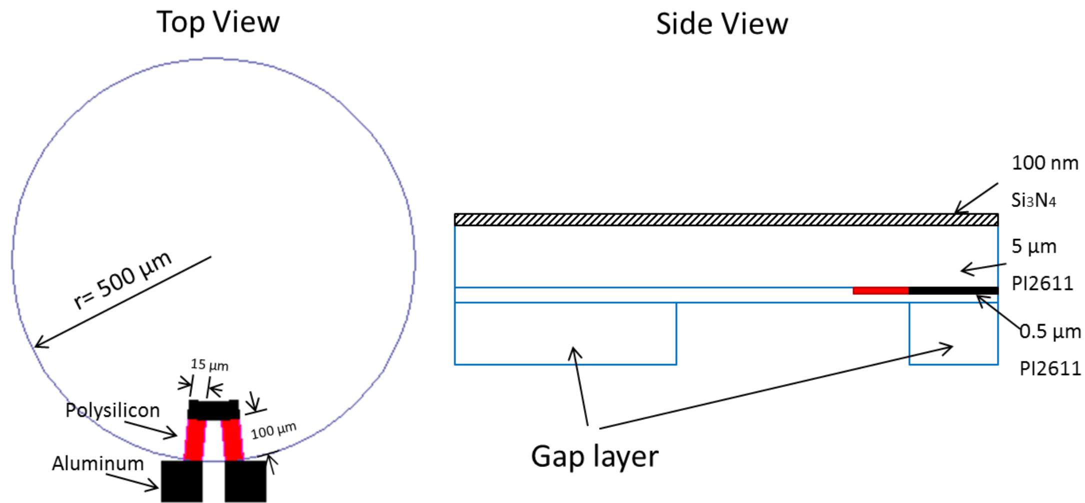

Figure 4-9. Dimensions of pressure sensor.

Microfabrication

To develop the flexible pressure sensor, PI2611 precursor (HD microsystem) was firstly spin-coated on silicon wafer and cured at 400 °C for 30 minutes to obtain 5 µm thick PI2611 film. Polysilicon thin film with thickness of 200 nm was developed on PI2611 with AIC. The polysilicon film was developed to polysilicon resistors pattern with standard photolithography. And 250 nm Aluminum layer was evaporated and patterned to form the electrical leads. 0.5 µm PI2611 film was applied on top to encapsulate the patterns. To obtain a thin PI2611 film with the thickness of 0.5 µm, PI2611 precursor was mixed with polyimide thinner T9039 (HD microsystem) (2:1 weight ratio) and then spin-coated on the patterns and cured. A gap with 20 µm height was constructed for the membrane deformation with photo-definable polyimide

PI8820 (HD microsystems). For electrical signal input and output, contacting pads for electrical connection were exposed by dry-etching the PI2611 film covering the pads with CF_4 and O_2 plasma. Finally the device was peeled off and a 100 nm thick silicon nitride layer was sputtered on top as an extra passivation layer.

Depends on the monitoring requirements, the developed sensor array can be used in either planer or curved form by wrapping the device around the curving surface. The major steps for mirofabrication are summarized in Fig. 4-10. The polysilicon piezoresistor pattern on membrane under microscope is shown in Fig. 4-11.

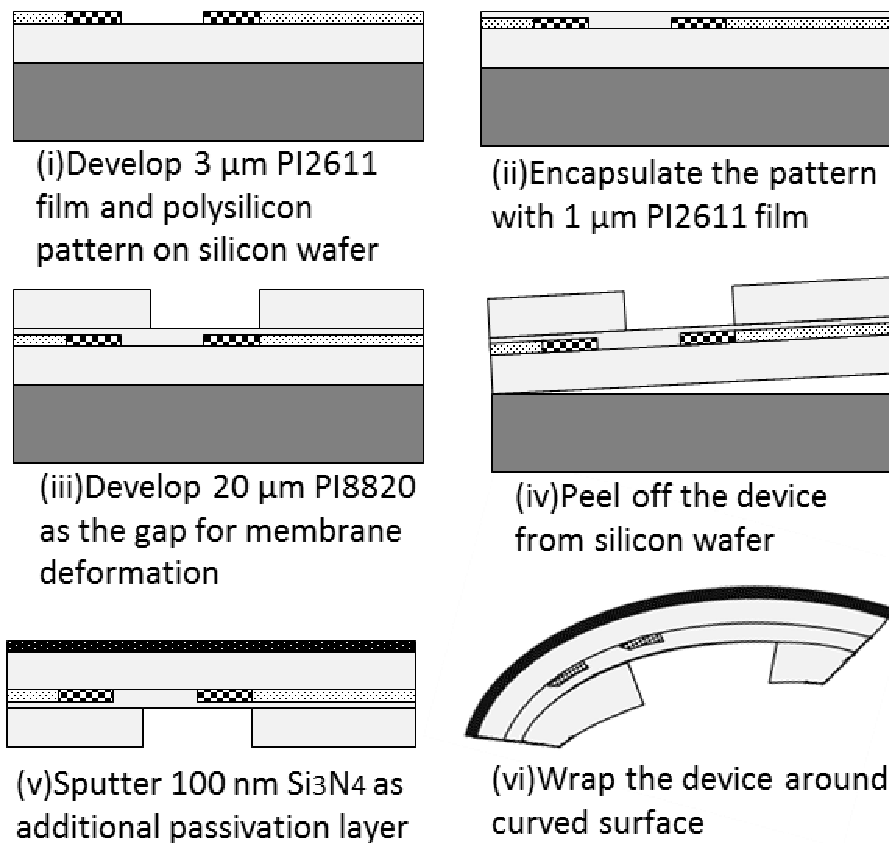

Figure 4-10. Summary of microfabrication process.

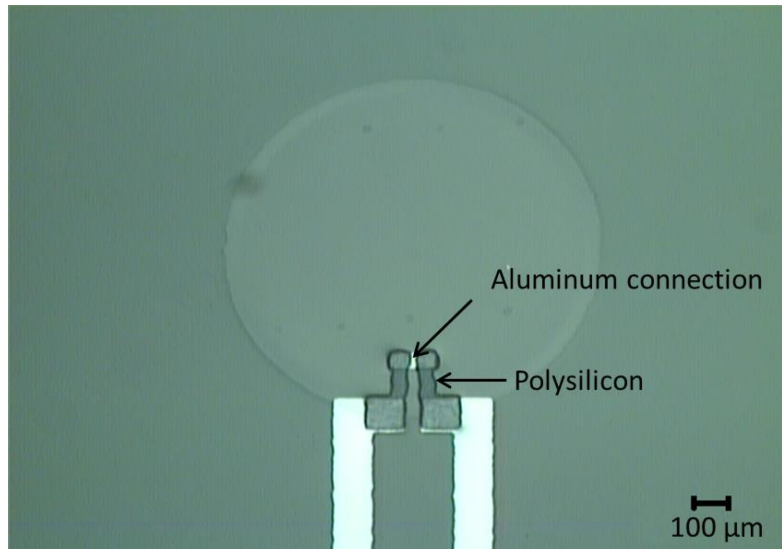

Figure 4-11. Polysilicon piezoresistor pattern on membrane under microscope: aluminum connection was used to connect two polysilicon radical resistors and prevent transverse effect.

Experiment Results

Measurement setup

The flexible pressure sensor was characterized in water. As shown in Fig. 4-12 (a), water column was used to apply pressure to the sensor, and a three valve was used to control the height of the water, thus the applied pressure. With the three-way valve, the water height can be increased, decreased, or held at a specific value.

Replaceable adapters were fabricated with milling machine and were used to hold the pressure sensor, either in planar form or curved form. Fig. 4-12 (b) shows two types of adapters for planar pressure sensor and curved pressure sensor respectively. Fig. 4-12 (c) shows the

planar form of pressure sensor attached to the adapter for testing. And Fig. 4-12 (d) shows the pressure sensor wrapped around a 2 mm diameter tube and placed in the adapter for measurement.

The resistance change of polysilicon resistor with water column height/pressure was measured with digital multimeter (Agilent 34461A). The sensitivity, resolution, and hysteresis of the pressure sensor were tested.

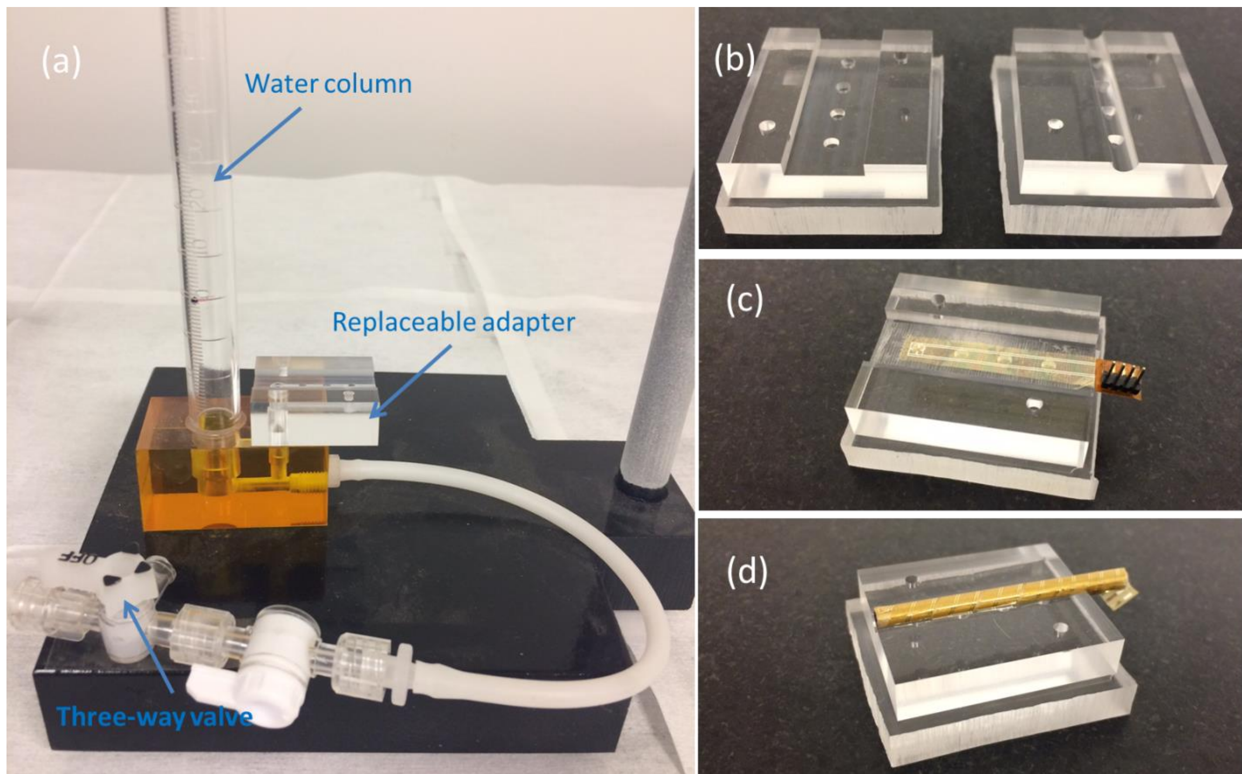

Figure 4-12. Test setup: (a) water column was used to apply pressure to the sensor, and a three valve was used to control the height of the water, thus the applied pressure. Replaceable adapters were fabricated with milling machine and were used to hold the pressure sensor; (b) Two types of adapters for planar pressure sensor and curved pressure sensor respectively; (c) The planar form of pressure sensor attached to the adapter for testing; and (d) Pressure sensor wrapped around a 2 mm diameter tube and placed in the adapter for measurement.

Sensitivity

The sensitivity of the pressure sensor was measured by increasing the pressure and recording the resistance change. The pressure was changed with 2 mmHg step and three pressure sensors were tested. As shown in Fig. 4-13, the developed pressure sensor has a linear change with pressure and a sensitivity of 6×10^{-4} / mmHg.

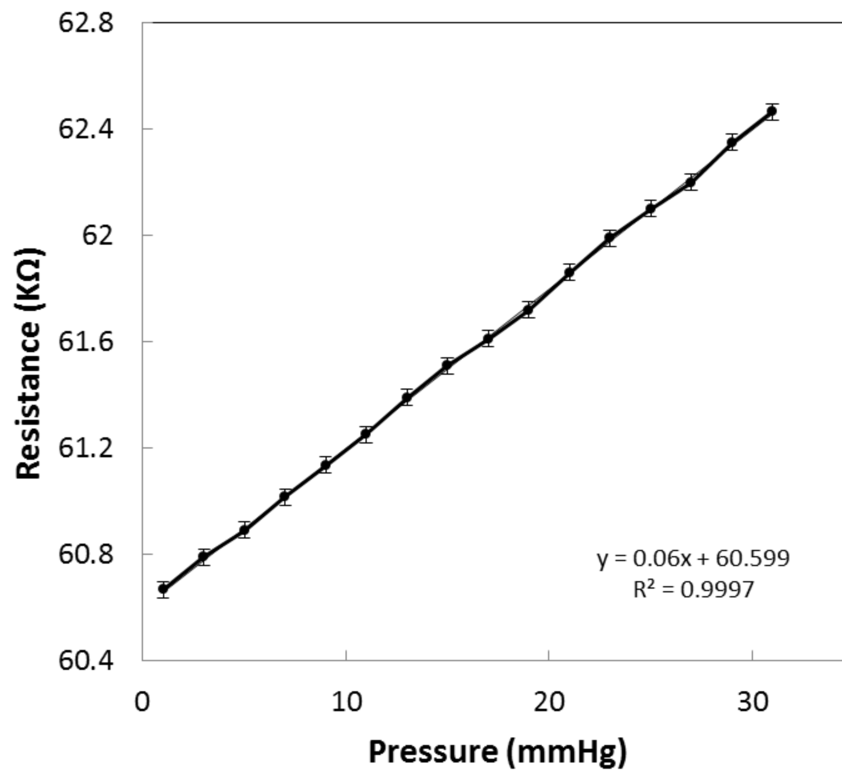

Figure 4-13. The developed pressure sensor showed a linear change with pressure and a sensitivity of 6.0×10^{-4} / mmHg.

Resolution

The resolution of the pressure sensor was measured by increasing the pressure from 1 mmHg to 30 mmHg with a 1mmHg step. The pressure was held for 3 minutes for each step and the resistance of the pressure sensor was recorded every minute. As shown in Fig. 4-14, the pressure sensor showed a stable resistance at each pressure and a clear increase with every pressure step of 1 mmHg.

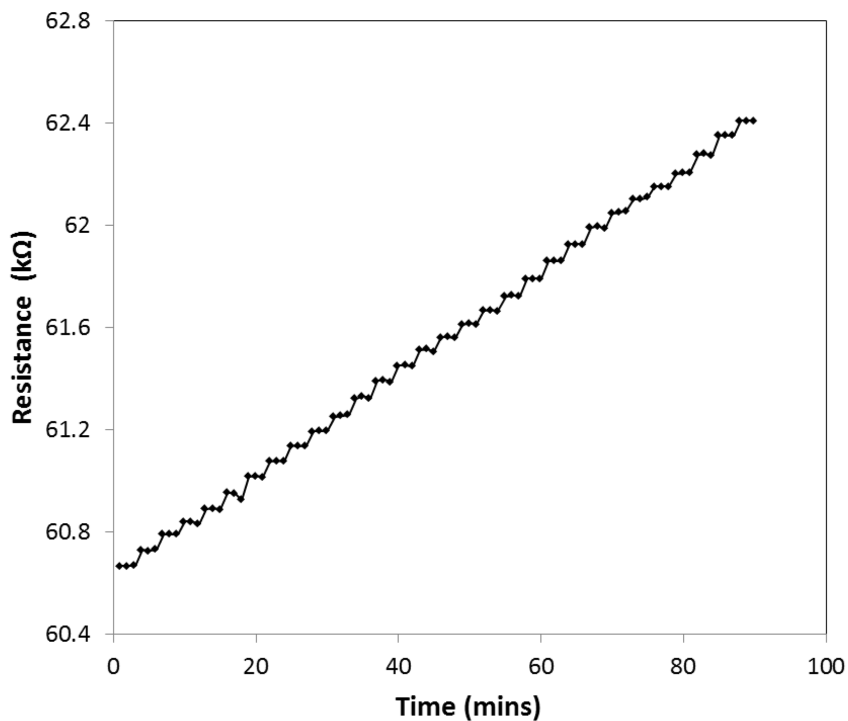

Figure 4-14. The pressure sensor showed a stable resistance at each pressure and a clear increase with every pressure step of 1 mmHg for the pressure range of 1 mmHg to 30 mmHg.

Hysteresis test

Hysteresis test was carried out for the pressure sensor by changing the water column height to increase and decrease the applied pressure. As shown in Fig. 4-15, the pressure sensor showed a hysteresis of less than 1 mmHg for a cycle ranging from 10 to 20 mmHg.

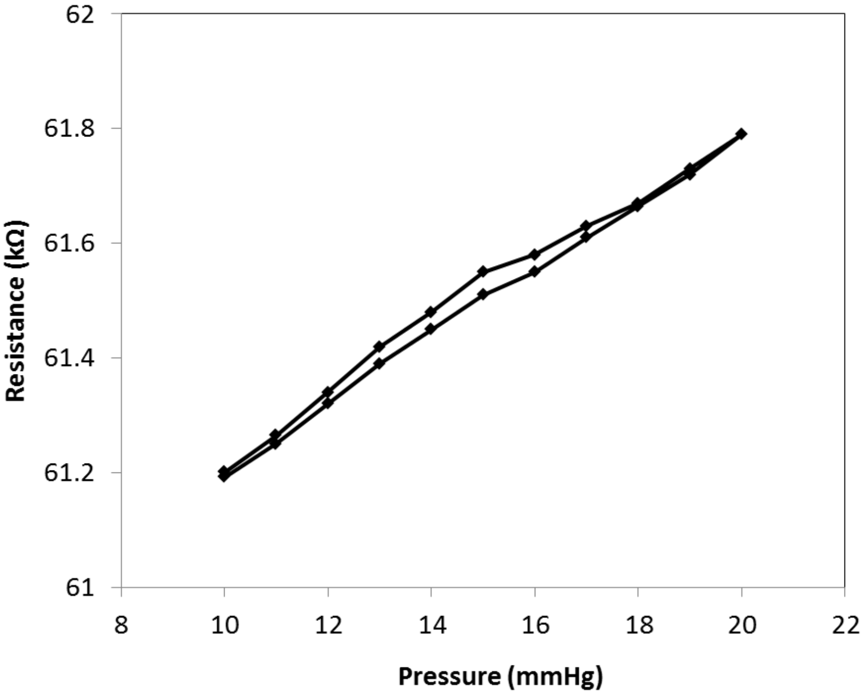

Figure 4-15. The pressure sensor showed a hysteresis of less than 1 mmHg for a cycle ranging from 10 to 20 mmHg.

Summary

A high sensitive flexible piezoresistive pressure sensor based on polysilicon thin film (PTF) was designed, developed and tested for ICP monitoring. The gauge factor of the polysilicon thin film was characterized. And the results showed polysilicon thin film had gauge factor of 10.316 and hysteresis of 0.3 % for the strains ranging from 0 to 0.005. With COMSOL Multiphysics, the strain, stress, and displacement of the membrane under desired pressure range were simulated, and the dimensions of the flexible piezoresistive pressure sensor was designed accordingly to achieve high sensitivity while maintain the linearity. The developed flexible pressure sensor was fully characterized in liquid environment. And the results showed a sensitivity of 6×10^{-4} / mmHg, resolution of 1 mmHg, and hysteresis of less than 1 mmHg for the pressure range of 10 to 20 mmHg.

The polysilicon based flexible piezoresistive pressure developed in this work has successfully achieved the sensitivity and resolution required for ICP monitoring, and showed the feasibility of developing the ICP sensor with high throughput and low cost.

CHAPTER 5

POLYSILICON PRESSURE SENSOR ARRAY

Introduction

Although elevated ICP is always associate with poor outcome, both cohort[123] and randomized, controlled trials[124] evaluating the clinical practice of monitoring ICP in the ICU setting have shown no improvements in outcome. Further, multiple randomized, controlled trials designed to treat elevated ICP have shown worse 6-month functional outcome in those treated compared to those left untreated[5,6,125].

One potential reason for these findings is simply that the likelihood of neurological deterioration depends on the location of the injury and the subsequent pressure gradients that develop when masses are asymmetrically present within the skull[13]. In a porcine animal model using multiple ICP monitors, ICP gradients were reliably produced by focal lesions, but the pressure gradients were distinct depending on the location of the mass lesions[126, 127]. In a study of 50 human subjects with moderate-to-severe TBI, two ICP monitors were placed - one on each side of the skull. Using data from just the first 24 hours of monitoring, the authors found that 20% had interhemispheric gradients in pressure; 70% had increased lesion volume or midline shift on repeated imaging[128] – findings that can prompt surgery in selected patients. In a smaller

cohort of patients with TBI, interhemispheric anteroposterior gradients were observed[129], and in post-surgical patients, a nearly 50% difference in ICP was reported comparing rostral to caudal compartments within the skull[130].

Currently, as shown in Fig. 5-1 (a), ICP is measured either through transducing the column of cerebrospinal fluid drained directly from the ventricle (through an external ventricular drain, or EVD) or by means of a mini-strain gauge placed within the brain tissue. Each sensor must be placed through an individual burr hold drilled through the skull. Each sensor measures pressure over time, but the spatial dynamics of ICP have not been studied yet. Thus, the development of a new high-sensitive pressure sensor array is very desirable for monitoring the pressure vectors in the injured brain.

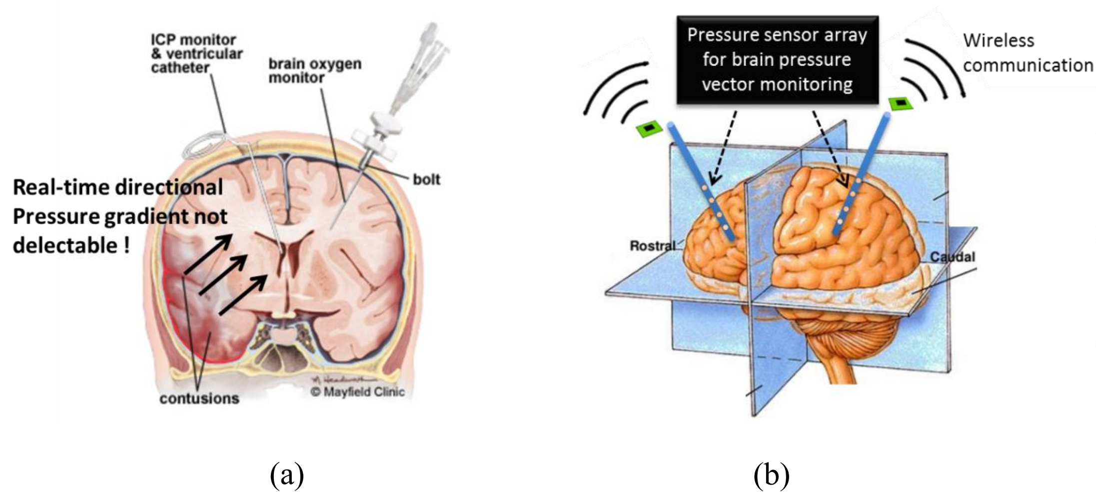

(a) (b)

Figure 5-1. Illustration of brain monitoring: (a) Current approach: single ICP, the real-time directional pressure gradient is not detectable and (b) New approach: lab-on-a-tube with pressure sensor arrays for monitoring pressure gradient and evaluating the pressure vectors within the skull.

Pressure sensor array

Concept

A lab-on-a-tube high sensitive temperature and pressure sensor array is designed as shown Fig. 5-2. The sensor array is firstly developed on polyimide and then spiral-rolled to form a catheter to detect the intracranial pressure gradient and brain temperature.

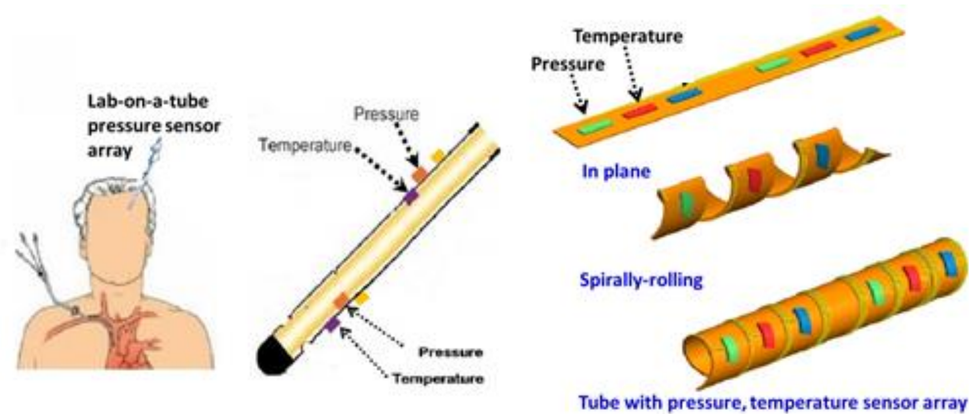

Figure 5-2. Spirally-assembled lab-on-a-tube integrated with pressure and temperature sensors.

Design

A temperature and pressure sensor array with four sensing units (1× 4) was designed with footprint of ~ 4 mm^2 for each unit and center-to-center distance of 4 mm. Each sensing unit contains a polysilicon piezoresistor for pressure sensing, and a polysilicon thermistor for

temperature sensing and eliminate the temperature effect for pressure determination. The dimension of the membrane was designed as the single pressure sensor as shown in Fig. 5-3.

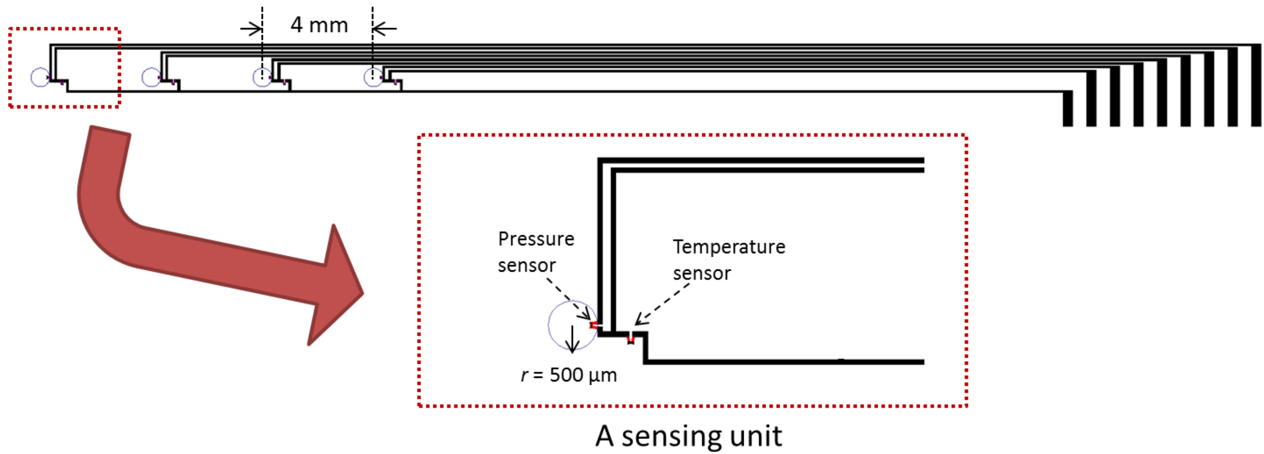

Figure 5-3. Layout of pressure and temperature sensors array.

Microfabrication

The microfabrication process of the sensor array was the same as developing a single pressure sensor. Polysilicon resistors with aluminum electrical leads were developed on PI2611 firstly, followed by the passivation layer and gap layer development. Contacting pads opening was achieved by dry etching PI2611. After the microfabrication process, the devices were peeled off from supporting silicon wafer for test. Fabricated devices are shown in Fig. 5-4.

Figure 5-4. Fabricated pressure sensor array.

Interface Circuit

Interface circuit was developed to provide constant current for the sensor array and also take output signal from the array into DAQ module to view the data on LabView. The constant current is designed to be 10 μA to minimize self-heating effect. The voltage of the each polysilicon resistor is the output signal. The resistance of each polysilicon resistor is designed as 60 kΩ. According to the sensitivity of the pressure sensor (6×10^{-4} / mmHg), the output voltage change for each 1mmHg pressure change will be around 0.36 mV with the constant current supply of 10 μA. To achieve a reasonable signal-to-noise ratio, the voltage accuracy of the

interface circuit should be in order 0.1 mV resolution. Any noise above the resolution will have an impact on the accuracy of the output voltage.

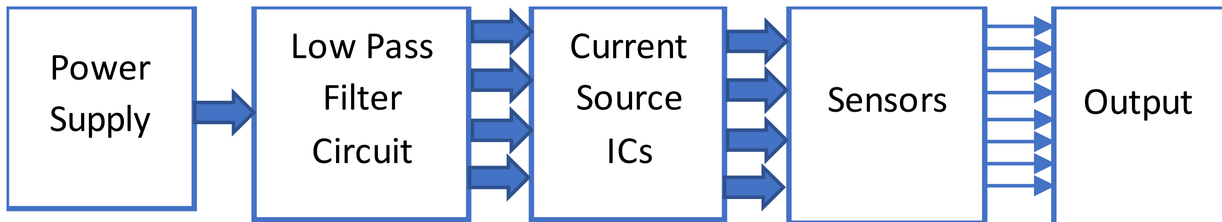

Figure 5-5. Block diagram of the circuitry.

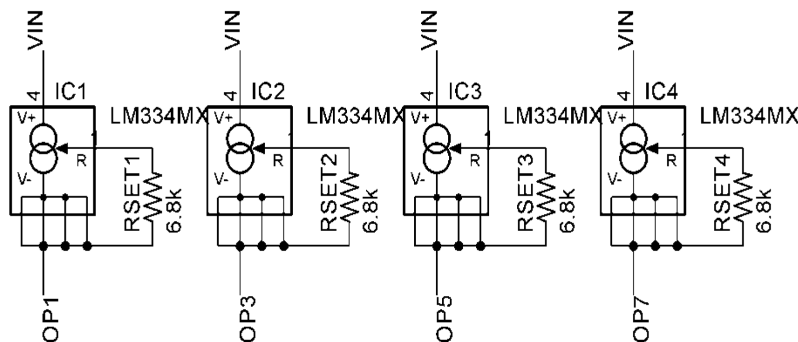

Figure 5-6. Current source IC Schematic.

Fig. 5-5 shows the block diagram of the circuit. A first order passive low pass filter to remove 50-60 Hz noise has been applied. The supply voltage for the current source is from 2.5-3.3 V. Low pass filter has been added into the input voltage circuitry to stabilize the voltage to the current source ICs. No passive filtering circuit was applied as the output voltage due to voltage divider configuration will remain constant even if there was a change in resistance.

Active filters will bring out an additional noise to the circuitry. A bypass capacitor of 10 nF has been connected at the input of the circuitry to dampen any AC noise or fluctuations.

Fig. 5-6 shows the schematic of each current source IC. LM334MX is an adjustable type current source. The current range of IC is from 10 μA - 10 mA. Since the constant current has been set as10 μA, Rset of 6.8 kΩ is chosen according to the datasheet of the IC.

The nine pins of the sensor contact pad was connected to the PCB which provides constant current and output voltage was taken with a National Instrument (NI) data acquisition (DAQ) Card. Fig. 5-7 shows the developed PCB of the designed interface circuit.

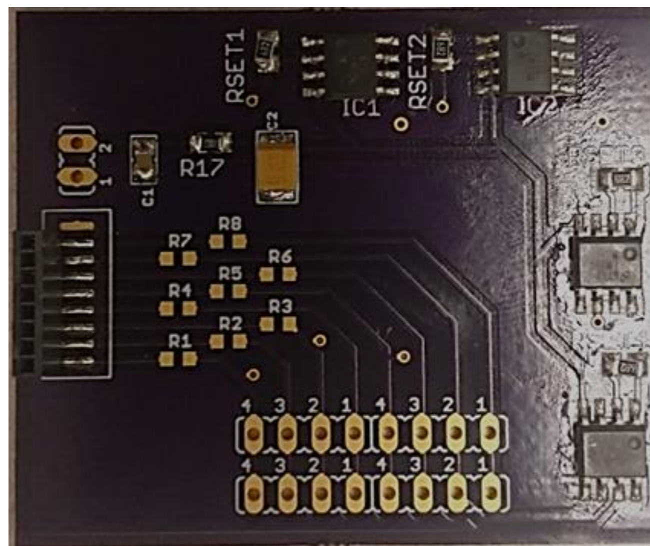

Figure 5-7. PCB of designed circuit.

Experimental Results

To test the sensor array's response to pressure and temperature, and examine the cross-talk between sensors, the sensor array was placed on a hotplate at room temperature of 25 °C. Lead rods with the radius of 500 μm and weight of 0.01 g, 0.02 g, 0.05 g were used to generate 1 mmHg, 2 mmHg, 5 mmHg pressure on the pressure sensor membrane (radius: 500 μm). To generate temperature change, the hot plate temperature was set to 40 °C for the sensor array to go through a temperature change of 25 °C to 40 °C. 10 μA constant current was supplied by the interface circuit to each temperature and pressure sensing elements and voltage was measured and recorded with Labview program. The pressure and temperature sensors were measured for two adjacent units to examine cross-talk. Signal from the two units, which include four polysilicon piezoresistors, were real-time and simultaneously recorded.

Fig. 5-8 shows the results of the temperature sensors from two units. Resistance of the polysilicon resistors decreases with temperature increase. Thus, voltage decreases were observed for temperature sensors from both unitswith the same slope. The resistance and voltage got stabled after hotplate reached to 40 °C. Fig. 5-9 shows the results of the pressure sensors for the twounits. As shown in the figure, in addition to the change to temperature, clear step change of voltage can be seen when pressure was applied or removed from the pressure sensor. 1, 2 and 5 mmHg generated about 0.8 mV, 1.5 mV and 4mV output voltages change respectively. No interference is shown between the two pressure sensors, indicating a low cross-talk.

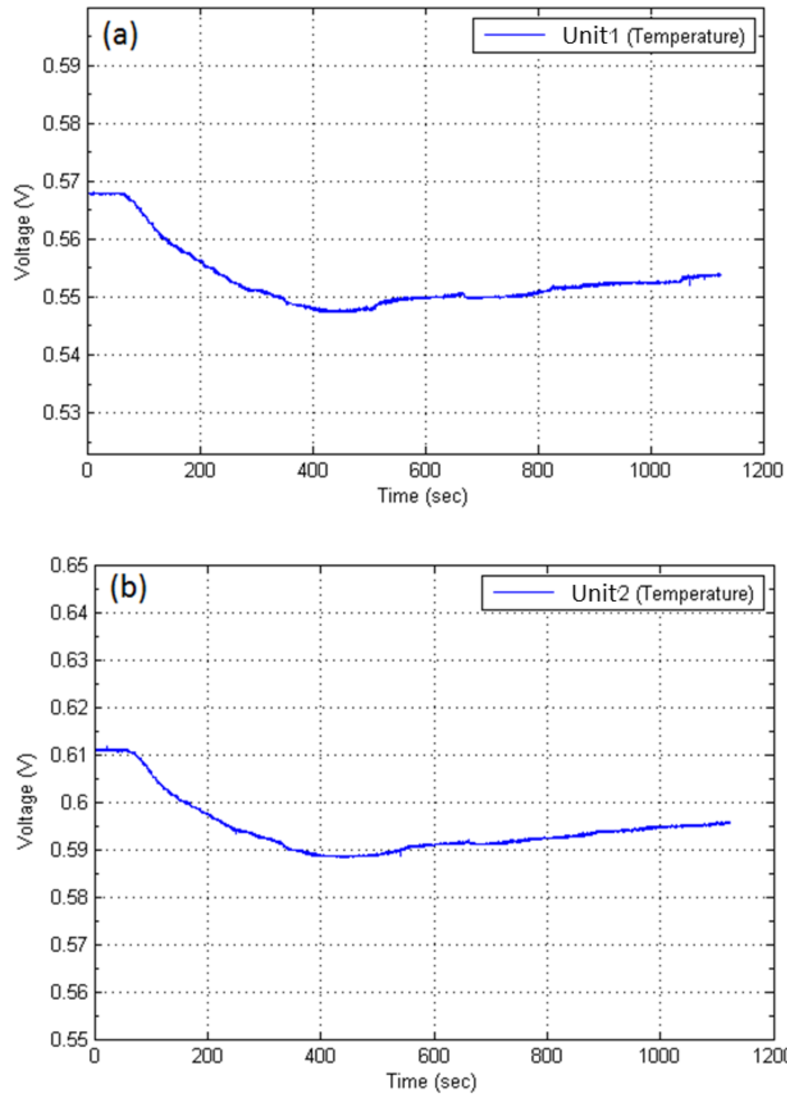

Figure 5-8. Temperature sensors of two adjacent sensing units responded to temperature change. Voltage decreased for both temperature sensors with the same slope as temperature increased, and the voltage got stabled after hotplate reached to the set temperature of 40 °C.

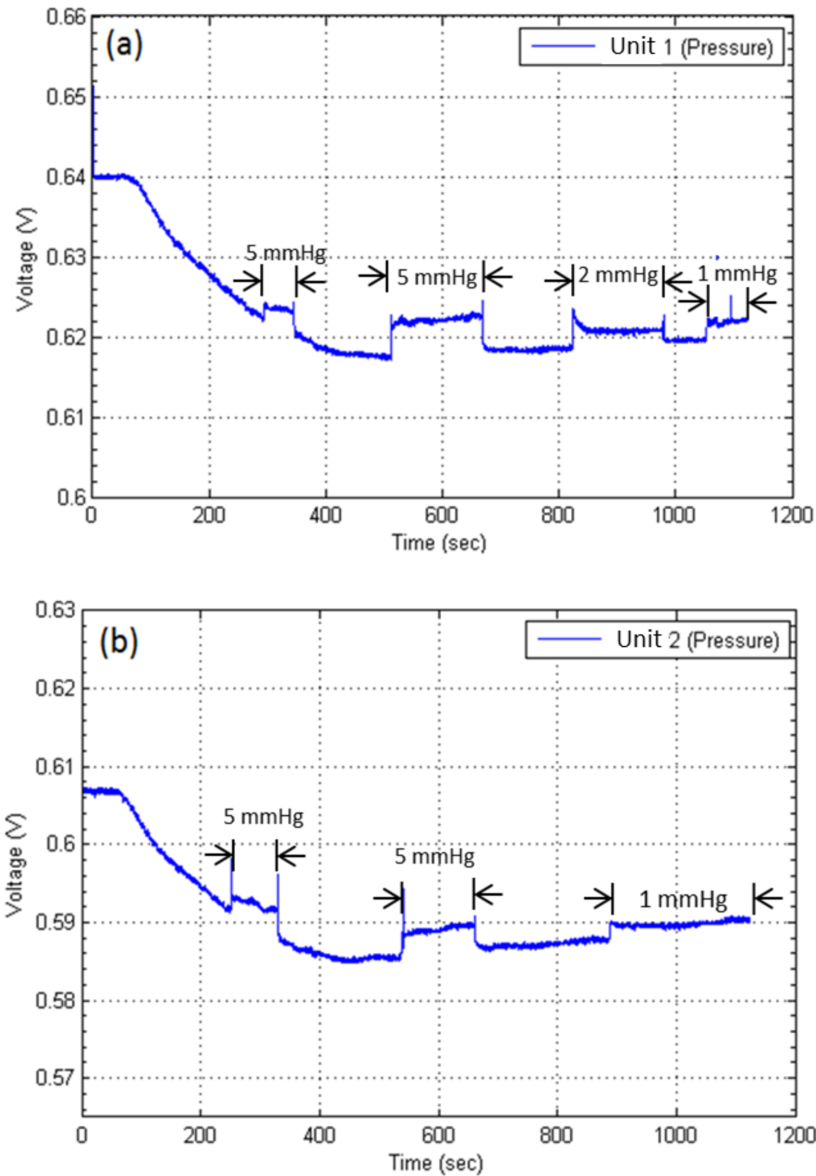

Figure 5-9. Pressure sensors of two adjacent units responded to both applied pressure and temperature. Pressures of 1 mmHg, 2 mmHg, and 5 mmHg were applied on the two elements and about 0.8 mV, 1.5 mV and 4 mV output voltages change were generated respectively. No interference is shown between the two sensors, indicating a low cross-talk.

A brain emulation model was further developed by filling a closed spherical ball (diameter: 10 mm) with agar gel (agar water weight ratio: 1.5%). As shown in Fig. 5-10, a balloon was placed in the ball and connected to a syringe of 60 ml. After inserting the pressure and temperature sensor array device, epoxy was applied to the entire surface of the spherical ball to develop a closed system. Syringe was then pushed or pulled to induce balloon expansion or shrinkage, and thus the pressure increase or decrease. 10 μA constant current was applied to each pressure and temperature sensor and voltage was recorded with Labview program with the 100 Hz frequency and displayed with laptop.

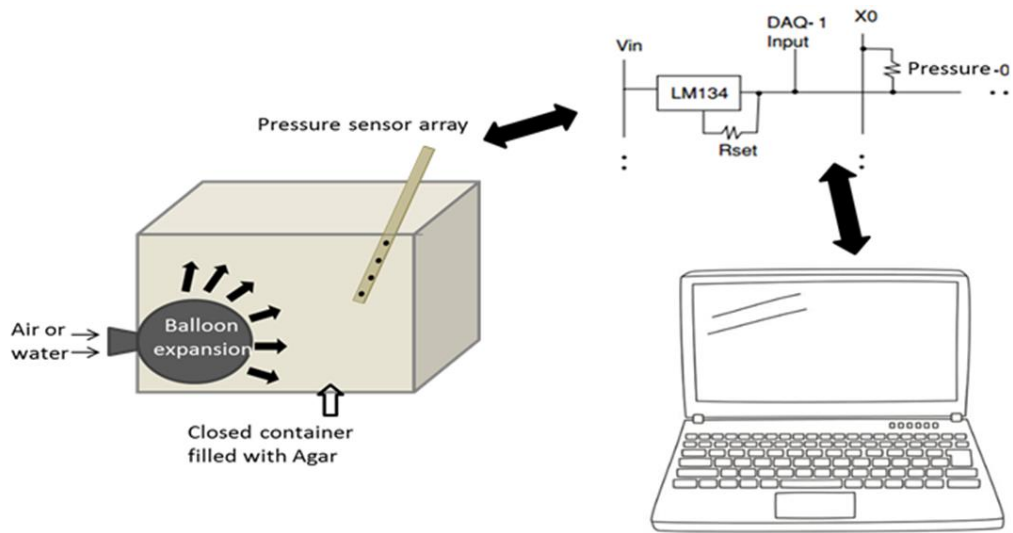

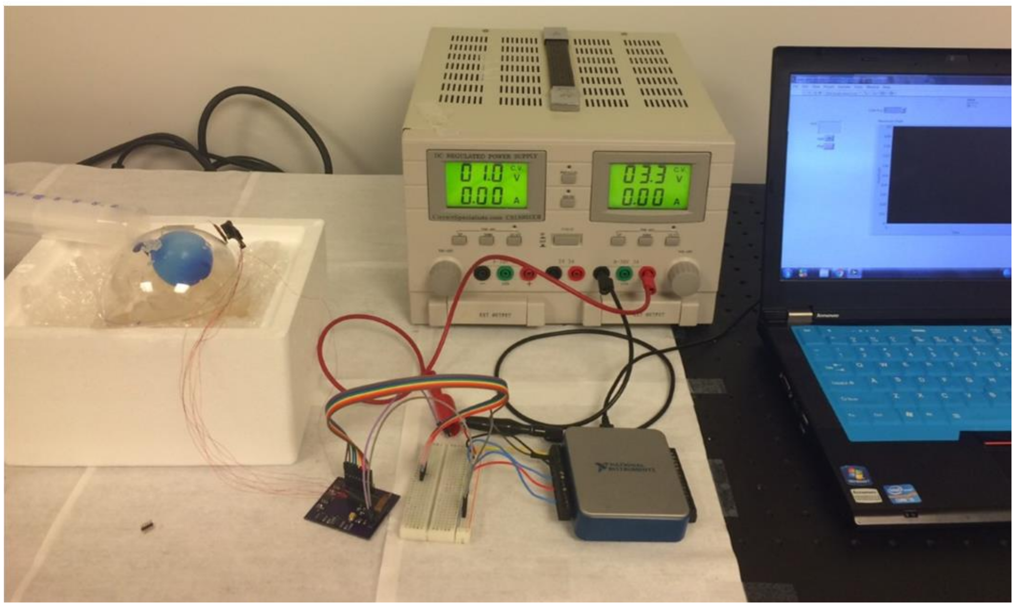

Figure 5-10. Test setup: a brain emulation model was developed for real-time pressure and temperature monitoring. 10 μA input constant current was applied with interface circuit and output voltage was recorded with Labview program with the 100 Hz frequency and displayed with laptop.

Real-time and dynamic pressure and temperature changes were monitored by the sensor array. Two sets of experiment results are shown in Fig. 5-11. As shown in Fig. 5-11, the output voltages of all three pressure sensors increased immediately with the balloon expansion with the same slope and no time difference, which means the pressure elevated simultaneously in the closed spherical ball.

To further check whether there was pressure gradient between each sensor, the output voltages of each pressure sensing arrays were normalized and compared. As shown in Fig. 5-12, the output voltages of the three pressure sensors overlaps well, which means there is no pressure gradient in the experiment.

To generate and measure pressure gradient, experiment model needs to be further explored in the future. Pressure change rates, the relative position between the balloon and sensor array, and directions of the sensor array need further optimization. However, it is very feasible to measure the pressure gradient using the developed pressure array. As shown in Fig. 5-12, the developed sensor array had high sensitivity and fast response time to detect the pressure differences or gradients if any. The development of an appropriate model may be another challenge for modelling the pressure variation in brain. In order to understand the correlation and effect between the source of pressure and the position of sensors, further experiments should be performed.

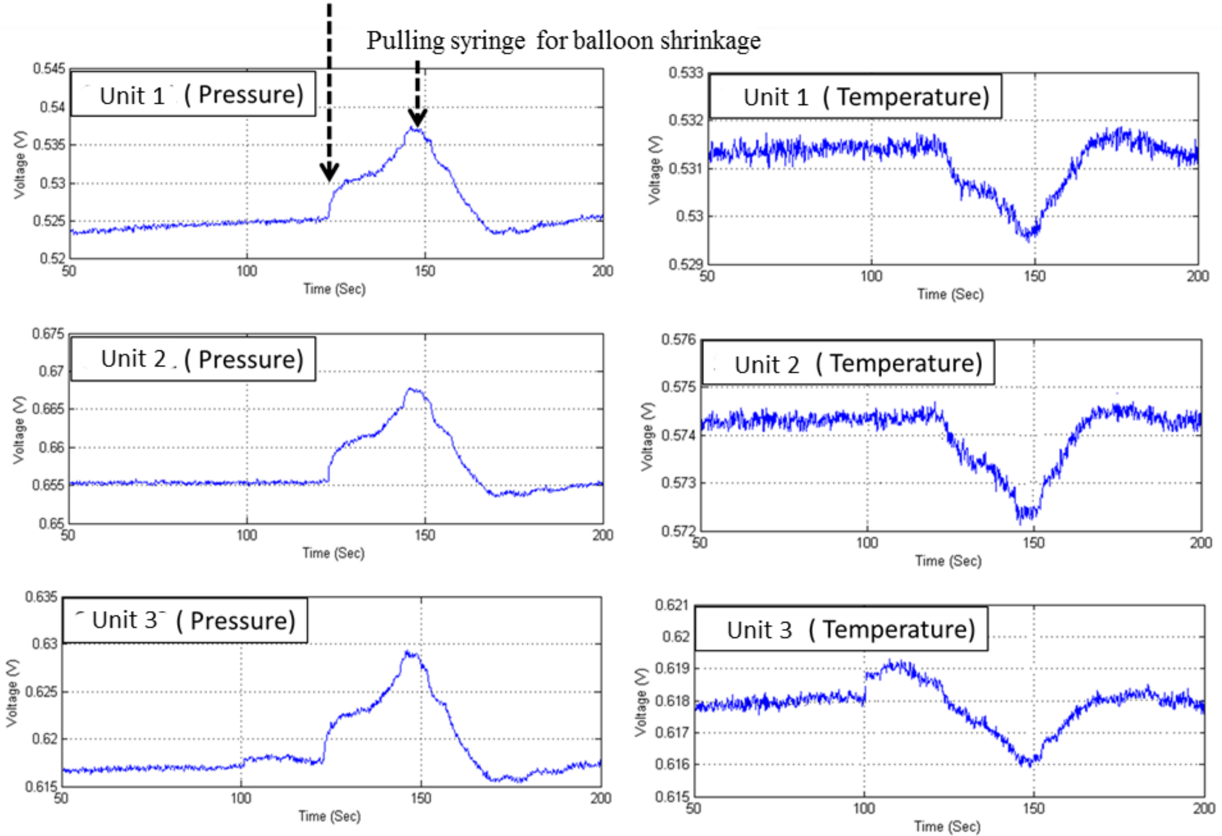

Figure 5-11. Real-time dynamic pressure and temperature measurement with a balloon expansion: the output voltage of all three pressure sensors changed with the pressure with the same slope, which increased when pushing the syringe to expand the balloon volume and increase the pressure inside the closed spherical ball, and decreased when pulling the syringe; the output voltage of temperature sensors also changed when pressure changes: which means temperature increased when agar pushed against the sensor.

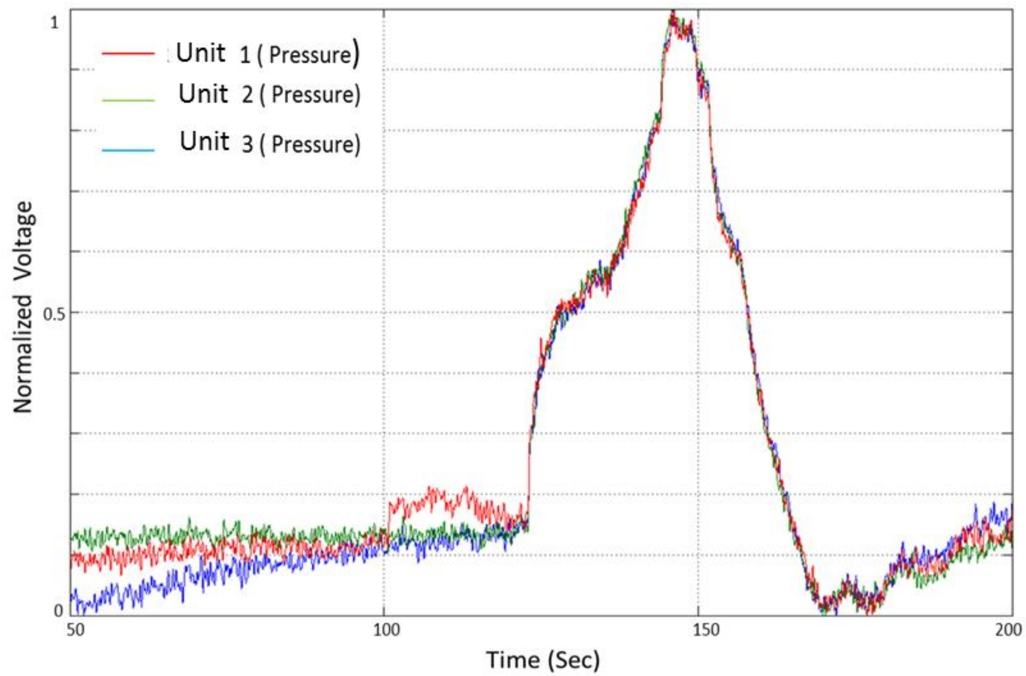

Figure 5-12. Comparison of normalized output voltage pressure of pressure sensors in three sensing units: Output voltages overlap well for three sensors, which mean there is no pressure gradient in the experiment.

Summary

A polysilicon based pressure and temperature sensor array was developed in this work. Following the same dimension of single pressure and temperature sensor, a 1×4 pressure and temperature sensor array with the footprint of 4 mm^2 and center distance of 4 mm was designed and developed. Interface circuit was designed to provide 10 μA constant current to the four pressure and temperature sensingunits. Labview program was designed to acquire and display the multichannel signal with a frequency of 100 Hz. The real-time simultaneous measurement of pressure and temperature was carried out. And the results showed a multichannel dynamic change to pressure and temperature with no interference. Thus, an array with the functionality of simultaneous pressure and temperature was successfully realized.

The pressure and temperature sensor array was further characterized in a brain emulation model and dynamic pressure and temperature measurement results were obtained. The preliminary experiment didn’t show pressure gradient. But the developed sensor array had enough sensitivity to detect the pressure differences or gradients in brain if any. Different pressure change rates and directions need to be further explored in the future for a thorough analysis of the gradient and vector of ICP.

CHAPTER 6

CONCLUTION

A high quality polysilicon thin film was directly developed on flexible PI2611 substrate with simple, fast, and low cost aluminum induced crystallization (AIC) as sensing material for ICP and ICT monitoring in this work. The polycrystalline structure and constitution of the film was verified with XRD, SEM, TEM and EDS measurements. Sheet resistance was measured with transfer length method (TLM). The results showed a high quality continuous P-type polysilicon film with the crystals' average size of 49 nm. The work shows that high quality polysilicon thin film can be directly developed on flexible substrate with ultra-simple, low cost, and fast process. With the wafer-size based high yield and uniformity, the developed polysilicon thin film shows a great potential for developing manufactural polysilicon-based flexible devices.

Based on the developed polysilicon thin film, a flexible thermistor array was designed and developed for brain temperature monitoring. The array has low mechanical stiffness and the ultra-small dimension of developed polysilicon thermistors can be applied for high spatial resolution measurement with sufficient accuracy and resolution. The developed polysilicon thermistors has achieved good *in vitro* performance with a sensitivity of -0.0031/°C, response

time of 1.5 s, a resolution of 0.1 °C, thermal hysteresis less than 0.1°C, and long term stability with drift less than 0.3 °C for 3 days of continuous operation in water. *In vivo* tests of the polysilicon thermistor showed a low noise level of 0.025±0.03 °C and the expected transient temperature increase associated with cortical spreading depolarization.

Furthermore, high sensitive flexible pressure sensor was designed and developed for ICP measurement with the polysilicon thin film. The developed flexible pressure sensor was fully characterized in liquid environment. And the results showed a sensitivity of 6×10^{-4} / mmHg, resolution of 1 mmHg, and hysteresis of less than 1 mmHg for the pressure range of 10 to 20 mmHg. The polysilicon based flexible piezoresistive pressure developed in this work has successfully achieved the sensitivity and resolution required for ICP monitoring, and showed the feasibility of developing the ICP sensor with high throughput and low cost.

Finally, a 1 × 4 polysilicon based pressure and temperature sensor array was designed and developed for monitoring plausible pressure vectors in the TBI. Following the same dimension design of single pressure and temperature sensor, a 1 × 4 sensor array with the center distance of 4 mm was developed and fully characterized. The real-time simultaneous measurement of pressure and temperature was performed. And the experiment results showed a multichannel dynamic change to pressure and temperature with no interference. Thus, an integrated ICP and ICT array, which can provide simultaneous monitoring of pressure and temperature, was successfully realized.

The pressure and temperature sensor array was further characterized in a brain emulation model and dynamic pressure and temperature measurement results were obtained. The preliminary experiment results didn’t show pressure gradient. However, the developed sensor

array had enough sensitivity to detect the pressure differences or gradients in brain if any. In the future, different pressure change rates and directions need to be further explored for a thorough analysis of the gradient and vector of ICP.

In conclusion, this work has proposed, developed and fully characterized innovative polysilicon-based flexible pressure and temperature sensors for ICP and ICT monitoring. . Polysilicon thin film has been showed to be developed on flexible polyimide with low cost, simple, and high yield process. The developed sensors have met the requirements of ICP and ICT monitoring with high sensitivity, high resolution, fast response, and low hysteresis. The sensors can be easily integrated with other biosensors and ECoG electrodes for a thorough brain monitoring with minimal cross-talk and interference.

REFERENCES

[1] Faul M, Xu L, Wald M, Coronado V. Traumatic Brain Injury in the United States: Emergency Department Visits, Hospitalizations and Deaths 2002–2006. Atlanta GA Cent Dis Control Prev Natl Cent Inj Prev Control. 2010;

[2] Corrigan JD, Selassie AW, Orman JAL." The epidemiology of traumatic brain injury. J Head Trauma Rehabil", 25(2), pp: 72–80, 2010.

[3] Faul M, Wald MM, Rutland-Brown W, Sullivent EE, Sattin RW. Using a Cost-Benefit Analysis to Estimate Outcomes of a Clinical Treatment Guideline: Testing the Brain Trauma Foundation Guidelines for the Treatment of Severe Traumatic Brain Injury: J Trauma Inj Infect Crit Care, 63(6), pp: 1271–1278, 2007.

[4] Malec JF, Brown AW, Leibson CL, Flaada JT, Mandrekar JN, Diehl NN, Perkins PK. The Mayo Classification System for Traumatic Brain Injury Severity. J Neurotrauma, 24(9), pp: 1417–1424, 2016.

[5] Cooper DJ, Rosenfeld JV, Murray L, Arabi YM, Davies AR, D'Urso P, Kossmann T, Ponsford J, Seppelt I, Reilly P, others. Decompressive craniectomy in diffuse traumatic brain injury. N Engl J Med, 364(16), pp: 1493–1502, 2011.

[6] Andrews PJD, Sinclair HL, Rodriguez A, Harris BA, Battison CG, Rhodes JKJ, Murray GD. Hypothermia for Intracranial Hypertension after Traumatic Brain Injury. N Engl J Med., 373(25), pp: 2403–2412, 2015.

[7] Wright DW, Yeatts SD, Silbergleit R, Palesch YY, Hertzberg VS, Frankel M, Goldstein FC, Caveney AF, Howlett-Smith H, Bengelink EM, Manley GT, Merck LH, Janis LS,

Barsan WG. Very Early Administration of Progesterone for Acute Traumatic Brain Injury. N Engl J Med, 371(26), pp:2457–2466, 2014.

[8] Collaborators CT, others. Final results of MRC CRASH, a randomised placebo-controlled trial of intravenous corticosteroid in adults with head injury—outcomes at 6 months. The Lancet. 365(9475), pp: 1957–1959, 2005.

[9] Thornhill S. Disability in young people and adults one year after head injury: prospective cohort study. BMJ, 320(7250), pp: 1631–1635, 2000.

[10] Foreman BP, Caesar RR, Parks J, Madden C, Gentilello LM, Shafi S, Carlile MC, Harper CR, Diaz-Arrastia RR. Usefulness of the Abbreviated Injury Score and the Injury Severity Score in Comparison to the Glasgow Coma Scale in Predicting Outcome After Traumatic Brain Injury: J Trauma Inj Infect Crit Care, 62(4), pp:946–950, 2007.

[11] Steyerberg EW, Mushkudiani N, Perel P, Butcher I, Lu J, McHugh GS, Murray GD, Marmarou A, Roberts I, Habbema JDF, others. Predicting outcome after traumatic brain injury: development and international validation of prognostic scores based on admission characteristics. PLoS Med.5(8):e165, 2008.

[12] Juul N, Morris GF, Marshall SB, Marshall LF. Intracranial hypertension and cerebral perfusion pressure: influence on neurological deterioration and outcome in severe head injury*. J Neurosurg, 92(1), pp:1–6, 2000

[13] Li, Chunyan, Pei-Ming Wu, WooSeok Jung, Chong H. Ahn, Lori A. Shutter, and Raj K. Narayan. "A novel lab-on-a-tube for multimodality neuromonitoring of patients with traumatic brain injury (TBI)." Lab on a Chip 9, no. 14 (2009): 1988-1990.

[14] Tisdall, M. M., and M. Smith. "Multimodal monitoring in traumatic brain injury: current status and future directions." British journal of anaesthesia 99, no. 1 (2007): 61-67.

[15] Tisdall, Martin M., and Martin Smith. "Cerebral microdialysis: research technique or clinical tool." British journal of anaesthesia 97, no. 1 (2006): 18-25.

[16] Smith M. Monitoring intracranial pressure in traumatic brain injury. Anesth Analg 2008; 106: 240-248

[17] Brain Trauma Foundation, American Association of Neurological Surgeons, Congress of Neurological Surgeons. Guidelines for the management of severe traumatic brain injury. J Neurotrauma. Suppl 1:S1-106, 2007

[18] Badri S, Chen J, Barber J, Temkin NR, Dikmen SS, Chesnut RM, Deem S, Yanez ND, Treggiari MM. Mortality and long-term functional outcome associated with intracranial pressure after traumatic brain injury. Intensive Care Med. 38(11), pp: 1800–1809, 2012

[19] Güiza F, Depreitere B, Piper I, Citerio G, Chambers I, Jones PA, Lo T-YM, Enblad P, Nillson P, Feyen B, Jorens P, Maas A, Schuhmann MU, Donald R, Moss L, Van den Berghe G, Meyfroidt G. Visualizing the pressure and time burden of intracranial hypertension in adult and paediatric traumatic brain injury, 41(6), pp:1067–1076, 2015

[20] Holloway, Kathryn L., Tom Barnes, Sung Choi, Ross Bullock, Lawrence F. Marshall, Howard M. Eisenberg, John A. Jane, John D. Ward, Harold F. Young, and Anthony Marmarou. "Ventriculostomy infections: the effect of monitoring duration and catheter exchange in 584 patients." Journal of neurosurgery 85, no. 3, pp: 419-424, 1996

[21] Yau, Yun-Hom, Ian R. Piper, Richard E. Clutton, and Ian R. Whittle. "An experimental evaluation of the Spiegelberg intracranial pressure and intracranial compliance monitor: Technical note." Journal of neurosurgery 93, no. 6, pp: 1072-1077, 2000

[22] Martínez-Mañas, Rosa M., David Santamarta, José M. de Campos, and Enric Ferrer. "Camino® intracranial pressure monitor: prospective study of accuracy and complications." Journal of Neurology, Neurosurgery & Psychiatry 69, no. 1, pp: 82-86, 2000

[23] Al-Tamimi, Yahia Z., Adel Helmy, Seb Bavetta, and Stephen J. Price. "Assessment of zero drift in the Codman intracranial pressure monitor: a study from 2 neurointensive care units." Neurosurgery 64, no. 1, pp: 94-99, 2009

[24] Eide, Per Kristian. "Comparison of simultaneous continuous intracranial pressure (ICP) signals from a Codman and a Camino ICP sensor." Medical engineering & physics 28, no. 6, pp: 542-549, 2006

[25] Rossi, S., E. Roncati Zanier, I. Mauri, A. Columbo, and N. Stocchetti. "Brain temperature, body core temperature, and intracranial pressure in acute cerebral damage." Journal of Neurology, Neurosurgery & Psychiatry 71, no. 4, pp: 448-454, 2001

[26] Mrozek, Ségolène, Fanny Vardon, and Thomas Geeraerts. "Brain temperature: physiology and pathophysiology after brain injury." Anesthesiology research and practice 2012

[27] J. Soukup, A. Zauner, E. M. R. Doppenberg et al., “The importance of brain temperature in patients after severe head injury: relationship to intracranial pressure, cerebral perfusion pressure, cerebral blood flow, and outcome,” Journal of Neurotrauma, vol. 19, no. 5, pp. 559–571, 2002

[28] R. H. Sacho, A. Vail, T. Rainey, A. T. King, and C. Childs, “The effect of spontaneous alterations in brain temperature on outcome: a prospective observational cohort study in patients with severe traumatic brain injury,” Journal of Neurotrauma, vol. 27, no. 12, pp. 2157–2164, 2010

[29] R. Busto, W. D. Dietrich, M. Globus, I. Valdes, P. Scheinberg, and M. D. Ginsberg, “Small differences in intraischemic brain temperature critically determine the extent of ischemic neuronal injury,” Journal of Cerebral Blood Flow and Metabolism, vol. 7, no. 6, pp. 729–738, 1987

[30] D. M. Greer, S. E. Funk, N. L. Reaven, M. Ouzounelli, and G. C. Uman, “Impact of fever on outcome in patients with stroke and neurologic injury: a comprehensive meta-analysis,” Stroke, vol. 39, no. 11, pp. 3029–3035, 2008

[31] W. D. Dietrich, O. Alonso, M. Halley, and R. Busto, “Delayed posttraumatic brain hyperthermia worsens outcome after fluid percussion brain injury: a light and electron microscopic study in rats,” Neurosurgery, vol. 38, no. 3, pp. 533–541, 1996

[32] McDannold, N. "Quantitative MRI-based temperature mapping based on the proton resonant frequency shift: review of validation studies." International journal of hyperthermia 21, no. 6, pp: 533-546, 2005

[33] Schwab, S., M. Spranger, A. Aschoff, T. Steiner, and W. Hacke. "Brain temperature monitoring and modulation in patients with severe MCA infarction." Neurology 48, no. 3 pp: 762-767, 1997

[34] Rossi, S., E. Roncati Zanier, I. Mauri, A. Columbo, and N. Stocchetti. "Brain temperature, body core temperature, and intracranial pressure in acute cerebral damage." Journal of Neurology, Neurosurgery & Psychiatry 71, no. 4, pp: 448-454, 2001

[35] Huschak, Gerald, Thomas Hoell, Christian Hohaus, Christian Kern, Yvonne Minkus, and Hans-Jörg Meisel. "Clinical evaluation of a new multiparameter neuromonitoring device: measurement of brain tissue oxygen, brain temperature, and intracranial pressure." Journal of neurosurgical anesthesiology 21, no. 2, pp: 155-160, 2009

[36] Stewart, Campbell, Iain Haitsma, Zsolt Zador, Diane Morabito, Geoffrey Manley, Guy Rosenthal, and J. Claude Hemphill III. "The new Licox combined brain tissue oxygen and brain temperature monitor: assessment of in vitro accuracy and clinical experience in severe traumatic brain injury." Neurosurgery 63, no. 6, pp: 1159-1165, 2008

[37] Soukup, Jens, Alois Zauner, Egon MR Doppenberg, Matthias Menzel, Charlotte Gilman, Ross Bullock, and Harold F. Young. "Relationship between brain temperature, brain chemistry and oxygen delivery after severe human head injury: the effect of mild hypothermia." Neurological research 24, no. 2, pp: 161-168, 2002

[38] http://www.integralife.com

[39] Opp, MARK R., F. Obal, and JAMES M. Krueger. "Effects of alpha-MSH on sleep, behavior, and brain temperature: interactions with IL 1." American Journal of Physiology-Regulatory, Integrative and Comparative Physiology 255, no. 6, pp: R914-R922, 1988

[40] Li, Chunyan, Pei-Ming Wu, Zhizhen Wu, Chong H. Ahn, David LeDoux, Lori A. Shutter, Jed A. Hartings, and Raj K. Narayan. "Brain temperature measurement: A study of in vitro accuracy and stability of smart catheter temperature sensors." Biomedical microdevices 14, no. 1, pp: 109-118, 2012

[41] Li, Chunyan, Frank E. Sauser, Richard G. Azizkhan, Chong H. Ahn, and Ian Papautsky. "Polymer flip-chip bonding of pressure sensors on a flexible Kapton film for neonatal catheters." Journal of Micromechanics and Microengineering 15, no. 9, pp: 1729, 2005

[42] Lichtenwalner, D.J., Hydrick, A. E., Kingon, A.I., “Flexible thin film temperature and strain sensor array utilizing a novel sensing concept”, Sensors and Actuators, A: Physical, 135(2), pp. 593-597, 2007.

[43] Someya, Takao, Tsuyoshi Sekitani, Shingo Iba, Yusaku Kato, Hiroshi Kawaguchi, and Takayasu Sakurai. "A large-area, flexible pressure sensor matrix with organic field-effect transistors for artificial skin applications." Proceedings of the National Academy of Sciences of the United States of America 101, no. 27, pp: 9966-9970, 2004

[44] Someya, Takao, Yusaku Kato, Tsuyoshi Sekitani, Shingo Iba, Yoshiaki Noguchi, Yousuke Murase, Hiroshi Kawaguchi, and Takayasu Sakurai. "Conformable, flexible, large-area networks of pressure and thermal sensors with organic transistor active matrixes." Proceedings of the National Academy of Sciences of the United States of America 102, no. 35, pp: 12321-12325, 2005.

[45] Mannsfeld, Stefan CB, Benjamin CK Tee, Randall M. Stoltenberg, Christopher V. HH Chen, Soumendra Barman, Beinn VO Muir, Anatoliy N. Sokolov, Colin Reese, and Zhenan Bao. "Highly sensitive flexible pressure sensors with microstructured rubber dielectric layers." Nature materials 9, no. 10, pp: 859-864, 2010.

[46] Miller, Sophie, and Zhenan Bao. "Fabrication of flexible pressure sensors with microstructured polydimethylsiloxane dielectrics using the breath figures method." Journal of Materials Research 30, no. 23, pp: 3584-3594, 2015

[47] Chen, Lisa Y., Benjamin C-K. Tee, Alex L. Chortos, Gregor Schwartz, Victor Tse, Darren J. Lipomi, H-S. Philip Wong, Michael V. McConnell, and Zhenan Bao. "Continuous wireless pressure monitoring and mapping with ultra-small passive sensors for health monitoring and critical care." Nature communications 5, 2014.

[48] Akiyama, Morito, Yukari Morofuji, Toshihiro Kamohara, Keiko Nishikubo, Masayoshi Tsubai, Osamu Fukuda, and Naohiro Ueno. "Flexible piezoelectric pressure sensors using oriented aluminum nitride thin films prepared on polyethylene terephthalate films." Journal of applied physics 100, no. 11, pp: 114318, 2006

[49] Li, Chunyan, Pei-Ming Wu, Soohyun Lee, Andrew Gorton, Mark J. Schulz, and Chong H. Ahn. "Flexible dome and bump shape piezoelectric tactile sensors using PVDF-TrFE copolymer." Journal of Microelectromechanical Systems 17, no. 2 (2008): 334-341.

[50] Harada, Shingo, Wataru Honda, Takayuki Arie, Seiji Akita, and Kuniharu Takei. "Fully printed, highly sensitive multifunctional artificial electronic whisker arrays integrated with strain and temperature sensors." ACS nano 8, no. 4, pp: 3921-3927, 2014.

[51] Athanassiou, Evagelos K., Robert N. Grass, and Wendelin J. Stark. "Large-scale production of carbon-coated copper nanoparticles for sensor applications." Nanotechnology 17, no. 6, pp: 1668, 2006.

[52] Gong, Shu, Willem Schwalb, Yongwei Wang, Yi Chen, Yue Tang, Jye Si, Bijan Shirinzadeh, and Wenlong Cheng. "A wearable and highly sensitive pressure sensor with ultrathin gold nanowires." Nature communications, 5, 2014.

[53] Pan, Lijia, Alex Chortos, Guihua Yu, Yaqun Wang, Scott Isaacson, Ranulfo Allen, Yi Shi, Reinhold Dauskardt, and Zhenan Bao. "An ultra-sensitive resistive pressure sensor based on hollow-sphere microstructure induced elasticity in conducting polymer film." Nature communications 5, 2014.

[54] Stampfer, C., T. Helbling, Dirk Obergfell, B. Schöberle, M. K. Tripp, A. Jungen, Siegmar Roth, V. M. Bright, and C. Hierold. "Fabrication of single-walled carbon-nanotube-based pressure sensors." Nano letters 6, no. 2, pp: 233-237, 2006.

[55] Lipomi, Darren J., Michael Vosgueritchian, Benjamin CK Tee, Sondra L. Hellstrom, Jennifer A. Lee, Courtney H. Fox, and Zhenan Bao. "Skin-like pressure and strain sensors based on transparent elastic films of carbon nanotubes." Nature nanotechnology 6, no. 12, pp: 788-792, 2011.

[55] Gelamo, R. V., F. P. Rouxinol, C. Verissimo, A. R. Vaz, MA Bica de Moraes, and S. A. Moshkalev. "Low-temperature gas and pressure sensor based on multi-wall carbon nanotubes decorated with Ti nanoparticles." Chemical Physics Letters 482, no. 4, pp: 302-306, 2009.

[56] Kim, Jaemin, Mincheol Lee, Hyung Joon Shim, Roozbeh Ghaffari, Hye Rim Cho, Donghee Son, Yei Hwan Jung et al. "Stretchable silicon nanoribbon electronics for skin prosthesis." Nature communications 5, 2014

[57] Kang, Seung-Kyun, Rory KJ Murphy, Suk-Won Hwang, Seung Min Lee, Daniel V. Harburg, Neil A. Krueger, Jiho Shin et al. "Bioresorbable silicon electronic sensors for the brain." Nature 530, no. 7588, pp: 71-76, 2016

[58] J. Viventi, D.-H. Kim, J.D. Moss, Y.-S. Kim, J.A. Blanco, N. Annetta, A. Hicks, J. Xiao, Y. Huang, D.J. Callans, J.A. Rogers and B. Litt, "A Conformal, Bio-Interfaced Class of Silicon Electronics for Mapping Cardiac Electrophysiology," Science Translational Medicine, 2010.

[59] Huang, Han, K. J. Winchester, A. Suvorova, B. R. Lawn, Y. Liu, X. Z. Hu, J. M. Dell, and L. Faraone. "Effect of deposition conditions on mechanical properties of low-

temperature PECVD silicon nitride films." Materials Science and Engineering: A 435, pp: 453-459, 2006.

[60] Nasuno, Y., M. Kondo, and A. Matsuda. "Microcrystalline silicon thin-film solar cells prepared at low temperature using PECVD." Solar energy materials and solar cells 74, no. 1, pp: 497-503, 2002.

[61] Carey, Paul G., Patrick M. Smith, Steven D. Theiss, and Paul Wickboldt. "Polysilicon thin film transistors fabricated on low temperature plastic substrates." Journal of Vacuum Science & Technology A: Vacuum, Surfaces, and Films 17, no. 4, pp: 1946-1949, 1999.

[62] Giust, Gary K., Thomas W. Sigmon, Paul G. Carey, B. Weiss, and Gary A. Davis. "Low-temperature polysilicon thin-film transistors fabricated from laser-processed sputtered-silicon films." IEEE Electron Device Letters 19, no. 9, pp: 343-344, 1998.

[63] Hsueh, Wei-Chieh, and Si-Chen Lee. "The fabrication of polysilicon thin film transistors by copper-induced lateral crystallization." IEEE Transactions on Electron Devices 50, no. 3, pp: 816-821, 2003.

[64] Herd, S. R., P. Chaudhari, and M_H Brodsky. "Metal contact induced crystallization in films of amorphous silicon and germanium." Journal of Non-Crystalline Solids 7, no. 4, pp: 309-327, 1972.

[65] Nast, Oliver, Tom Puzzer, Linda M. Koschier, Alistair B. Sproul, and Stuart R. Wenham. "Aluminum-induced crystallization of amorphous silicon on glass substrates above and below the eutectic temperature." Applied Physics Letters 73, no. 22, pp: 3214-3216, 1998.

[66] Yoon, Soo Young, Ki Hyung Kim, Chae Ok Kim, Jae Young Oh, and Jin Jang. "Low temperature metal induced crystallization of amorphous silicon using a Ni solution." Journal of applied physics 82, no. 11, pp: 5865-5867, 1997.

[67] M. Iwami, K. Okuno, S. Kamei, T. Ito and A. Hiraki, “Electronic States of Ni-Silicides and Its relation to metal-silicide/Si interfaces” J. Electrochem. Soc.,127 (7), PP.1542-1545, 1980.

[68] Gall, S., M. Muske, I. Sieber, O. Nast, and W. Fuhs. "Aluminum-induced crystallization of amorphous silicon." Journal of Non-Crystalline Solids 299, pp: 741-745, 2002.

[69] Uhlig, Steffen, Stephan Rau, and Günter Schultes. "Piezoresistivity of polycrystalline silicon applying the AIC process-route." Sensors and Actuators A: Physical 172, no. 2, pp: 447-454, 2011.

[70] Patil, Suraj Kumar, Zeynep Celik-Butler, and Donald P. Butler. "Nanocrystalline piezoresistive polysilicon film by aluminum-induced crystallization for pressure-sensing applications." IEEE Transactions on Nanotechnology 9, no. 5, pp: 640-646, 2010.

[71] Patil, Suraj Kumar, Zeynep Çelik-Butler, and Donald P. Butler. "Piezoresistive polysilicon film obtained by low-temperature aluminum-induced crystallization." Thin Solid Films 519, no. 1, pp: 479-486, 2010.

[72] Patil, Suraj K., Zeynep Celik-Butler, and Donald P. Butler. "Microcrystalline piezoresistive polysilicon film obtained by aluminum induced crystallization." In Nanotechnology, 2008. NANO'08. 8th IEEE Conference on, pp. 767-770. IEEE, 2008.

[73] Hatalis, M. K., D. N. Kouvatsos, J. H. Kung, A. T. Voutsas, and J. Kanicki. "Thin film transistors in low temperature as-deposited and reduced-crystallization-time polysilicon on 665° C strain point glass substrates." Thin Solid Films 338, no. 1, pp: 281-285, 1999.

[74] Nast, Oliver, and Stuart R. Wenham. "Elucidation of the layer exchange mechanism in the formation of polycrystalline silicon by aluminum-induced crystallization." Journal of applied physics 88, no. 1, pp: 124-132, 2000.

[75] Nast, Oliver, and Andreas J. Hartmann. "Influence of interface and Al structure on layer exchange during aluminum-induced crystallization of amorphous silicon." Journal of Applied Physics 88, no. 2, pp: 716-724, 2000.

[76] https://www.researchgate.net/file.PostFileLoader.html?id...assetKey...

[77] Vinod, P. N. "Specific contact resistance measurements of the screen-printed Ag thick film contacts in the silicon solar cells by three-point probe methodology and TLM method." Journal of Materials Science: Materials in Electronics 22, no. 9, 1248-1257, 2011.

[78] Ford, Jenny M. "Al/Poly Si specific contact resistivity." Electron Device Letters, IEEE 4, no. 7,255-257, 1983.

[79] Childs, Charmaine. "Human brain temperature: regulation, measurement and relationship with cerebral trauma: part 1," British journal of neurosurgery, Vol. 22, No.4, pp: 486-496, 2008.

[80] Busto, Raul, et al, "Small differences in intraischemic brain temperature critically determine the extent of ischemic neuronal injury," Journal of Cerebral Blood Flow & Metabolism, Vol.7, No.6, pp: 729-738, 1987.

[81] Michenfelder, John D. et al, "The relationship among canine brain temperature, metabolism, and function during hypothermia," Anesthesiology, Vol.75, No.1, pp: 130-136, 1991.

[82] Mrozek, Ségolène, et al, "Brain temperature: physiology and pathophysiology after brain injury," Anesthesiology research and practice, 2012.

[83] Schwab, S., et al, “Brain temperature monitoring and modulation in patients with severe MCA infarction,” Neurology, Vol. 48, No.3, pp: 762-767, 1997.

[84] Marshall I et al, “Measurement of regional brain temperature using proton spectroscopic imaging: validation and application to acute ischemic stroke,” Magn. Reson. Imaging, Vol. 24, No. 6, pp: 438-446, 2006.

[85] Mack MG et al, “MR-guided ablation of head and neck tumors,” Magn Reson Imaging Cli N Am., Vol. 10, No. 4, pp: 707-713, 2002.

[86] Kim JH et al, “Clinical and biological studies of localized hyperthermia,” Cancer Res., Vol. 39, pp: 2258-2261, 1979.

[87] Arthur, R. M., et al. "Non-invasive estimation of hyperthermiatemperatures with ultrasound," International journal of hyperthermia, Vol 21, No.6, pp: 589-600, 2005.

[88] Hand, J. W., et al. "Monitoring of deep brain temperature in infants using multi-frequency microwave radiometry and thermal modelling." Physics in Medicine and Biology, Vol 46, No.7, pp: 1885-1903, 2001.

[89] Rieke, Viola, and Kim Butts Pauly. "MR thermometry," Journal of Magnetic Resonance Imaging, Vol. 27, No. 2, pp: 376-390, 2008.

[90] Kuroda K., et al. “Temperature mapping using the water proton chemical shift: self-referenced method with echo-planar spectroscopic imaging.” Magn Reson Med, Vol. 43, pp: 220-225, 2000.

[91] Michael J. Thrippleton et al, “Reliability of MRSI brain temperature mapping at 1.5 and 3 T,” NMR in Biomedicine, pp: 183-190, 2014.

[92] Krafft, Christoph, et al., “Methodology for fiber-optic Raman mapping and FTIR imaging of metastases in mouse brains,” Analytical and bioanalytical chemistry, Vol. 389, No.4, pp: 1133-1142, 2007.

[93] C. Li et al., “Brain temperature measurement: A study of in vitro accuracy and stability of smart catheter temperature sensors,” Biomed. Microdevices, vol. 14, No. 1, pp: 109-118, 2012.

[94] Schwab, S., et al., “Brain temperature monitoring and modulation in patients with severe MCA infarction,” Neurology, Vol.48, No.3, pp: 762-767, 1997.

[95] E. Kiyatkin et al., “Fluctuations in neural activity during cocaine self-administration: clues provided by brain thermorecording,” Neuroscience, Vol.116, pp: 525–538, 2003.

[96] C. Merino et al., “Application of a digital deconvolution technique to in vivo brain temperature measurement as an index of metabolic regulation,” Lisbon, Portugal, pp: 111–119, 2004.

[97] Raymann et al., “Skin deep: enhanced sleep depth by cutaneous temperature manipulation,” Brain, Vol. 131, No.2, pp: 500-513, 2008.

[98] Thayne R. Larson et al., “An accurate technique for detailed prostatic interstitial temperature-mapping in patients receiving microwave thermal treatment,” Journal of Endourology, Vol. 9, No. 4, pp: 339-347, 1995.

[99] B. C. Lee et al, “Microfabricated neural thermocouple arrays probe for brain research,” in Proc. Int. Solid-state Sens., Actuators Microsyst. Conf., pp: 338-341, 2009.

[100] G Urban et al., “High-resolution Thin-film temperature sensor arrays for medical applications,” Sensors and Actuators, A21-A23, pp: 650-654, 1990.

[101] Moinuddin Ahmed et al., “Temperature sensor in a flexible substrate,” IEEE Sensors, vol. 12, No. 5, pp: 864-869, 2012.

[102] Mylee W. Billard et al., “A flexible vanadium oxide thermistor array for localized temperature field measurements in brain,” IEEE Sensors, vol. 16, No.8, pp: 2211-2212, 2016.

[103] Obermeier, E. et al, “Polysilicon as a material for microsensor applications,” Sensors and Actuators A: Physical, Vol. 30, No.1-2, pp: 149-155, 1992.

[104] Z. Bendekovi et al, “Polysilicon temperature sensor,” Electrotechnical Conference, MELECON 98., 9th Mediterranean, Tel-Aviv, vol. 1, pp. 362-366, 1998

[105] French, P. J. “Polysilicon: a versatile material for microsystems,” Sensors and actuators A: Physical, Vol.99, No.1, pp: 3-12, 2002.

[106] Wu, Z. H et al, “A new high-temperature thermal sensor based on large-grain polysilicon on insulator,” Sensors and Actuators A: Physical, Vol.130, pp: 129-134, 2006.

[107] Wu, Zhizhen et al, “Polysilicon Thin Film Developed on Flexible Polyimide for Biomedical Applications,” JMEMS, in press, 2016.

[108] Tseng, I-Hsiang, et al., “Effect of magnetron sputtered silicon nitride on the water-vapor-permeation-rate of polyimide thin film,” Surface and Coatings Technology, Vol.231, pp: 496-500, 2013.

[109] Li, Chunyan, Kanokwan Limnuson, Zhizhen Wu, Aseer Amin, Anjali Narayan, Eugene V. Golanov, Chong H. Ahn, Jed A. Hartings, and Raj K. Narayan. "Single probe for real-

time simultaneous monitoring of neurochemistry and direct-current electrocorticography." Biosensors and Bioelectronics 77, pp: 62-68, 2016.

[110] Carcia, P. F. et al., "Gas diffusion ultrabarriers on polymer substrates using Al 2 O 3 atomic layer deposition and SiN plasma-enhanced chemical vapor deposition," J. Appl. Phys, Vol.106, pp: 023533, 2009.

[111] Iwamori, Satoru, et al., "Silicon oxide gas barrier films deposited by reactive sputtering," Surface and coatings technology, Vol. 166, No.1, pp: 24-30, 2003.

[112] Tsai, Mei-Hui, et al., "Properties of magnetron-sputtered moisture barrier layer on transparent polyimide/graphene nanocomposite film," Thin Solid Films, Vol.544, pp: 324-330, 2013.

[113] Li, Chunyan, et al., "Development and application of a microfabricated multimodal neural catheter for neuroscience," Biomedical microdevices, Vol.18, No.1, pp: 1-10, 2016.

[114] Brain Trauma Foundation, American Association of Neurological Surgeons, Congress of Neurological Surgeons. Guidelines for the management of severe traumatic brain injury. J Neurotrauma. 2007;24 Suppl 1:S1-106. PMID: 17511534

[115] Chesnut, Randall M., Nancy Temkin, Nancy Carney, Sureyya Dikmen, Carlos Rondina, Walter Videtta, Gustavo Petroni et al. "A trial of intracranial-pressure monitoring in traumatic brain injury." New England Journal of Medicine 367, no. 26, pp: 2471-2481, 2012.

[116] Lane, Peter L., Terry G. Skoretz, Gordon Doig, and Murray J. Girotti. "Intracranial pressure monitoring and outcomes after traumatic brain injury." Canadian Journal of Surgery 43, no. 6, pp: 442, 2000.

[117] Steffen Uhlig, Stephan Rau, Gunter Schultes, "Piezoresistivity of polycrystalline silicon applying the AIC process-route", Sensors and Actuators A 172 pp: 447-454, 2011

[118] S.K. Patil, Z. Celik-Butler, D. Butler, "Characterization of mems piezoresistive pressue sensor using afm", Ultramicroscopy, 110(9), pp.1154-1160, 2010

[119] S.K. Patil, Z. Celik-Butler, D. Butler, "Piezoresistive polysilicon film obtained by low-temperature aluminum-induced crystallization", Thin Solid Films, 519(1) (2010) 479-486.

[120] M. Iwami, K. Okuno, S. Kamei, T. Ito and A. Hiraki, "Electronic States of Ni-Silicides and Its relation to metal-silicide/Si interfaces" J. Electrochem. Soc.,127 (7), PP.1542-1545, 1980.

[121] Zhizhen Wu, Chunyan Li, Jed A. Hartings, Go, Raj K. Narayan and Chong H. Ahn, "Polysilicon-based flexible temperature sensor for brain temperature monitoring with high spatial resolution", Journal of Micromechanics and Microengineering, Vol. 27, No. 2, 2017.

[122] Lin, Liwei, and Weijie Yun, "Design, optimization and fabrication of surface micromachined pressure sensors", Mechatronics, No. 5, pp. 505-519, 1998.

[123] Cremer OL, van Dijk GW, van Wensen E, Brekelmans GJF, Moons KGM, Leenen LPH, Kalkman CJ. "Effect of intracranial pressure monitoring and targeted intensive care on functional outcome after severe head injury": Crit Care Med., 33(10), pp:2207–2213, 2005.

[124] Chesnut RM, Temkin N, Carney N, Dikmen S, Rondina C, Videtta W, Petroni G, Lujan S, Pridgeon J, Barber J, Machamer J, Chaddock K, Celix JM, Cherner M, Hendrix T. A Trial of Intracranial-Pressure Monitoring in Traumatic Brain Injury. N Engl J Med 367(26) pp:2471–2481, 2012

[125] Hutchinson PJ, Kolias AG, Timofeev IS, Corteen EA, Czosnyka M, Timothy J, Anderson I, Bulters DO, Belli A, Eynon CA, Wadley J, Mendelow AD, Mitchell PM, Wilson MH, Critchley G, Sahuquillo J, Unterberg A, Servadei F, Teasdale GM, Pickard JD, Menon DK, Murray GD, Kirkpatrick PJ. "Trial of Decompressive Craniectomy for Traumatic Intracranial Hypertension". N Engl J Med. 375(12), pp: 1119–1130, 2016.

[126] Wolfla CE, Luerssen TG, Bowman RM. "Regional brain tissue pressure gradients created by expanding extradural temporal mass lesion". J Neurosurg. 86(3) pp: 505–510, 1997.

[127] Wolfla CE, Luerssen TG, Bowman RM, Putty TK. "Brain tissue pressure gradients created by expanding frontal epidural mass lesion". J Neurosurg, 84(4), pp: 642–647, 1996.

[128] Sahuquillo J, Poca M-A, Arribas M, Garnacho A, Rubio E. "Interhemispheric supratentorial intracranial pressure gradients in head-injured patients: are they clinically important?" J Neurosurg, 90(1), pp: 16–26, 1999.

[129] Broaddus WC, Pendleton GA, Delashaw JB, Short RV, Kassell NF, Grady MS, Jane JA. Differential Intracranial Pressure Recordings in Patients with Dual Ipsilateral Monitors. In: Hoff JT, Betz AL, editors. Intracranial Press VII]. Berlin, Heidelberg: Springer Berlin Heidelberg; 1989 p. 41–44.

[130] Rosenwasser RH, Kleiner LI, Krzeminski JP, Buchheit WA. "Intracranial pressure monitoring in the posterior fossa: a preliminary report." J Neurosurg, 71(4), pp:503–505, 1989.